# Ecology of vector-borne diseases at the interface of theory and data

by

Tsukushi Kamiya

A thesis submitted in conformity with the requirements
for the degree of Doctor of Philosophy
Graduate Department of Ecology and Evolutionary Biology
University of Toronto

# Abstract

Ecology of vector-borne diseases at the interface of theory and data

Tsukushi Kamiya
Doctor of Philosophy
Graduate Department of Ecology and Evolutionary Biology
University of Toronto
2020

Infectious diseases continue to impact human lives. However, surprisingly little is known about the fundamental biology of disease-causing organisms and their interactions with the host. This thesis focuses on vector-borne diseases which account for 17% of all known human infections and put more than half of the global population at risk of infection. An overarching focus of the work presented is heterogeneity within species, which is ubiquitous and fundamental to biology, yet has often been neglected outside of evolutionary biology. In infectious disease biology, a better understanding of individual heterogeneity is needed across scales. At the within-host level, infection dynamics and health outcomes are highly variable between hosts. Therefore, a single clinical intervention strategy will likely not achieve the desired cure in all individuals infected with the same parasite. At the between-host level, it is important to map the consequences of heterogeneity because a small fraction of the host population contributes disproportionately to disease transmission and determines the fate of an epidemic. By combining mathematical modelling and empirical data, this thesis develops conceptual and methodological frameworks that are rooted in ecology, but shift away from the strict focus on the average often found in biological sciences, dubbed the "tyranny of the golden mean". This thesis uncovers within-host origins, and explores the between-host consequences, of heterogeneities in vector-borne diseases. In the first half, I outline how differences in within-host ecological processes generate variation in parasite population dynamics and health outcomes of malaria infection across inoculum sizes and host genetic backgrounds. In the latter half, I present host population-level consequences of variation generated by tri-trophic interactions between parasites, hosts, and arthropod disease vectors, and of temperature-dependent heterogeneity in within-vector processes that govern the timing of infectivity. Overall, this thesis showcases the synergistic benefit of combining mathematical and computational modelling with empirical data to achieve better understanding and management of infectious diseases.

To my parents, Yuko and Kiyotaka Kamiya

# Acknowledgements

*"Life is unpredictable. Not everything's in our control. But as long as you're with the right people, you can handle anything."*

Amy Santiago (Brooklyn Nine-Nine)

My foremost gratitude goes to my supervisor Nicole Mideo. I couldn't have hoped for a more supportive and understanding mentor. I also credit Nicole for feeding me interesting ideas that became my PhD chapters and seedlings for many future projects.

I was fortunate to work with wonderful collaborators. I am particularly grateful to Megan Greischar, who has been a great collaborator and a friend. I appreciated many a discussions we had, both about science and non-science. A big thanks goes to David Schneider, who hosted me in his lab for three months. David's creativity reminds me that I do science because I enjoy it. I'm also grateful to Nicole Davis, who was very generous with her time in our collaborative projects even in the months coming up to finishing her own PhD. Krijn Paaijmans kindly shared his expertise on mosquito disease ecology, which was crucial for my fourth chapter. I am also grateful to Benjamin Gilbert whose expertise in community and quantitative ecology was invaluable to my fourth chapter.

I appreciate my committee members, Aneil Agrawal and Benjamin Gilbert who have provided insightful feedback in our meetings. I also appreciate Njal Rollinson and Art Weis for their contribution to my appraisal exam.

I would like to recognise the invaluable assistance that I received from other EEB faulty and staff, including Helen Rodd, Kitty Lam, Olivera Joksimovic and Aneil Agrawal for their support of graduate students, and Ryan MacDonald and Adam Hotchin for IT support. I am also grateful to patient SciNet support staff in particular, Alexey Fedoseev and Daniel Gruner.

My time during PhD would not have been enjoyable without friends and colleagues including the current and former members of the Mideo Group, my EEB friends and members of the Schneider lab.

I would like to thank my mother, Yuko, for always looking out for me and my father, Kiyotaka, for instilling intellectual curiosity in my childhood.

Finally, I am grateful to Katie for her love and support.

My PhD was supported by Natural Sciences and Engineering Research Council (Vanier Scholarship), Compute Canada (Resource Allocation Competition), National Science Foundation (Infectious Disease Evolution Across Scales, Research Exchange Award), University of Toronto (Professor R. Paul Young Fellowship), Mitacs (Globalink Research Award), and Council of Ontario Universities (Ontario Graduate Scholarship).

# Contents

# List of Figures

# Introduction

Infectious diseases continue to shape human society. For millennia, scientists have sought an understanding of infectious diseases that plagued human societies, albeit mostly without the knowledge that they were caused by biological organisms. The commonly held view was that *miasma* (meaning pollution in ancient Greek) emanating from rotting organic matter, ground and swamp, was responsible for outbreaks that are now known to have been caused by bacteria such as *Vibrio cholera* or *Yersinia pestis*, the aetiological agent of bubonic plague (Last, 2007). This idea remained mainstream throughout the middle ages and the Renaissance: in his 24-page doctoral dissertation, Carl Linnaeus, the father of modern taxonomy, proposed a hypothesis that malaria — derived from *mal aria* in Medieval Italian meaning "bad air" — was caused by clay particles (Hempelmann and Krafts, 2013). It was not until the invention of microscopes in the 17th century and development of the germ theory in the subsequent centuries that the scientific community widely accepted the biological origin of infectious diseases, like cholera, bubonic plague and malaria. Aided by the rapid improvement of scientific instruments, studies of infectious diseases since the 20th-century have sought discovery of ever-finer details of specific disease systems (Prosser et al., 2007). Classic microbiologists, for instance, were concerned with the structure and classification of bacteria and other infectious agents while immunologists traditionally catalogued components of the host immune system at the molecular and cellular levels and examined their functions in specific controlled settings (Rivas et al., 2017).

The vast knowledge base generated by these disciplines traditionally associated with studying diseases largely conforms to reductionism — an approach that simplifies complex biological processes by isolating effects to a small number of static components (Rivas et al., 2017). However, critics point out that reductionist disciplines fail to consider that biological processes are complex — consisting of many interacting components, and are dynamic — variable over time. It has been argued, therefore, that traditional disciplines are individually ill-equipped to provide full explanations of complex disease phenotypes, or to address clinically or epidemiologically relevant questions (Trochim et al., 2006; Aderem et al., 2011; Tran et al., 2012; Eckhardt et al., 2020). The limitation of reductionism in the context of infectious diseases is perhaps best highlighted by the fact that the precise mechanistic knowledge of the immune system alone does not predict sickness and recovery of a host in any disease system (Schneider, 2011). Therefore, a fuller understanding and prediction of infectious diseases demands a conceptual framework and a quantitative toolbox that is capable of mapping complex and dynamic disease systems. This thesis aims to highlight that ecological concepts and the ecologists' toolbox offer a unified framework for better understanding and management of infectious diseases, both at the level of individual hosts (i.e., within-host, or clinical) and populations (i.e., between-host, or epidemiological).

Biological processes and phenomena do not occur in isolation but rather span multiple levels of organisation. An individual organism consists of organs, tissues, cells and molecules while the organism itself is a member of a population, community and ecosystem. A universal challenge in biological sciences is to understand the relationship within and across these levels that constitutes a complex and dynamic system. For example, ecologists focus on interactions between organisms (e.g., parasitism, competition, predation) and their influence on the population, community and ecosystem-level properties (e.g., emergence, proliferation, coexistence, extinction, evolution). These ecological concepts are an example of "systems thinking" which seeks to explain interactions between components and overall phenomena of a system, which are unpredictable from the knowledge about individual components in isolation (Cabrera et al., 2008; Verhoeff et al., 2018).

Mathematical modelling has been an integral part of systems thinking because intuition often fails to

track the knock-on implications of numerous interacting processes in complex systems. As early as at the beginning of the 20th century, Ronald Ross — who was also among the first to empirically demonstrate the role of mosquitoes in transmitting malaria (Ross, 1897) — developed a series of mathematical models to understand the transmission and control of malaria (Ross, 1908, 1911*a*,*b*, 1921). Remarkably, an iteration of his model by George Macdonald (Macdonald, 1957) (known as the Ross-Macdonald model) still serves as the starting block of vector-borne disease models (Smith et al., 2012; Reiner et al., 2013). The historical significance of the Ross-Macdonald model is glaring as it provided rational justification for the World Health Organisation's (WHO) worldwide DDT spraying campaign against mosquitoes, which successfully eliminated malaria in many countries by the late 1970s (Smith et al., 2012; Mendis et al., 2009).

Many contemporary models used to study the population ecology of infectious diseases are grounded in dynamic systems and nonlinear systems theory. These models are used to investigate the interactions between organisms and their physical, chemical and biological environments from the first principles of ecological and evolutionary dynamics (Smith et al., 2005; Bjørnstad, 2015). In epidemiology, dynamical modelling is widely used to describe the spread of infection and immunity in a population. For example, the commonly used Susceptible-Infected-Recovered (SIR) model tracks the fraction of a population divided into three compartments: susceptible to an infectious disease (S), carrying infection and infectious to others (I) or recovered or vaccinated and hence immune to future infections (R). The SIR model and its extensions have been applied to inform the required vaccination threshold (i.e., minimum proportion of a population required to be vaccinated), for example, to prevent childhood measles infections (Keeling and Rohani, 2008). Dynamical models have also been used to investigate the time-course of infection and immune responses within hosts, including malaria (Mideo et al., 2008*c*) and HIV (Perelson and Ribeiro, 2013). These within-host models share conceptual parallels with population ecology and epidemiological models, as they track the population dynamics of the focal parasite and its target cells (i.e., resource population) and can incorporate immune systems (analogous to "predators" feeding on their prey, the focal parasites) and coinfecting parasites which are in competition with the focal parasite for the shared host resource. Furthermore, dynamical models have been applied to study feedbacks between the two levels, which are important considerations for rapidly evolving viruses (Mideo et al., 2008*a*). Today, application of dynamical models to infectious disease systems is more accessible to biologists than ever before, thanks to the development of user-friendly packages in high-level programming languages (e.g., R, Python and Mathematica) and excellent educational resources in the field (e.g., Otto and Day, 2011; Keeling and Rohani, 2008)

A thematic goal of this thesis is to uncover the origin of variation in the interactions between hosts and parasites, and to map the impact of individual variation on disease spread. Trait variation within species is ubiquitous and fundamental to organismal evolution. Outside of evolutionary biology, however, individual variation has often been neglected. Population ecology, for instance, focuses typically on homogenised, "average" populations, ignoring variability between individuals (Vindenes and Langangen, 2015) while many biological disciplines have traditionally disregarded individual variation as undesirable experimental noise to be minimised (Herzfeld and Shadmehr, 2014; Roche et al., 2016; Nikinmaa and Anttila, 2019). In recent years, there has been increasing attention on intraspecific variation (Roche et al., 2016), shifting away from the strict focus on the average that has been described as the "tyranny of the golden mean" (Bennett, 1987). In modern disease ecology, better understanding the origin and consequences of individual heterogeneity has emerged as a central theme (VanderWaal and Ezenwa,

2016). At the within-host level, it is crucial to understand individual heterogeneity because infection dynamics and outcomes are highly variable between individual hosts. Thus, a critical applied implication is that a single clinical intervention strategy does not achieve the desired cure in all individuals infected with the same parasite (Moser et al., 2019). At the population level, an empirical relationship of the 20/80 rule often holds, where 20% of individuals are responsible for 80% of total parasite transmission (Woolhouse et al., 1997). Thus, it is essential to identify the small fraction of the host population that can contribute disproportionately to transmission and decide the fate of an outbreak (Lloyd-Smith et al., 2005).

This thesis focuses on infectious diseases transmitted by arthropod vectors — like mosquitoes, sand flies, and ticks —, which account for 17% of all known human infections, and put more than half of the global population at risk of infection (World Health Organization, 2014). Mosquitoes alone are responsible for diseases such as malaria, dengue, West Nile virus, chikungunya, yellow fever, filariasis and Zika. More than a century after the role of mosquitoes in malaria transmission was discovered (Ross, 1897), the WHO estimates that malaria alone continues to claim over half a million lives annually (World Health Organization, 2014). Despite the common notion that vector-borne diseases are only a problem for the tropics, threats are now expanding worldwide. For example, *Aedes* mosquitoes — the genus that carries dengue fever among other diseases — were considered eradicated from Europe over half a century ago (Schaffner and Mathis, 2014). Today, *Aedes aegypti* is found in 20 European countries and, climatic and environmental conditions are suitable for establishment across the entire region of southern Europe (Rogers and Hay, 2012). Following the expansion of mosquitoes, there have been dengue outbreaks reported in France, Croatia and the Portuguese archipelago Madeira since 2010 — breaking a 55-year absence after the last European outbreak in 1945 (Schaffner and Mathis, 2014). Similarly, in the US, reported incidences of West Nile virus and Lyme disease have been on the rise since the early 2000s (Petersen et al., 2014). The increasing global threat from vector-borne diseases calls for renewed momentum to combat their spread. In response, the WHO has committed to preventing all vector-borne disease outbreaks worldwide by 2030 (World Health Organization, 2017).

## Thesis outline

In this thesis, I investigate both within- (Chapter 1 & 2) and between-host (Chapter 3 & 4) ecology of vector-borne diseases using various dynamical modelling techniques. Each chapter of this thesis is also closely inspired by data: I quantitatively describe longitudinal data of within-host infection (Chapter 1 & 2) and predict population-level consequences of overlooked empirical observations (Chapter 3 & 4).

### Within-host ecology (Chapter 1 & Chapter 2)

The dynamics of parasites within their hosts is a key determinant of host immune activity, disease severity, between-host transmission and the evolution of parasite traits such as drug resistance (Paul et al., 2003; Greischar et al., 2016*b*). In Chapter 1 and 2, I focus on the within-host dynamics of malaria. The within-host stage of malaria is characterised by asexual proliferation and occasional sexual reproduction. Following an infectious bite, malaria parasites first migrate to the liver. The asexual cycle begins when an extracellular stage parasite, released from the liver, enters a red blood cell. Depending on the species of *Plasmodium*, parasite development within a red blood cell takes approximately 24 to 72 hours, and the cycle is typically synchronised among asexual clones infecting the same host (Mideo et al., 2013).

The end of each asexual cycle is marked by rupturing of the red blood cell and bursting of extracellular parasites into the bloodstream where they have only minutes to find the next red blood cell to infect and repeat the cycle. As red blood cells are depleted and host immunity clears parasites, the parasite number eventually declines. Aided by the decreasing parasite number and up-regulation of red blood cell replenishment (i.e., erythropoiesis), the host starts to recover from anaemia marking the end of the acute phase of malaria infection. Mathematical modelling has been applied extensively to describe these processes of within-host malaria infection (Mideo et al., 2008*c*), yet few have incorporated dynamical immune regulation coupled with the infection dynamics. I developed two distinct dynamical models of blood-stage malaria ecology and host responses, one using classic differential equations (Chapter 1) and another using recursion equations (Chapter 2). I fitted the models to time-series data of experimental rodent infections to study variation in infection dynamics caused by the initial infection dose (Chapter 1) and to uncover functional diversity of host resilience to malaria infection among host genotypes (Chapter 2).

## Between host ecology (Chapter 3 & Chapter 4)

Variation in transmission has been recognised as an important factor in disease emergence and persistence. Some host traits underlying the variation in transmission may be best conceptualised as distinct groups. For example, while age is, in reality, a continuous variable, it is often useful to categorise age structure into discrete classes to reflect the underlying variation in immune status between children and adults due to vaccination and history of infection. By ignoring individual variability within discrete classes, such class-structured models allow for estimation of the infection risk structure associated with a known source of variation without explicit knowledge about the nature of variation at the individual level (Keeling and Rohani, 2008). Using the class-structured approach, I developed, in Chapter 3, a general model of vector-borne disease to explore the effect of the variation in host immune status generated by bites of uninfected vectors.

Another way to conceptualise heterogeneity is to consider a statistical distribution of trait values representing continuous variation in a population. Most commonly, events of an epidemiological model, like the aforementioned SIR model, are assumed to follow an exponential distribution. Consider, for example, the standard expression of the mean duration of infection, $\gamma^{-1}$ where $\gamma$ is the rate of host recovery. In this formulation, it is assumed that the time until recovery (or infectious period) is exponentially distributed, which implies that the average waiting time, e.g., $\gamma^{-1}$, is accompanied by large variance, e.g., $\gamma^{-2}$, with the mode of the distribution at 0. This means many individuals are assumed to recover from infection immediately after exposure. However, the infectious period is rarely exponentially distributed in nature (Keeling and Rohani, 2008), and neither are many processes that require parasite development (e.g., the incubation period of measles, chickenpox and mumps (Simpson, 1952) and within-mosquito incubation period of malaria and dengue (Paaijmans et al., 2011; Chan and Johansson, 2012)). In SARS, for example, precise assumptions made about the distribution of the infectious period had profound implications for disease spread. When realistic variation is considered, epidemics were predicted to be rarer, yet more potent (Lloyd-Smith et al., 2005). With increasing availability of data on the effects of temperature on parasite development within vectors (Paaijmans et al., 2011; Chan and Johansson, 2012), there is an opportunity to incorporate realistic developmental variation into mathematical models to predict its consequences. In Chapter 4, I focused on dengue virus for which the most comprehensive data is available. Using an individual-based stochastic simulation model, I investigated

the impact of temperature-dependent variation in the dengue virus extrinsic incubation period on the probability of disease emergence.

## Thesis contributions

This thesis aims to advance the current understanding of the origin and consequences of individual variation in the ecology of infectious diseases, both within- and between-hosts. It merges knowledge in the fields of microbiology, parasitology, and immunology through the lens of ecological concepts. The originality of this thesis is demonstrated also in its methodological approaches. It showcases a variety of quantitative techniques that are instrumental to incorporating biological variation, but are still underutilised in studies of infectious diseases. By combining these techniques with empirical data, the work presented here reveals subtle signals in data, projects consequences of overlooked empirical patterns, and generates new hypotheses that will motivate future experiments. Finally, this thesis offers practical insights of clinical and public health importance.

# Chapter 1

# Uncovering drivers of dose-dependence and individual variation in malaria infection outcomes

This work was carried out in collaboration with Megan Greischar (University of Toronto), David Schneider (Stanford University) and Nicole Mideo (University of Toronto).

Contents of this chapter have been provisionally accepted by *PLOS Computational Biology*.

## 1.1 Abstract

To understand why some hosts get sicker than others from the same type of infection, it is essential to explain how key processes, such as host responses to infection and parasite growth, are influenced by various biotic and abiotic factors. In many disease systems, the initial infection dose impacts host morbidity and mortality. To explore drivers of dose-dependence and individual variation in infection outcomes, we devised a mathematical model of malaria infection that allowed host and parasite traits to be linear functions (reaction norms) of the initial dose. We fitted the model, using a hierarchical Bayesian approach, to experimental time-series data of acute *Plasmodium chabaudi* infection across doses spanning seven orders of magnitude. We found evidence for both dose-dependent facilitation and debilitation of host responses. Most importantly, increasing dose reduced the strength of activation of indiscriminate host clearance of red blood cells while increasing the half-life of that response, leading to the maximal response at an intermediate dose. We also explored the causes of diverse infection outcomes across replicate mice receiving the same dose. Besides random noise in the injected dose, we found variation in peak parasite load was due to unobserved individual variation in host responses to clear infected cells. Individual variation in anaemia was likely driven by random variation in parasite burst size, which is linked to the rate of host cells lost to malaria infection. General host vigour in the absence of infection was also correlated with host health during malaria infection. Our work demonstrates that reaction norms describing parameters of a mechanistic model provide a useful approach for examining the impact of an environmental gradient in within-host infection processes.

## 1.2 Introduction

Infections produce divergent outcomes. In human malaria, for example, outcomes of infection with the same parasite, *Plasmodium falciparum*, range from sub-clinical to fatal (Galatas et al., 2015). Understanding drivers of variation in infection outcomes is central to explaining why some hosts get sicker than others. Some host and parasite factors underlying this variation have well-understood mechanisms. For example, heterozygosity in the haemoglobin coding gene (i.e., sickle-cell trait, or HbAS) confers partial protection against falciparum malaria: sickle-cell trait individuals experience lower parasite load and reduced likelihood of life-threatening cerebral malaria and severe anaemia (Luzzatto, 2012). The resistance mechanism of this single locus trait has been corroborated by four decades of research demonstrating that sickling enhances clearance of infected red blood cells (iRBCs) by host immune effectors like macrophages (Luzzatto, 2012). However, unlike the sickle-cell trait, there are numerous sources of heterogeneity — including in the initial infection dose, nutrition, coinfection, and other genetic factors — for which quantitative impacts on outcomes have been observed, but causal mechanisms have remained elusive (Shankar, 2000; Haydon et al., 2003; Weatherall, 2008; Hochman and Kim, 2009). To establish a causal link between complex factors and infection outcomes, a key challenge is to quantify how a factor of interest mediates key host and parasite processes, such as host responses to infection and parasite growth (Lazzaro and Little, 2008).

In many disease systems, the initial infection dose is a key biotic factor that varies widely across infection events (Schmid-Hempel and Frank, 2007; Leggett et al., 2012). Experimental infections in diverse systems show that increasing infection dose negatively impacts host fitness through reduced host vigour, survival and fecundity (Nie and Kennedy, 1993; Ashworth et al., 1996; Michael and Bundy,

1989; Mackinnon and Read, 1999; Ebert et al., 2000; Timms et al., 2001; Tan et al., 2010; Brunner et al., 2005), which is likely linked to variation in the within-host parasite dynamics due to dose-dependence in parasite growth and host immune responses (Michael and Bundy, 1989; McLean and Bostock, 2000; Hughes et al., 2002; Haydon et al., 2003; Li and Handel, 2014; Handel et al., 2018). Complex interactions between immune responses and the initial infection dose have been revealed by molecular immunology studies of viral and bacterial systems. For example, the expression of pro-inflammatory cytokines (i.e., signalling molecules) and immune cells, can decrease with infection dose (Schmidt et al., 2013; Morris et al., 2014), presumably due to enhanced evasion and escalated damage of host immune machinery through an increased abundance of reactive oxygen species(Schmidt et al., 2014). Conversely, it has been shown that higher doses trigger distinct, and sometimes more robust, activation of innate and adaptive immune pathways (Hatta et al., 2010; Marois et al., 2012; Segueni et al., 2016; Pagan et al., 2016). From an applied perspective, a better understanding of the immunogenic dose-response relationship is pertinent for optimising vaccine dosing to ensure improved safety and efficacy (Handel et al., 2018; Rhodes et al., 2018, 2019; Afrough et al., 2020). However, because the functional output of immune activities (e.g., the rate of immune-mediated iRBC clearance) is difficult to measure directly, it remains an open question how the initial infection dose influences host responses overall.

In malaria infections, the initial density of iRBCs at the start of blood-stage infection likely ranges in the order of hundreds to over millions (Garnham, 1966; Rosenberg et al., 1990; Beier et al., 1991; Lines and Armstrong, 1992; Beier, 1993), with greater numbers generally shown to increase mortality and worsen morbidity (Mackinnon and Read, 1999; Timms et al., 2001). Experimental manipulations of the initial infection dose, ranging from 100 to 100 million iRBCs, have demonstrated that larger doses increase the pace of infection with each order of magnitude reducing the time until peak infection by roughly 24 hours (Timms et al., 2001) (Fig. 1.1a). Dose also impacts the peak parasite load: mice initially infected with 100 million parasites harbour roughly 60% more iRBCs at peak compared to those infected with 100 parasites (Timms et al., 2001) (Fig. 1.1b). Furthermore, high doses induced more severe anaemia measured by the minimum red blood cell (RBC) count in mice on average (Timms et al., 2001) (Fig. 1.1c). Previous mathematical modelling studies interpret these dose-dependent infection outcomes as a reflection of the underlying dose-dependence in host immune responses (Haydon et al., 2003; Metcalf et al., 2011).

While dose clearly influences malaria infection dynamics, these experimental data also reveal striking variability within dose treatments (Timms et al., 2001) (Fig. 1.1), meaning that quantitatively diverse infection outcomes were observed across individuals receiving the same infection dose. This is despite the fact that hosts were inbred to homozygosity and parasites were also of single strain origin in the experiment (Timms et al., 2001). Identifying the sources of such individual variation — usually considered experimental "noise" — may reveal biologically interesting, subtle trait variation among hosts and/or parasites, and thus new therapeutic targets (e.g., host responses to boost).

In the study of acute malaria infection, mathematical models have been fitted to the time course of experimental infections in mice to provide a quantitative understanding of parasite growth, pathogenesis and host responses to infection (e.g., (Kochin et al., 2010; Miller et al., 2010; Mideo et al., 2011; Wale et al., 2019); see (Mideo et al., 2008*c*) for a review of earlier work). Infection triggers a variety of host responses, for example, indiscriminate clearance of RBCs, targeted clearance of iRBCs (Miller et al., 2010) and production of new RBCs to compensate for those lost to infection (Miller et al., 2010; Wale et al., 2019). It is well documented that these responses involve a complex cascade of interactions

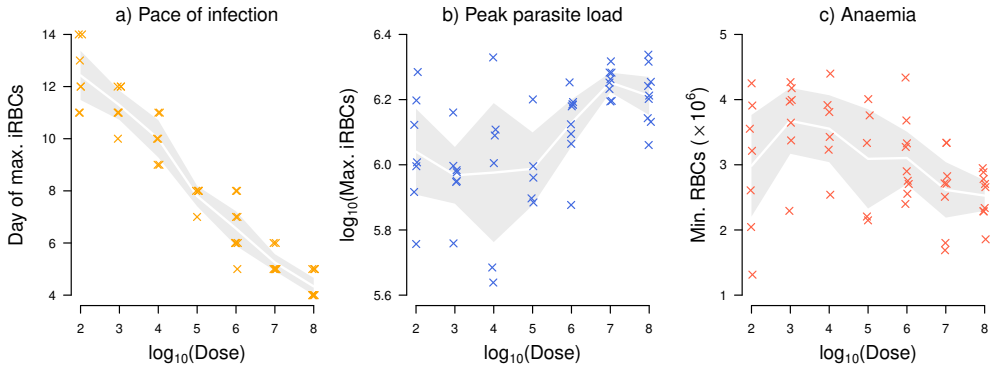


Figure 1.1: Higher initial infection doses increase a) the pace of infection (i.e., time until peak iRBC density), b) peak parasite load measured as the maximum iRBC count, and c) severity of anaemia during malaria infection measured as the minimum RBC count. There is also considerable variation in quantitative infection outcomes (i.e., parasite load and anaemia) within infection dose treatments. Data from Timms et al. (2001) with 5 to 9 mice infected with the CW strain of *P. chabaudi*, at each dose. The crosses indicate data and the white lines and grey bands correspond to the means and 95% confidence intervals.

across multiple organisational scales from molecules, cells, and tissues to organ systems (Stevenson and Riley, 2004; Gazzinelli et al., 2014). However, it remains a challenge to scale up the details of finer level processes to an understanding of the net effect of host responses on parasite load and host health (Schneider, 2011). Data-driven mathematical modelling allows for the inference of these net effects, without necessarily requiring a detailed understanding of the underlying mechanisms.

Here, we fitted a dynamical model of within-host malaria infection to experimental data spanning seven orders of magnitude of initial doses, using a Bayesian statistical approach. By modelling the influence of dose on model parameters as a reaction norm, which describes the pattern of phenotypic expression of an organism across an environmental gradient, we identified drivers of the observed dose-dependent malaria parasite load and severity of malaria-induced anaemia. By explicitly modelling individual variation as model parameters, we also examined the origin of quantitatively diverse infection outcomes observed within single initial infection dose treatments.

## 1.3 Methods

### 1.3.1 System and experimental set-up

The rodent malaria system offers unique opportunities to investigate infection ecology, pathogenesis and host responses (Stephens et al., 2012). We examined previously published experimental data of C57BL/6 female mice infected with the CW strain of *Plasmodium chabaudi* (Timms et al., 2001). In this experiment (Timms et al., 2001), infection was initiated with an intraperitoneal injection of iRBCs at seven different doses: $10^2$, $10^3$, $10^4$, $10^5$, $10^6$, $10^7$, $10^8$ — and considerable variation in quantitative infection outcomes was observed both among and within dose treatments (Fig. 1.1b & c). Details of the experiment are provided by Timms et al. (2001).

### 1.3.2 Model

**Innate host responses to malaria infection**

Hosts trigger a variety of responses to resist, tolerate and/or recover from infections. Here, we focused on two forms of rapid immune responses on the order of minutes (on the order of minutes, Safeukui et al., 2008; White, 2017) that have been identified as the most pertinent to describing the acute blood-stage malaria infection (Kochin et al., 2010; Miller et al., 2010; Mideo et al., 2011).

The first response we modelled was general clearance of RBCs which may involve mechanisms such as retention of RBCs by the spleen and destruction of RBCs by immune effector cells (Price et al., 2001; Castro-Gomes et al., 2014). Clearing RBCs indiscriminately has been proposed as a host adaptation in the presence of malaria parasites to directly clear the parasites (i.e., top-down effect) as well as to limit the resource for the parasite (i.e., bottom-up effect) (Metcalf et al., 2012). The second response we considered was the induction of innate immunity targeting iRBCs only, which is considered predominantly responsible for controlling the acute phase of malaria infection (Stevenson and Riley, 2004).

We modelled regulation of host responses without delving into fine mechanistic details (i.e., we avoided mathematical descriptions of cytokine storms and subsequent cascades of effector responses). In part, this modelling choice was out of necessity because there is no complete map of innate immune responses against malaria (Stephens et al., 2012). Yet, it was also by design so that we would gain a functional understanding of host responses with minimal complexity. Biologically, responses modelled here may reflect the output of an entire module of proteins and signal transduction pathways that lead to the production of effector cells. Specifically, we used a single ordinary differential equation (ODE) to describe the change in the functional output of each response (Fig. 1.2a; yellow and green block, respectively). We assumed that the maximum possible activity of each response is fixed, at one, and we tracked the dynamics of its proportional activity, $N_i$, where $i$ indicates the response identity (general RBC clearance, $i = 1$; targeted iRBC clearance $i = 2$)

$$\frac{dN_i(t)}{dt} = \psi_i\, C_i(t)\Big(1 - N_i(t)\Big) - \frac{N_i(t)}{\phi_i}. \tag{1.1}$$

We defined the activity of $N_1$ and $N_2$ as the proportion of RBCs and iRBCs cleared by indiscriminate and targeted mechanisms per day, respectively. We assumed that there is no response output in the absence of infection, i.e., $N_1(t = 0) = N_2(t = 0) = 0$, consequently assuming a stable RBC population and that there is no constitutive immune activity.

We modelled the signalling input that activates each response as a function of a within-host cue, $C_i(t)$ and a constant determining the strength of activation, $\psi_i$ (Eq. 1.1). Host innate immune responses against malaria are thought to be triggered by pathogen-associated molecular patterns (PAMPs) such as GPI anchors, haemozoin, parasite DNA and RNA (Stephens et al., 2012; Gazzinelli et al., 2014). Assuming that the abundance of PAMPs reflects that of iRBCs, our model considers the relative density of iRBCs compared to its observed maximum in any infection across all treatment groups, as the within-host cue for general RBC clearance and targeted iRBC clearance, i.e., $C_1(t) = C_2(t) = \frac{I(t)}{\max I}$ where $I(t)$ and $\max I$ are the iRBC density at time $t$ and the maximum observed iRBC density, respectively. The latter was reported at $2.18 \times 10^6$ from this dataset (Timms et al., 2001). We assumed that each response activity decays spontaneously with a half-life of $\phi_i$.

Our two-parameter approach — involving only an activation constant, $\psi_i$, and activity half-life, $\phi_i$ — to modelling each host response was inspired by Kochin et al. (2010) who used a single ODE to

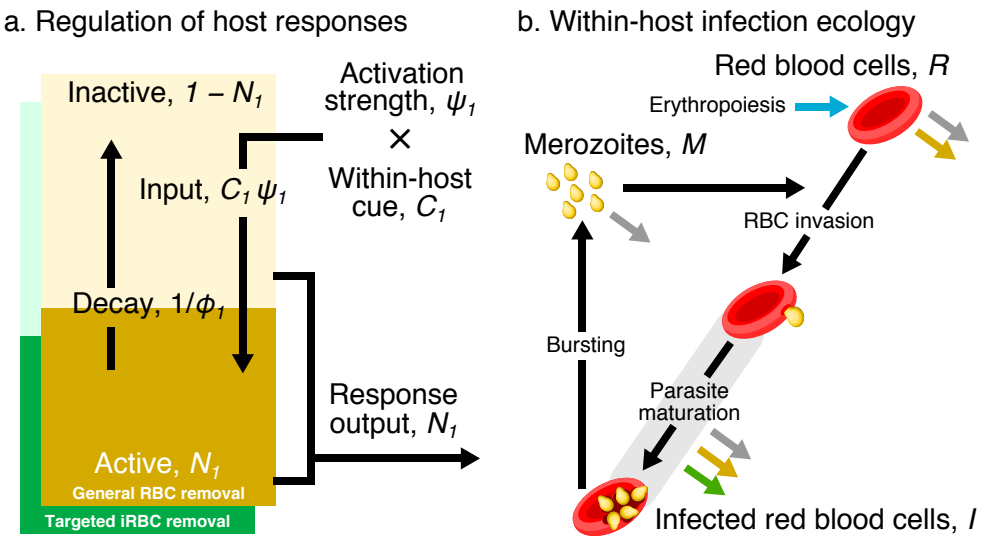


Figure 1.2: a) A dynamical regulation model of host responses against blood-stage malaria. We condensed the complexity of the vertebrate innate response against malaria into two independent pathways responsible for general RBC clearance and targeted iRBC clearance (represented by the yellow and green block, respectively). We modelled each pathway using a single differential equation, the activity of which is denoted $N_i$ where the subscript $i$ indicates the identity of each response: general RBC clearance, $i = 1$; and targeted iRBC clearance, $i = 2$. (The schematic shows the example of $i = 1$.) For each response type, the host detects a within-host cue, $C_i$. The product of the cue and the strength constant, $\psi_i$, activates the response. The activity of a response decays spontaneously with a half-life, $\phi_i$. The output of each host response feeds back to influence the within-host infection dynamics (indicated by the coloured arrows in panel b). b) Dynamics of RBCs and blood-stage malaria parasites within the host. Recruitment into and transitions among components of the asexual cycle are indicated with black arrows. Background mortality for different components is indicated by grey arrows. General clearance of RBCs and targeted clearance of iRBCs are marked with yellow and green arrows, respectively. Replenishment of RBCs (erythropoiesis) is indicated in blue.

model innate immunity against malaria parasites governed by density-dependent response activation and constant decay. However, we interpreted host response activity differently from their study: i.e., we modelled the proportion of RBCs and iRBCs cleared per day whereas they modelled the number of immune cells. Our study also extends the approach to the dynamics of general RBC clearance.

### Within-host infection dynamics of blood-stage rodent malaria

We used a system of ODEs to model the blood-stage asexual cycle of *P. chabaudi*, tracking the density of uninfected RBCs (hereafter, uRBCs), $R$, iRBCs, $I$, and extracellular parasites called merozoites, $M$, in a microlitre of blood (Fig. 1.2b). In this model, we assumed that RBCs are constantly replenished to maintain a homeostatic equilibrium, thus the daily rate of erythropoiesis in the absence of infection is defined as $R_c\,\mu_R$, where $\mu_R$ is the baseline RBC mortality rate. We estimated $R_c$ at $8.89 \times 10^6$ from data (Timms et al., 2001) as the average RBC density of 10 uninfected mice between Day 7 and 14 during which time the RBC density appears stable. During the acute phase of malaria infection, the host upregulates erythropoiesis to restore RBCs lost to malaria-induced anaemia (Chang et al., 2004; Bunn, 2013). Following a previous study (Miller et al., 2010), we modelled this upregulation as a product of the deviation from the homeostatic equilibrium, $R_c - R(t)$ where $R(t)$ is the RBC density at time $t$,

and the proportion of the deviation from the homeostatic equilibrium restored by the host per day, $\rho$.

Given that $N_1$ and $N_2$ were defined as the proportion of cells cleared by indiscriminate and targeted mechanisms per day, respectively, it was convenient to convert the proportions into daily rates at which cells are cleared in the dynamical within-host model. To do this, we equate $N_i = 1 - e^{-X_i}$, where $X$ is the daily rate of clearance. Solving for $X$, we obtained the rate of general RBC clearance as $-ln(1-N_1)$ and the rate of targeted iRBC clearance as $-ln(1-N_2)$. Therefore, the sum of the baseline rate, $\mu_R$ and $-ln(1-N_1)$ constitutes the daily mortality rate of uRBCs. uRBCs then become infected at a rate proportional to the density, $M$, and invasion rate, $p$, of merozoites. Together the dynamics of uRBCs is expressed as:

$$\frac{dR(t)}{dt} = R_c\,\mu_R + \rho(R_c - R(t)) - (\mu_R - ln(1-N_1))\,R(t) - p\,R(t)\,M(t). \tag{1.2}$$

Following merozoite invasion, iRBCs remain subjected to background mortality, $\mu_R$ and general RBC clearance, $-ln(1-N_1)$. In addition, infected cells are cleared by targeted immunity at a rate $-ln(1-N_2)$: here, we note that estimates of $-ln(1-N_2)$ may be slightly inflated by iRBCs that commit to sexual reproduction (usually less than 2% of iRBCs, Greischar et al., 2016*a*) because our model does not consider *Plasmodium* sexual reproduction. We modelled the development of iRBCs using a gamma-chain trick (also known as linear chain trick, Gravenor et al., 2002; Smith, 2011), which consists of a series of ODEs:

$$\frac{dI_1(t)}{dt} = p\,R(t)M(t) - (\mu_R - ln(1-N_1) - ln(1-N_2) + \tau)I_1(t) \tag{1.3}$$

$$\frac{dI_i(t)}{dt} = \tau\,I_{i-1}(t) - (\mu_R - ln(1-N_1) - ln(1-N_2) + \tau)I_i(t) \quad \text{for } 2 \le i \le n \tag{1.4}$$

where $\tau = {}^{n}/_{\alpha}$, and $\alpha$ is the average cell cycle duration, which is 24 hours for *P. chabaudi* (Paul et al., 2003). The number of compartments in the series, $n$, reflects the assumption about the variance in the developmental time, which is inversely proportional to $n$ (Gravenor et al., 2002). At one compartment per cycle (i.e., $n = 1$, e.g., Anderson et al., 1989; Hellriegel, 1992), the assumption is that the developmental time is exponentially distributed, with large variance, i.e., $\alpha^2$ (Saul, 1998). The variance decreases with the number of compartments, and the variance tends to disappear as the number of compartments approaches infinity (i.e., $n \to \infty$) — a scenario equivalent to discrete-time models (e.g., White et al., 1992; Molineaux et al., 2001) and delay-differential equation models (Greischar et al., 2013) that assume there is no variation in the developmental period (Gravenor et al., 2002). It has been shown that models with few compartments tend to estimate greater asexual multiplication, compared to discrete-time models (Saul, 1998; Crooks, 2008). With enough compartments (e.g., one compartment per hour of parasite development, Gravenor et al., 2002), however, the outcome of a gamma-chain ODE model converges to the discrete-time model (Crooks, 2008). We arrived at the choice of $n = 12$ (one compartment every two hours) for computational efficiency, and because our preliminary analysis showed that the infection dynamics were quantitatively comparable to that of a 24 compartment model (one compartment per hour).

Finally, the production of merozoites is determined by parasite burst size (i.e., the number of progeny parasites emerging from an iRBC), $\beta$, and the number of bursting cells, $\tau\,I_n(t)$. Merozoites are lost as they invade new RBCs and through background mortality, $\mu_M$. We ignored immune-mediated clearance of merozoites because its effect on the parasite dynamics is functionally similar to clearing iRBCs and

comparatively less important for describing the acute phase of malaria infection than general RBC clearance or targeted iRBC clearance (Haydon et al., 2003; Miller et al., 2010),

$$\frac{dM(t)}{dt} = \beta\,\tau\,I_n(t) - p\,R(t)M(t) - \mu_M\,M(t). \tag{1.5}$$

**Initial conditions**

We set the initial RBC density, $R(t = 0)$, to the values reported per mouse by Timms et al. (2001). In the experiment (Timms et al., 2001), malaria infection was initiated with an intraperitoneal injection to mimic the initial cohort of blood-stage malaria parasites following release from the liver. Assuming that the initial parasite growth is near-exponential (for the first three records of iRBCs per mouse), we estimated the initial infection dose per $\mu l$ of blood in each mouse as the intercept of a linear regression model with the natural logarithm of iRBCs as the response and the time since infection as a predictor. At a preliminary phase, we also estimated the initial infection dose simultaneously with the rest of the model parameters. Because these two methods for estimating initial dose yielded analogous results (see Appendix 1.6.1) and the regression method allowed us to estimate one fewer parameter in the main Bayesian parameter inference procedure (described below), we present results based on the initial infection dose estimated by the regression method. Finally, we defined the age structure of the inoculated iRBCs to schedule the bursting of iRBCs in the initial cohort. Assuming that all inoculated iRBCs commit to producing merozoites (i.e., ignoring the possibility that some of them produce transmission stages instead), the timing of bursting can be described using a symmetrical beta distribution (Greischar et al., 2013). We assumed a moderately synchronised blood-stage cycle (i.e., with the shape parameter, $s = 10$). Our preliminary exploration indicated that the daily RBC and iRBC measurements were insensitive to the $s$ parameter. We discretised the beta distribution into 12 compartments (for Eq. 1.3 and 1.4) by dividing the cumulative density function into 12 intervals.

### 1.3.3 Bayesian statistical inference

Bayesian causal inference is an effective tool to paint a picture of processes that generated data (McElreath, 2018). We fitted our ODE model describing the dynamics of RBCs (Eq. 1.2) and iRBCs (Eq. 1.3 and 1.4) to the corresponding time-series data from 51 mice (Timms et al., 2001) using a Bayesian statistical approach. Statistical inference in a Bayesian framework incorporates prior knowledge and uncertainty about model parameters and updates the belief about them (by computing the posterior probability of parameters) based on observations (through a likelihood function) (Gelman et al., 2013). Besides its conceptual merits (Gelman, 2011; Gelman et al., 2013), Bayesian inference has a pragmatic appeal for its ability to estimate parameters in high dimensional space, for example, in hierarchical models, which are used when observations are organised in multiple levels of sampling units (Mugglin et al., 2002; Cressie et al., 2009). In this study, we considered two levels of sampling units: treatments (i.e., infection doses) and subjects (i.e., individual mice).

**Dose and individual-specific effects** For the dynamical model (Eq. 1.1 to 1.5), we estimated dose- and individual-specific effects in a set of seven parameters including the response activation strength of host responses $N_1$ and $N_2$ ($\psi_1$ and $\psi_2$, respectively), half-life of those responses ($\phi_1$ and $\phi_2$, respectively), erythropoiesis upregulation ($\rho$) and parasite burst size ($\beta$). Below, we collectively refer to the parameter set as $\theta$ ($\theta \ni \psi_1, \psi_2, \phi_1, \phi_2, \rho, \beta$) and refer to a parameter in the set using an index, $k$. The prior

Table 1.1: Descriptions of model parameters and their fixed values, or prior distributions used in Bayesian statistical inference. Estimated parameters are indicated by an asterisk on the description. We assigned a generic, weakly informative prior, except for erythropoiesis upregulation, $\rho$, burst size, $\beta$, and standard deviations of $\log_{10}$ RBC and iRBC density, $\sigma_{\text{RBC}}$ and $\sigma_{\text{iRBC}}$, for which there exist specific prior information from previous studies. Further details of the priors and comparisons with estimated posterior probability densities, and prior sensitivity analyses are provided in Appendix 1.6.2.

| Symbol | Description | Fixed value or prior | [Source] |
|---|---|---|---|
| Host responses | | | |
| $\psi_i$ | *Activation strength of $N_i$ | $\exp(\mathcal{N}(ln(1)+5,\sqrt{5})$ | |
| $\phi_i$ | *Half-life of $N_i$ | $\exp(N(ln(1)+5,\sqrt{5})$ day | |
| Within-host infection dynamics | | | |
| $R_c$ | RBC density at homeostatic equilibrium | $8.89\times10^6$ per $\mu l$ | (Timms et al., 2001) |
| $maxI$ | Maximum iRBC density observed in Timms et al. | $2.18\times10^6$ per $\mu l$ | (Timms et al., 2001) |
| $\mu_R$ | Baseline RBC mortality rate | 0.025 per day | |
| $\rho$ | *Proportion of deviation from $R_c$ restored per day | $0.25\times\exp(\mathcal{N}(0,0.25))$ | (Miller et al., 2010) |
| $\beta$ | *Parasite burst size | $7\times\exp(\mathcal{N}(0,0.25))$ | (Miller et al., 2010) |
| $p$ | Merozoite invasion rate | $8\times10^{-6}$ per day | (Miller et al., 2010) |
| $\alpha$ | *P. chabaudi* RBC cycle duration | 1 day | (Paul et al., 2003) |
| $n$ | Number of RBC cycle components | 12 | |
| $s$ | Degree of synchronous bursting | 10 | |
| $\mu_M$ | Merozoite mortality rate | 48 per day | (McAlister, 1977) |
| Reaction norms and individual variation | | | |
| $\delta_p$ | *Dose-dependent reaction norm slope for parameter $p$ | $\mathcal{N}(0,2.5)$ | |
| $\sigma_{u,p}$ | *Individual deviation for intercept | $\mathcal{N}(0,1)$ | |
| $\sigma_{v,p}$ | *Individual deviation for slope | $\mathcal{N}(0,1)$ | |
| Measurement errors | | | |
| $\sigma_{\text{RBC}}$ | *Standard deviations for total RBC density | $\mathcal{N}(5\times10^5, 5\times10^5/10)$ | (Miller et al., 2010) |
| $\sigma_{\text{iRBC}}$ | *Standard deviations for $\log_{10}$ iRBC count | $\mathcal{N}(0.13, 0.13/10)$ | (Miller et al., 2010) |

distributions for these parameters are provided in Table 1.1 and further detailed in Appendix 1.6.2.

Instead of modelling each dose treatment as a discrete group (or a character state), we consider the entire range of the initial infection dose as an environmental gradient. In other words, we modelled each parameter of the dynamical model, $\theta_k$, as a reaction norm, which describes the pattern of phenotypic expression of an organism across an environmental gradient (Martin et al., 2011; Dingemanse and Dochtermann, 2013). The simplest and most commonly used reaction norm assumes a linear relationship between the environment and phenotype expression and consists of two components: the mean intercept, i.e., the phenotype expressed against the "average" environment, and the slope, i.e., the degree of phenotypic change along with the environment. We estimated the mean intercept, $\hat{\theta}_k$ (dose was centred so that the intercept is at the middle dose of $10^5$) and the mean slope of the reaction norms, $\hat{\delta}_k$.

Within each dose treatment, Timms et al. (2001) dataset contains repeated measures from replicate mice that showed marked individual variability (Fig. 1.1b & c). We sought to identify the source of this variability by explicitly modelling individual variation in $\theta_k$ among mice through partial pooling. This means that a given parameter was considered a sample from a common population distribution with a mean — in this case the intercept, $\hat{\theta}_k$, and the slope, $\hat{\delta}_k$ — and the deviation of the parameter from the mean for each individual, $i$, which we express as $u_{k,i}$ and $v_{k,i}$ for the intercept and slope variation, respectively. We assumed that the individual deviations, $u_{k,i}$ and $v_{k,i}$, are samples of a normal distribution with standard deviations, $\sigma_{u,k}$ and $\sigma_{v,k}$ that we estimated from data (Gelman, 2006).

Together, dose- and individual-specific parameter, $\theta_{k,i}$, is expressed as:

$$\theta_{k,i} = \hat{\theta}_k + u_{k,i} + (\hat{\delta}_k + v_{k,i}) \times Dose_i \tag{1.6}$$

where $Dose_i$ indicates the dose treatment applied to individual $i$. *Dose* was coded as $\{-3, -2, -1, 0, 1, 2, 3\}$ such that the intercept was centred at the initial infection dose of $10^5$. As is customary in quantitative genetics (Martin et al., 2011), we modelled a covariance structure describing the association among parameters in individual deviation following (Sorensen et al., 2016).

**MCMC sampling** Estimating the posterior probability density of parameters of a complex model requires a Markov Chain Monte Carlo (MCMC) sampling algorithm, which can be computationally intensive for large statistical models. Our model was written in Stan 2.18.2 and fitted through the RStan interface (Carpenter et al., 2017; Stan Development Team, 2019), which provides an efficient general-purpose MCMC sampler (No-U-Turn Hamiltonian Monte Carlo) and a Bayesian inference environment. The model was fitted in parallel in four independent chains, each with 4000 sampled iterations and 1000 warmup iterations. For diagnostics, we confirmed over 400 effective samples and ensured convergence of independent chains using the $\hat{R}$ metric (values below 1.1 are considered an indication of multi-chain convergence) for all parameters (Gelman et al., 2013; Stan Development Team, 2018).

**Likelihood** A Bayesian approach requires a likelihood function to assess the probability of observing the data given model parameters and associated predictions. Our log-likelihood function assumed that the measurement error for the total density of RBCs (i.e., sum of uRBCs and iRBCs), and iRBCs is distributed normally and $log_{10}$-normally, respectively (Mideo et al., 2008*b*, 2011):

$$\begin{aligned} \ln L \;=\; & \sum_{i}^{n_{\text{mice}}} \Bigg\{ \sum_{t}^{n_{\text{time}}} \ln\Bigg\{ \frac{1}{\sigma_{\text{RBC}}\sqrt{2\pi}} \exp\Bigg[ -\frac{(D_{i,t}^{\text{RBC}} - M_{i,t}^{\text{RBC}})^2}{2(\sigma_{\text{RBC}})^2} \Bigg] \Bigg\} \\ + \; & \sum_{t}^{n_{\text{time}}} \ln\Bigg\{ \frac{1}{\sigma_{\text{iRBC}}\sqrt{2\pi}} \exp\Bigg[ -\frac{(\log_{10}(D_{i,t}^{\text{iRBC}}+1) - \log_{10}(M_{i,t}^{\text{iRBC}}+1))^2}{2(\sigma_{\text{iRBC}})^2} \Bigg] \Bigg\} \Bigg\} \end{aligned} \tag{1.7}$$

where $D_{i,t}^{\text{RBC}}$ and $D_{i,t}^{\text{iRBC}}$ are the observed count of total RBCs and iRBCs, $M_{i,t}^{\text{RBC}}$ and $M_{i,t}^{\text{iRBC}}$ are the model predictions of total RBCs and iRBCs for individual $i$ at time $t$. We estimated standard deviations, $\sigma_{\text{RBC}}$ and $\sigma_{\text{iRBC}}$ for the total RBC and iRBC count, respectively, with specific informative priors based on (Mideo et al., 2008*b*, Table 1.1).

Our modelling focused on the first wave of infection before iRBCs recrudesce and adaptive immunity starts to take effect (Miller et al., 2010). Thus, $n_{\text{time}}$ was defined $\{16, 16, 13, 11, 11, 10, 8\}$ for the seven dose treatments, respectively, noting that higher doses lead to shorter time series because of the faster pace of infection (Fig. 1.1a). We further subsetted the dataset by removing instances of atypical dynamics (Appendix 1.6.3 for more details). In total, we fitted data from 51 individual mice ($n_{\text{mice}} = 51$).

## 1.4 Results and Discussion

Our fitted model accurately describes the daily time course of RBCs and iRBCs during the acute phase of malaria infection in mice, initiated at doses spanning seven orders of magnitude, from $10^2$ to $10^8$ iRBCs (Fig. 1.3; Appendix 1.6.4). We found evidence for dose-dependence in key parameters of host

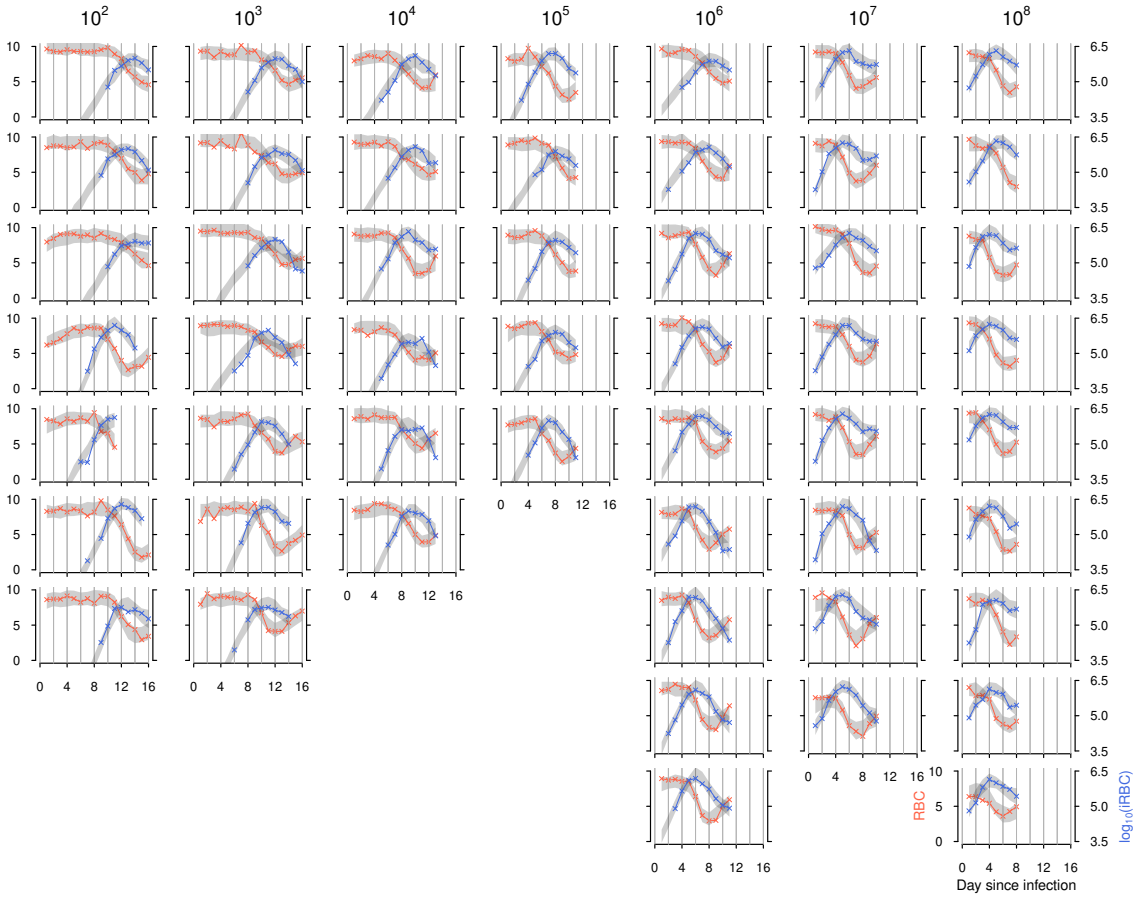


Figure 1.3: The fit of the full model (with parameters defined by Eq. 1.6) to the density of RBCs (orange) and iRBCs (blue) for individual mice inoculated at $10^2$, $10^3$, $10^4$, $10^5$ ,$10^6$, $10^7$ and $10^8$ infected cells. Each column corresponds to the initial infection dose given at the top. The crosses indicate data and grey bands correspond to 95% predictive intervals of the full model, incorporating uncertainty in parameter estimation and sampling.

responses underlying the dynamics of RBCs and iRBCs. Additionally, even under the highly controlled condition of Timms et al.'s experiment (Timms et al., 2001) — with the single strain combination of hosts (C57/BL6) and *P. chabaudi* parasites (CW) — we identified individual variation in host and parasite traits that influences the variation in infection outcomes independent of the dose treatment. Below, we closely examine the sources and impacts of dose-dependence and individual variation in different parameters of infection and initial conditions.

### 1.4.1 Dependence on the initial infection dose

We found evidence that increasing dose had two opposing effects on general RBC clearance. First, increasing dose reduces the activation strength of this response (Fig. 1.4a). The lower peak responses estimated for high doses (Fig. 1.5a) were attributable to a negative influence of the initial dose on the response activation strength (Fig. 1.4a), supporting the notion that higher infection doses enhance the parasites' ability to evade/suppress host responses and/or damage host machinery (Schmidt et al., 2014). In contrast, we found that dose facilitates the same response by inducing a longer action (Fig. 1.4b).

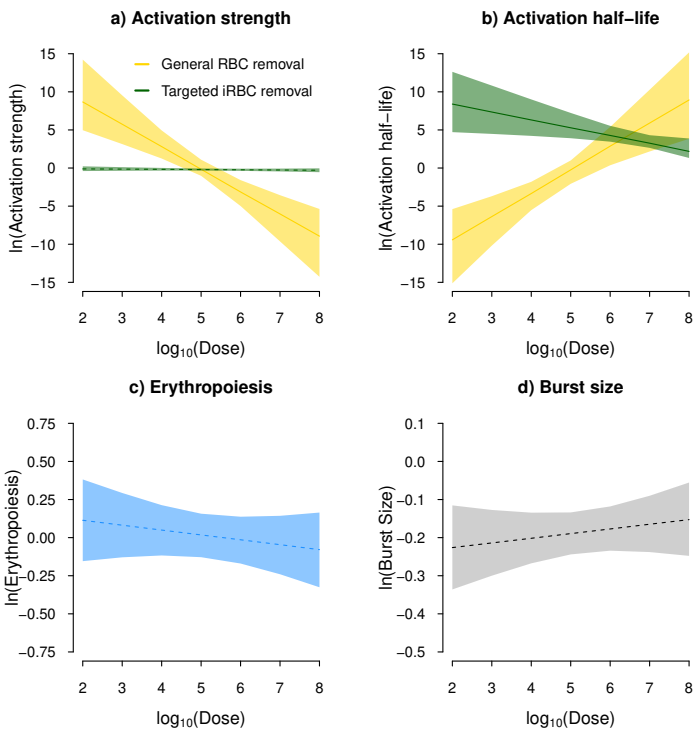


Figure 1.4: Dose dependence in some parameters of host responses, but not parasite traits. Plotted are the estimated relationship between the initial infection dose and a) the activation strength ($\psi_1$ and $\psi_2$), b) activity half-life ($\phi_1$ and $\phi_2$) of general RBC clearance (yellow) and targeted iRBC clearance (green), c) erythropoiesis upregulation, $\rho$, and d) parasite burst size, $\beta$. The line and band indicates the median prediction and 95% predictive intervals, respectively. The solid line indicates a statistically significant sign of dose-dependence (See Appendix 1.6.2 for the prior and posterior distributions).

The positive relationship between dose and activity half-life of these responses (Fig. 1.4b) explained the relatively low peak response at low doses (Fig. 1.5a). As a result of these two opposing effects of dose, the strongest host response in general RBC clearance was predicted at an intermediate dose, $10^5$ (white squares in Fig. 1.5a). This finding draws a comparison to another data-driving modelling work demonstrating that the maximum immune protection against influenza is generally achieved at an intermediate dose due to an interplay between innate and adaptive responses (Handel et al., 2018). Further studies in other disease systems are desired to probe the generality of the intermediate peak and understand diverse mechanisms that may generate this pattern.

Following the peak infection day, malaria parasites find themselves in a hostile within-host environment as over 70% of the iRBC population per day is cleared by host immunity targeting iRBCs (Fig. 1.5b). Combining targeted and indiscriminate responses, up to 80% of iRBCs were cleared per day by the host one to three days after the peak of infection (Fig. 1.5a). The activation of targeted iRBC clearance was estimated to be independent of the initial infection dose (Fig. 1.4a) while we found that the half-life of this response decreased with infection dose (Fig. 1.4b). This result is consistent with the faster waning of parasite clearance with dose observed by Metcalf et al. (2011) who speculate mechanisms including enhanced antigen escape, reduced immune memory due to low RBC availability, depleted immune effectors and downregulation by the host or parasites. Without this dose-dependent effect, our sensitivity analysis demonstrated that the peak targeted iRBC clearance would occur at high

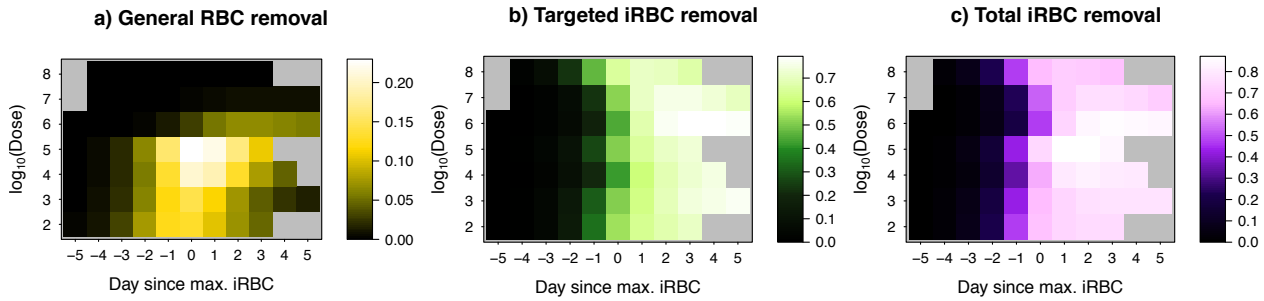


Figure 1.5: Host responses against malaria depend on the initial infection dose. Shown are the median predicted host responses (colour) as a function of time centred around the dose-dependent day of peak infection (x-axis) and the initial infection dose (y-axis) for a) general RBC clearance (i.e., proportion of RBCs, indiscriminately of their infection status, cleared by the host per day), b) targeted iRBC clearance (i.e., proportion of iRBCs cleared by the host per day), c) the total iRBC clearance (the sum of a and b). The grey region indicates that the model was not fitted for the day because either data do not exist or the day is beyond the first wave of infection.

doses, where higher iRBC density triggers an elevated response (Appendix 1.6.5).

To assess the relative importance of dose-dependence in the host responses, we examined the sensitivity of the model fit to whether host response parameters were dose-dependent (by setting $\theta_{k,i} = \hat{\theta}_k + u_{k,i}$, where $k = \{\psi_1, \phi_1\}$, $k = \{\psi_2, \phi_2\}$, for the two responses, respectively). We found that the dynamics of RBCs were most sensitive to dose-dependence in general RBC clearance: goodness of model fit declined by 2.6-fold and 3.4-fold, respectively, when dose-dependence in activation strength or activity half-life was ignored (Fig. 1.6). Interestingly, even though the targeted response clears more iRBCs than the general response (Fig. 1.5a & b), we found that iRBC dynamics were also overwhelmingly more sensitive to dose-dependence in general RBC clearance (Fig. 1.6): goodness of model fit declined by 3.6-fold and 7-fold, respectively, when dose-dependence in either activation strength or activity half-life (Fig. 1.6) was ignored. While the mechanism through which the host clears RBCs indiscriminately remains an open question, the functional importance of general clearance of RBCs is apparent from our work here and the work of others (Wale et al., 2019). Furthermore, the distinct patterns of dose-dependence we found (Fig. 1.4 a & b) suggest that there is separate host machinery for specifically clearing iRBCs and clearing RBCs indiscriminately.

Previously, dose-dependence in infection dynamics has been attributed to ineffective clearance of iRBCs at high doses due to handling time in innate immune effectors targeting iRBCs (Metcalf et al., 2011). Our findings offer an alternative explanation that dose promotes some aspects of some response while debilitating others. Of largest effects, we found that dose increases the half-life, but reduces activation strength, of general RBC clearance (Fig. 1.4 & 1.6). This finding likely reflects complex mechanisms through which the initial infection dose impacts different aspects of host response machinery (Schmidt et al., 2014; Chong et al., 2017; Hatta et al., 2010; Marois et al., 2012; Segueni et al., 2016; Pagan et al., 2016). Regardless of the mode of defence involved (i.e., indiscriminate or targeted iRBC clearance) and mechanisms (i.e., handling time, damage to host machinery, or immune evasion), the two distinct modelling frameworks demonstrate that malaria parasites are at an advantage at high initial infection dose due to less efficient host responses to clear iRBCs. We did not find significant evidence that upregulation in erythropoiesis or parasite burst size depends on the initial iRBC density (Fig. 1.4c & d). Therefore, our findings suggest that dose-dependent variation in infection dynamics observed

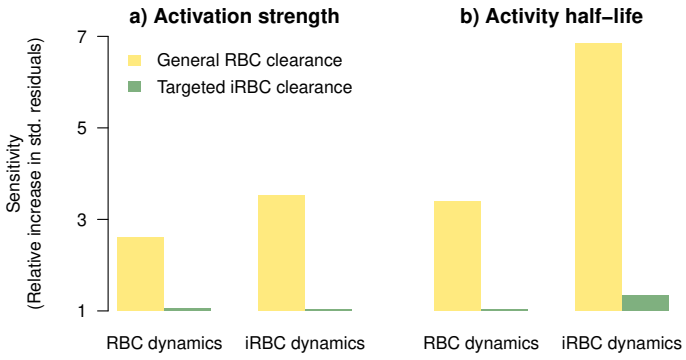


Figure 1.6: RBC and iRBC dynamics are most sensitive to dose-dependence in general RBC clearance. Plotted is the sensitivity of RBC and iRBC dynamics to dose-dependence of a) activation strength and b) activity half-life in general RBC clearance and targeted iRBC clearance (green), calculated as the sum of absolute standardised residuals (see Appendix 1.6.4 for details) relative to the full model (with parameters defined by Eq. 1.6).

across initial infection dose treatments in Timms et al. (2001) was driven by the interaction between the initial infection dose and host responses, but not plasticity in malaria parasites injected at different doses as predicted by Mideo et al. (2008*b*).

### 1.4.2 Individual variation

We explicitly modelled individual variation in each fitted parameter among the inbred mice using hyperparameters, $\sigma_{u,k}$ and $\sigma_{v,k}$. These sources of variation — analogous to subject-level random effects in regression analyses — capture unobserved heterogeneity among individuals in a sample, independent of the experimental manipulation in the initial infection dose. We found evidence of individual variation in every host and parasite parameter of the model describing malaria infection ecology (Fig. 1.7a; Appendix 1.6.2). There was no evidence of moderate or stronger correlation ($r > 0.3$) among individual variation in parameter values (Appendix 1.6.6), suggesting that there are no clear trade-offs nor facilitation among different arms of host responses.

To understand the functional importance of individual variation in estimated model parameters, as well as random variation in the reported initial RBC density, host weight, and initial infection dose, we computed the correlation coefficient, $r$, between individual variation and two key infection outcomes: parasite load (maximum iRBC density) and anaemia severity (minimum RBC density). We identified two individual-level correlates of the maximum iRBC density (Fig. 1.7b). First, we found that better suppression of the peak parasite load was associated with mice that activated the response to clear iRBCs more strongly than average through a targeted mechanism (Fig. 1.7b). While it is not clear what underlies this within-strain variation, our finding, nonetheless, demonstrates the functional importance of non-genetic heterogeneity in immune responses, drawing parallels to invertebrate systems in which intrinsic within-clone variation (e.g., differences in sizes at birth and molecular mechanisms of immune responses) are thought to impact susceptibility to infection (Dwyer et al., 1997; Watson et al., 2005; Ben-Ami et al., 2008). With the rodent malaria system, it may be possible to identify the mechanistic causal agents, for example, by characterising within-strain variation in immune effector expression prior

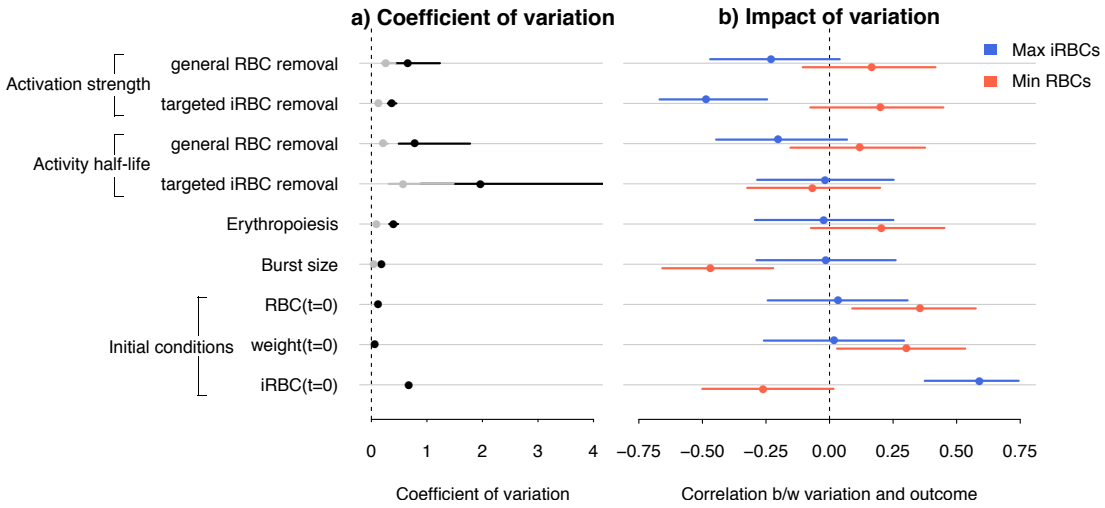


Figure 1.7: Individual variation in parameters of host responses and parasite growth impacts quantitative infection outcomes. a) Coefficient of variation among individuals in specific model parameters and initial conditions. Variation in the dose-independent (intercept) term, $\sigma_{u,k}$ and dose-dependent (slope) term $\sigma_{v,k}$. is indicated in black and grey, respectively. b) Correlation coefficients between individual-level estimates of parameters or initial conditions, and the infection outcome measured as the maximum and minimum densities of iRBCs (blue) and RBCs (red), respectively. The error bars indicate the 95% confidence interval. Statistical significance is indicated when the confidence interval does not intersect 0 (dashed line).

to and throughout the course of infection. We also found that variation in the initial infection dose within dose treatments correlated positively with the peak parasite load (Fig. 1.7b). In the context of Timms et al. (2001)'s experiments, variation in the initial infection dose may be attributable, for example, to random experimental variability in sampling by a syringe and in the parasites' ability to reach blood vessels following intraperitoneal injection. While neither of these sources of random variation are relevant outside the lab, the observation that higher doses — both among and within dose treatments — increase parasite burden (Timms et al., 2001, Fig. 1.1 & 1.7b) highlights the need to better understand causes of variation in pre-blood-stage parasite densities in natural malaria infections, both within and among *Plasmodium* species (Paul et al., 2003). One such source of variation is pre-blood-stage host immunity that develops in response to exposure to the parasite stage injected by mosquitoes (sporozoites) and has been shown effective in reducing the number of liver-stage parasites from which blood-stage merozoites originate (Nahrendorf et al., 2015).

There were also three significant individual-level correlates of anaemia severity (Fig. 1.7b). First, we found a significant negative effect of burst size meaning that infections initiated with a parasite population that happens to proliferate and exhaust RBCs faster than average caused more severe anaemia (Fig. 1.7b). In addition, mice that were heavier or had more RBCs before infection suffered less severe anaemia (Fig. 1.7), suggesting that general host vigour in the absence of infection is an indicator of host health under malaria infection. Because these measurements of host vigour did not correlate with the peak parasite load, host vigour can be interpreted as an indicator of tolerance (i.e., a host's ability to minimise anaemia), rather than a resistance (i.e., a host's ability to minimise parasite burden) mechanism (Schneider and Ayres, 2008).

In general, we found that the magnitude of individual variation, estimated here as the coefficient of

variation, did not coincide with whether or not a particular trait impacted an infection outcome. For example, we estimated large individual-level variation in the half-life of host response for targeted clearance of iRBCs (Fig. 1.7a), yet infection outcomes were insensitive to this variation (Fig. 1.7b). Conversely, we detected a small coefficient of variation in burst size (Fig. 1.7a), but this small variation showed a marked impact on the severity of anaemia (Fig. 1.7b). The misalignment between the magnitude and impact of individual variation poses a challenge from a clinical perspective because it is not clear whether those parameters can be estimated with sufficient precision from patient data. Finally, despite the fact that the dynamics of RBCs and iRBCs are ecologically coupled (i.e., malaria parasites are consumers of RBCs), we found that the impact of individual variation on anaemia severity was not coupled to that of parasite load. These findings indicate that resistance and tolerance are likely uncorrelated at the individual level in the rodent malaria system.

## 1.5 Conclusion

We examined drivers of dose-dependent malaria parasite load and the severity of malaria-induced anaemia. We also shed light on the role of unobserved heterogeneity in producing diverse infection outcomes, identifying sources of subtle variation beneath an experimental treatment. More often than not, infection experiments are structured in multiple levels of sampling units (e.g., host, parasite genotypes, presence of coinfection, and drug treatments) with many replicates within treatment groups. Observations from such experiments contain multiple sources of variation whose effects on infection outcomes are difficult to disentangle directly. Our study demonstrates that the combination of dynamical within-host model and a Bayesian approach is a powerful tool for causal inference of infection outcome variation.

## 1.6 Appendices

### 1.6.1 Estimation of the initial infection dose in individual mice

We estimated the initial infection dose for each mouse using two methods. First, assuming that the initial parasite growth rate is near-exponential (for the first three days of observations), we estimated the initial infection dose per microliter of blood in each mouse as the intercept of a linear regression model with the natural logarithm of iRBCs as the response and the time since infection as a predictor. We extrapolated this estimate to the initial injected dose using the information about the individual mouse weight reported by Timms et al. (2001) and assuming that there is 95 ml of blood per kg of a female mouse (Riches et al., 1973, Fig. 1.8a; blue circles). Alternatively, we estimated the initial infection dose simultaneously with the rest of the model parameters using a Bayesian approach detailed in the main text (95% predictive band of which is shown in grey; Fig. 1.8a). We found that the two methods converge and both estimate higher than reported injected doses at low doses (Fig. 1.8a). Crucially, the rank order of the reported infection dose was preserved in our estimates (Fig. 1.8a).

We explored the possibility that the regression method was affected differently among dose treatments by dose-dependent iRBC clearance at an early stage of infection. We did not find evidence that the estimated slopes in the regression method were affected by the initial infection dose (Fig. 1.8b). Thus, it is unlikely that our estimates of the initial infection dose were biased differently among dose treatments by early host immunity.

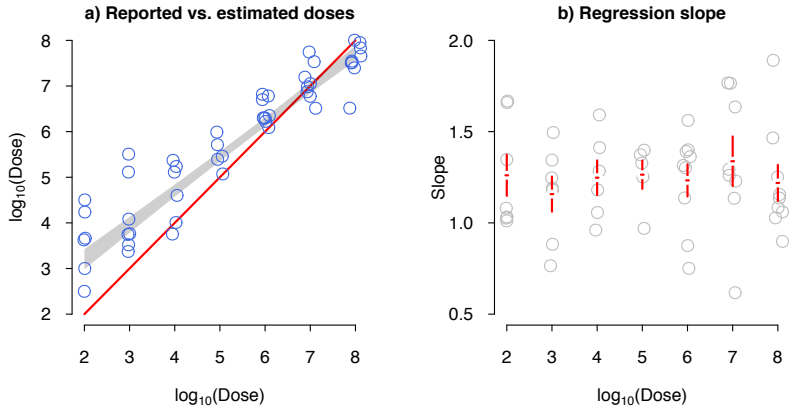


Figure 1.8: a) The reported and estimated initial infection dose. The blue circles represent the individual-level estimate of the initial infection dose using the regression method and the grey band represents the 95% predictive band when the initial infection dose was estimated simultaneously with the rest of the model parameters. The reported initial infection dose is shown in red. b) The slope in a linear regression model with the natural logarithm of iRBCs per mouse as the response and the time since infection as a predictor. The red bars indicate 95% confidence intervals.

### 1.6.2 Graphical summary of prior and posterior distributions

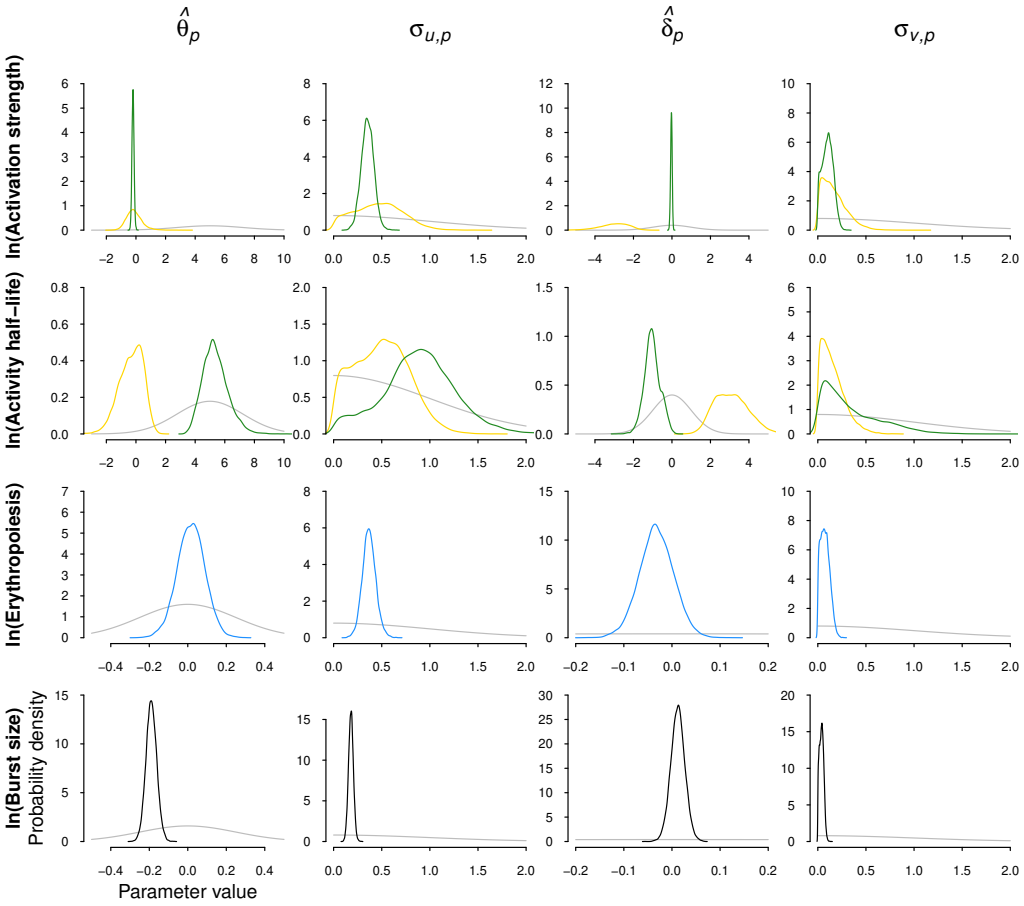


Figure 1.9: Graphical summary of prior (grey) and posterior distributions. Erythropoiesis, general RBC clearance and targeted RBC clearance are represented by blue, yellow and green, respectively. The mathematical descriptions of prior distributions are provided in Table 1.1 in the main text.

### 1.6.3 Mice excluded from model fitting

Table 1.2: List of mice in Timms et al. (2001) excluded from model fitting and the rational for exclusion.

| Dose | Block | Mouse | Rational |
|---|---|---|---|
| $10^2$ | 1 | 1 | Infection peaks orders of magnitude lower than the rest. |
| $10^2$ | 1 | 5 | Infection does not peak during the fitted time scale. |
| $10^2$ | 2 | 3 | Infection never takes off. |
| $10^3$ | 1 | 5 | Infection peaks occurs five days later than the average. |
| $10^3$ | 2 | 3 | Infection does not peak during the fitted time scale. |
| $10^3$ | 2 | 5 | Infection never takes off. |
| $10^4$ | 1 | 1 | Infection never takes off. |
| $10^4$ | 1 | 4 | Infection peaks two days later than average. |
| $10^4$ | 2 | 1 | Infection peaks orders of magnitude lower than the rest. |
| $10^4$ | 2 | 2 | RBC density crashes on day 1 for an unknown reason. |
| $10^7$ | 2 | 2 | Infection peaks two days later than the average. |
| $10^8$ | 2 | 1 | RBC density crashes on day 1 for an unknown reason. |

### 1.6.4 Assessment of model fit: standardised residuals

To provide a rigorous assessment of the model fit, we examined the standardised residuals for RBC and iRBC densities following Miller et al (Miller et al., 2010). By integrating over the probability density of each parameter, $\Phi$, the marginal standardised residual of each data point $i$ was defined as:

$$r_{x,i} = \frac{1}{\sigma_x} \int_{\Phi} (x_{data,i} - x_{model,i}(\Phi)) d\Phi \tag{1.8}$$

where $\sigma_x$ is standard deviation of $x$, which is either RBC or iRBC density. The fit of the full model (the parameters of which are defined by Eq. 1.6) to RBC and iRBC density was accurate without a significant sign of bias (Fig. 2.7).

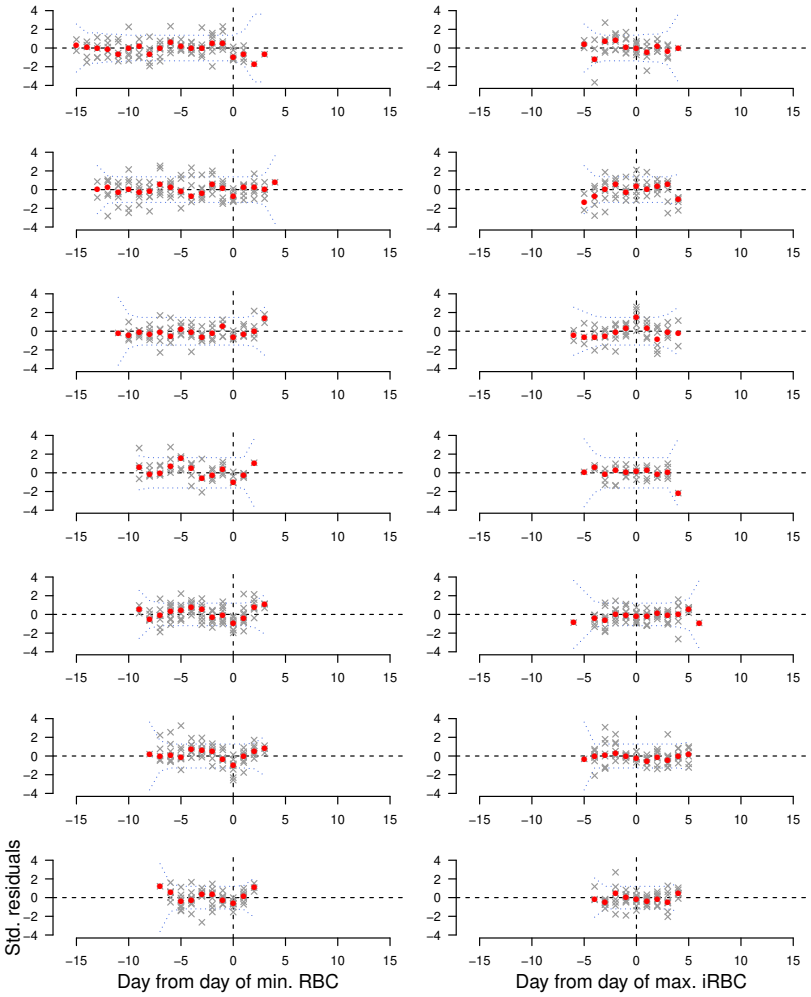


Figure 1.10: a) Standardised model residuals of the full model (with parameters defined by Eq. 1.6 in the main text). Poor fits are indicated by the mean residuals deviating from confidence intervals. Blue dotted lines indicated the Bonferroni-corrected 95% intervals.

### 1.6.5 Sensitivity of targeted iRBC clearance to dose-dependent half-life

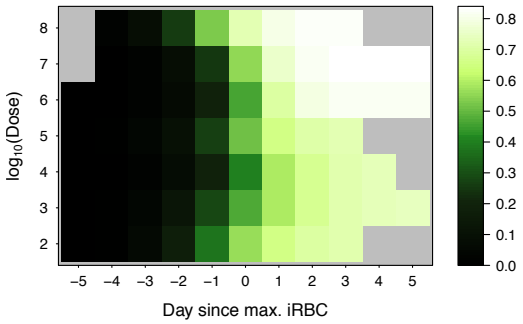


Figure 1.11: The peak targeted iRBC clearance would increase with dose if activity half-life of this response was independent of the initial infection dose. The colour shows the median predicted targeted iRBC clearance (i.e., proportion of iRBCs cleared by the host per day) as a function of time centred around the day of peak infection (x-axis) and the initial infection dose (y-axis). The grey region indicates days beyond model fitting: our model was designed for and fitted to acute dynamics.

### 1.6.6 Correlations among individual variation

We estimated a correlation matrix between parameters at the individual level using an LKJ prior with a shape parameter, $\eta = 5.0$. For further details of concepts and implementation of correlation matrices in Stan models (Stan Development Team, 2019), we refer the readers to Sorensen et al. (Sorensen et al., 2016). We found no moderate ($> 0.3$) or strong ($> 0.5$) correlations indicating that there is little sign of trade-offs or facilitation among parameters of host responses.

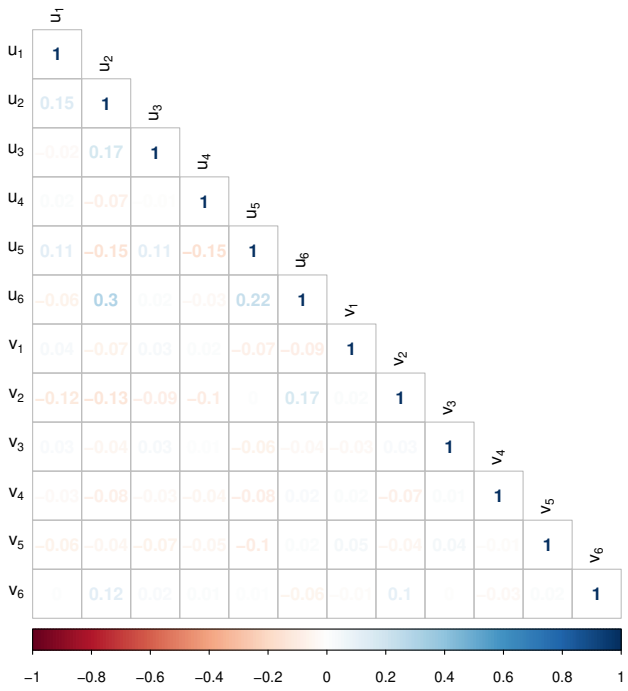


Figure 1.12: Pairwise correlations of individual-level parameter deviations. The indexing (i.e., 1 to 6) refers to the position of the parameter set, $\theta \ni \{\psi_1, \psi_2, \phi_1, \phi_2, \rho, \beta\}$, and $u$ and $v$ indicate the intercept and slope variation, respectively.

# Chapter 2

# Understanding functional diversity of host resilience to malaria infection

This work was carried out in collaboration with Nicole Davis (equal contribution, Stanford University), Megan Greischar (University of Toronto), David Schneider (Stanford University) and Nicole Mideo (University of Toronto).

## 2.1 Abstract

Infection outcomes range widely from sub-clinical to fatal in human malaria. By fitting a mathematical model of within-host malaria infection to experimental infection data from eight inbred mouse strains, we aimed to identify aspects of within-host ecological interactions that explain variation in host resilience to malaria infection. Among the eight mouse strains that collectively span 90% of the common genetic diversity of laboratory mice, we demonstrated that well-regulated immune responses are the primary functional motif correlated with survival from malaria infections, more so than than differences in red blood cell production or interactions between parasites and red blood cells. Our model also identified two dichotomous mechanisms of host mortality. For most non-resilient strains, we found evidence for weak activation of host responses that specifically target infected cells. Alternatively, one non-resilient strain showed the strongest tendency to trigger a response that clears red blood cells indiscriminately. We carried out cross-sectional assays of pro- (TNF-$\alpha$ and IFN-$\gamma$) and anti-inflammatory (IL-10 and TGF-$\beta$) cytokines to corroborate that highly resilient strains exhibit balanced cytokine expressions, indicative of well-regulated immune responses. In contrast, mouse strains that succumb to infection showed either little signs of inflammation or imbalanced expression with relative few anti-inflammatory cytokines to maintain a healthy balance. Our work highlights the power of combining a dynamical within-host infection model with a hierarchical Bayesian approach to uncover functional mechanisms governing within-host dynamics and infection outcomes. By validating our model predictions with cytokine data, the present study narrows the gap between mechanistic knowledge of molecular and cellular immunity and clinically relevant infection phenotypes.

## 2.2 Introduction

In human malaria, infection outcomes range widely from sub-clinical to fatal. While it is difficult to disentangle the factors contributing to this variation in resilience to malaria, host genetics is a major determinant (Hernandez-Valladares et al., 2005; López et al., 2010; Hedrick, 2011). In experimental rodent malaria infections, where environment, diet, and as many other factors as possible are highly controlled, different mouse strains infected with the same strain of *Plasmodium chabaudi* demonstrate remarkable variation in infection dynamics and malaria mortality. Among eight strains of inbred laboratory mice (129S1/SvImJ, A/J, C57BL/6, CAST/EiJ, NOD/ShiLtJ, NZO/HILtJ, PWK/PhJ, WSB/EiJ) that collectively span 90% of the mouse genetic diversity commonly used in laboratory experiments (Roberts et al., 2007), survival from malaria infection ranges from 5 to 100% (Fig. 2.1). Underlying this survival variation is likely differences in functional properties of within-host ecology (i.e., parasite growth, immune responses, and replenishment of RBCs), which are difficult to measure directly. However, longitudinal measurements of host health and parasite burden can inform processes of within-host ecology (i.e., red blood cells (RBCs) and infected red blood cells (iRBCs), respectively, in malaria infections). For example, a "disease curve" — longitudinal data of health and parasites plotted against each other in a phase plane — helps visualise the process of parasite growth, host sickness and recovery at the individual host level (Fig. 2.2) (Schneider, 2011). Furthermore, a mathematical model fitted to these data can identify particular functional mechanisms (e.g., parasite proliferation (Mideo et al., 2011), specific versus non-specific immunity (Wale et al., 2019) and dose-dependent host responses (Chapter 1)) that lead to divergent infection dynamics (Mideo et al., 2008*c*). Here, we employ a model-fitting approach

to explore the diversity of functional mechanisms among mouse strains that impact resilience to malaria infection.

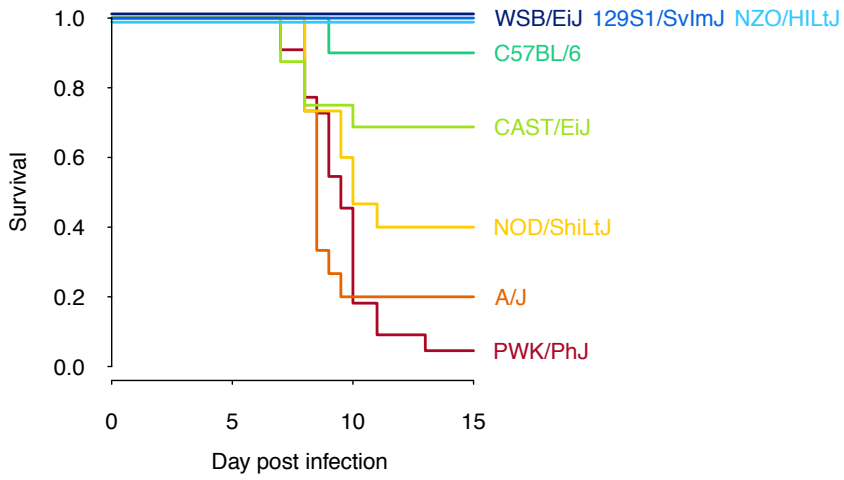


Figure 2.1: Proportion of mice surviving over the course of infections initiated with $10^5$ *P. chabaudi* AJ parasites. Eight mouse strains are shown (with total sample sizes given by in brackets): WSB/EiJ (30), 129S1/SvImJ (10), NZO/HILtJ (10), C57BL/6 (10), CAST/EiJ (16), NOD/ShiLtJ (15), A/J (15), and PWK/PhJ (22). The dataset is a compilation of three experiments (Davis et al. unpublished a, Davis et al. unpublished b and Gupta et al. unpublished). The lines for WSB/EiJ, 129S1/SvImJ and NZO/HILtJ are jittered as 100% of mice of each strains survived for 15 days.

The immune system is one critical proximate mechanism of host genetic resilience to infection (López et al., 2010). Failure to mount a robust immune response can lead to unchecked parasite proliferation while dysregulated responses may cause collateral damage, i.e., immunopathology. While the benefit of immune protection often outweighs any costs associated with these responses (Sorci et al., 2017), severe outcomes of many infectious diseases are a consequence of immunopathology rather than direct damage caused by parasites (Graham et al., 2005). Thus, a "healthy" immune response requires striking a delicate balance.

During the acute phase of blood-stage malaria infection, innate responses target and remove iRBCs as well as short-living extracellular parasites known as merozoites (Stevenson and Riley, 2004). In addition, RBCs — regardless of infection status — are also susceptible to clearance by immune effectors such as macrophages (Jakeman et al., 1999; Chua et al., 2013). While the targeted response removes more iRBCs, data-driven modelling studies highlight the importance of indiscriminate RBC clearance for lowering parasite burden (Miller et al., 2010; Metcalf et al., 2012; Wale et al., 2019, Chapter 1). Functionally, this self-destruction of RBCs can have both favourable and unfavourable consequences for host health. On the one hand, it has been proposed as a host adaptation in the presence of malaria parasites to clear the parasites directly (i.e., top-down effect) as well as to limit resources for the parasite (i.e., bottom-up effect, Haydon et al., 2003; Cromer et al., 2009; Metcalf et al., 2012; Wale et al., 2019). On the other hand, an excessive loss of RBCs brings forth adverse health implications. In immune naive infants and children, severe malarial anaemia is the most common severe manifestation of disease and its associated mortality rate can reach 30% (Perkins et al., 2011). Malaria-related anaemia is caused by a variety of processes including loss due to parasite exploitation, RBC clearance (e.g., phagocytosis of both infected and uninfected cells), suppression of RBC production, and defective RBC development

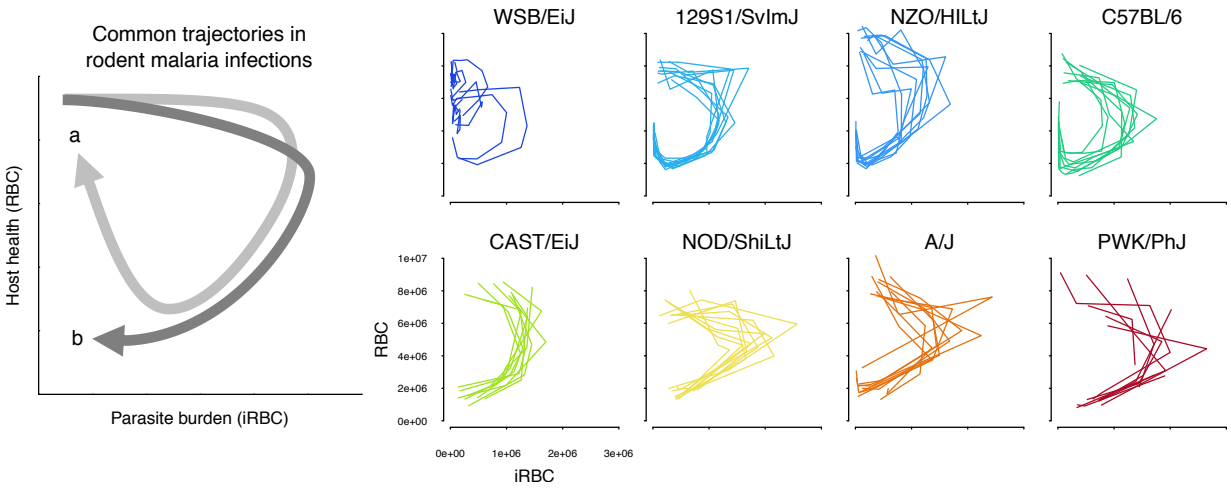


Figure 2.2: Longitudinal data of infection contain features of within-host ecology that influence infection outcomes. In a phase plot bound by parasite burden and host health (i.e., disease space, *sensu* Schneider, 2011; Torres et al., 2016), infection progresses clockwise from the top-left corner (i.e., many RBCs, few iRBCs). Left panel illustrates common trajectories. Following a rapid parasite growth phase (x-axis), host health deteriorates (y-axis) during acute malaria infection. In the meantime, the parasite density starts to decline due to resource limitation and/or upregulated immunity. If a host is resilient, the trajectory tends towards the starting healthy state as parasites further decline and RBCs get replenished (path a, light grey). In contrast, the damage to host health may be irreparable in non-resilient hosts (path b, dark grey, Schneider, 2011). The small, coloured plots show the empirically-observed trajectories of the first wave of malaria infection in 80 mice across eight strains in disease space, with the densities of iRBCs and RBCs on the x- and y-axis, respectively. Generally speaking, highly resilient strains (WSB/EiJ, 129S1/SvImJ, NZO/HlLtJ, C57BL/6) follow path a and poorly resilient strains (CAST/EiJ, NOD/ShiLtJ, A/J, PWK/PhJ) follow path b.

(Chua et al., 2013). Among them, clearance is the most significant process as between 75% and 90% of the total RBC deficit during malaria infections has been attributed to it (Jakeman et al., 1999). In comparison, direct exploitation by malaria parasites has been estimated to account for less than 10% of the RBC deficit (Jakeman et al., 1999; Price et al., 2001; Fonseca et al., 2016).

At the molecular level, vertebrate host responses are regulated by immune signalling molecules, known as cytokines (Lamb et al., 2006). Acute malaria infection induces pro-inflammatory cytokines required for mounting a timely and robust response while anti-inflammatory cytokines inhibit excess immune reactions to safeguard against collateral damage (Lamb et al., 2006). For instance, tumour necrosis factor alpha (TNF-$\alpha$) and interferon gamma (IFN-$\gamma$), are pro-inflammatory cytokines responsible for a myriad of inflammatory responses including production of nitric oxide and reactive oxygen species (Bouharoun-Tayoun et al., 1995; Bogdan et al., 2000), which are associated with rapid clearance of *Plasmodium falciparum*, the deadliest human malaria parasite (Rockett et al., 1992; Kremsner et al., 1995; Mordmüller et al., 1997; Hernandez-Valladares et al., 2006; Franklin et al., 2007). However, the same inflammatory responses can also be damaging to the organisms that produce them (Clark et al., 1991; King and Lamb, 2015). For example, TNF-$\alpha$ overproduction — which can result from a deficit of anti-inflammatory cytokines like interleukin 10 (IL-10) and transforming growth factor beta (TGF-$\beta$) — could lead to adverse effects including worsened anaemia, weight loss and survival in the mouse model (Omer and Riley, 1998; Li et al., 2003; Long et al., 2006, 2008). Therefore, differences in cytokine

expression are likely to contribute to variation in survival from malaria infection.

To uncover the functional mechanisms underlying malaria survival and variation thereof, we formulated a mathematical model of the within-host malaria ecology that describes the asexual replicative cycle and qualitatively distinct components of host immunity. Rather than aiming for a mechanistically precise description of host immunity, we designed a model to track the net effects of host responses, i.e., clearance rate of iRBCs and RBCs. By fitting the model to longitudinal data of RBCs and iRBCs from eight mouse strains with varied resilience to malaria, we identified functional diversity of host responses, including insufficient and dysregulated responses associated with elevated mortality risk. We then compared our model predictions to pro- and anti-inflammatory cytokine expression data. We corroborated the association between host resilience and robust and well-balanced expression of pro- and anti-inflammatory cytokines. On the contrary, we found that both low pro-inflammatory cytokine expression and unbalanced regulation (high pro- and low anti-inflammatory cytokines) were associated with poor host survival.

## 2.3 Methods

### 2.3.1 Data

#### Infection experiment

Mice were purchased from Jackson Laboratories (WSB/EiJ stock #001145), 129S1/SvImJ stock #002448, NZO/HILtJ stock #002105, CAST/EiJ stock #000928, A/J stock #000646, NOD/ ShiLtJ stock #001976, and PWK/PhJ stock #003715) and Charles River (C57BL/6). A subset of mice (WSB/EiJ, NZO/HILtJ, and PWK/PhJ) were also bred in-house at Stanford University.

We administered the AJ strain of *Plasmodium chabaudi* to the experimental animals at a dose of $10^5$ iRBCs and monitored infections longitudinally, for 15 days, as previously described (Torres et al., 2016). RBCs were quantified using a BD Accuri C6 Plus cytometer. We quantified parasitemia (i.e., proportion of RBCs infected) via thin blood smears and manual microscope counting. We then calculated the number of iRBCs per microliter of blood, which was calculated by multiplying parasitemia by the number of total RBCs per microliter of blood.

From a compilation of experiments (Davis et al. unpublished a, Davis et al. unpublished b and Gupta et al. unpublished), we recorded that three strains (129S1/SvImJ, NZO/HILtJ and WSB/EiJ) were fully resilient to the *P. chabaudi* AJ strain injected at $10^5$, meaning we did not observe mortality for 15 days following infection. Other strains, C57BL/6, CAST/EiJ, NOD/ShiLtJ, A/J and PWK/PhJ exhibited 90%, 69%, 40%, 20%, and 5% survival by day 15 post-infection, respectively.

#### Cross-sectional cytokine assay

In a separate experiment focused on collecting cytokine data, we initiated infections under the same condition in each of the eight mouse strains. For cross-sectional sampling, between three and five infected mice of each strain were euthanised each day from days 3-12 post-infection. For each mouse strain, two uninfected control animals were euthanised at baseline and generally on odd-numbered days. Following euthanasia, 75 microliters of plasma was used for immunoassay using the mouse 38-plex kit (eBiosciences/Affymetrix).

### 2.3.2 Model

**Dynamical model of malaria asexual cycle**

Blood-stage malaria infection begins when extracellular merozoites, which are initially released from the liver, invade an RBC. Following invasion, *P. chabaudi* parasites develop within RBCs for approximately 24 hours. Synchronously at midnight, iRBCs rupture, releasing a new generation of merozoites into the bloodstream (Paul et al., 2003). These merozoites then rapidly invade further RBCs and the cycle continues. We assumed that regulation of immune responses takes place continuously throughout the day ($0 < t \leq 1$ where $t$ is the fraction of a day) and demographic processes of the host and parasite (i.e., turnover of RBCs, iRBC bursting and RBC invasion by merozoites) happen at the end of each day at midnight ($t = 1$).

**Regulation of host responses** Malaria infection triggers a variety of host responses (Stevenson and Riley, 2004; Price et al., 2001; Castro-Gomes et al., 2014), of which we considered two previously identified as most quantitatively important: indiscriminate clearance of RBCs and targeted clearance of iRBC (Miller et al., 2010). We formulated a set of ordinary differential equations to track the change in the activity of each response $N_i$, where $i$ indicates the response identity (general RBC clearance, $i = 1$; targeted iRBC clearance, $i = 2$):

$$\frac{dN_i(t)}{dt} = \psi_{N_i} \frac{I}{I_{max}} - \phi_{N_i} N_i(t), \tag{2.1}$$

where $\psi_{N_i}$ and $\phi_{N_i}$ are the activation and decay strength of $N_i$, respectively. We defined $N_1$ and $N_2$ as the rate of RBC and iRBC clearance, respectively. Assuming that the abundance of iRBCs reflects that of pathogen-associated molecular patterns (PAMPs), we considered the scaled density of iRBCs, $\frac{I}{I_{max}}$, as the within-host cue driving these responses, where $I_{max}$ is the maximum observed iRBC density in the experiment. We assumed that there is no activity in the absence of infection, consequently assuming that there is no constitutive immunity. Because demographic events are formulated in discrete time with a unit of one day, the iRBC density, $I$, is assumed a constant during the time scale of immune regulation (i.e., $0 < t \leq 1$); thus $I = I_{(t=0)}$. After substituting $\psi_{N_i} \frac{I}{I_{max}}$ and $\phi_{N_i}$ with constants $a_i$ and $b_i$, respectively, we solved Eq. 2.1 as an initial value problem to obtain the solution, $N_i$ at time $t$:

$$N_i(t) = \frac{e^{-b_i t}(a_i(e^{b_i t} - 1) + b_i N_{i(t=0)})}{b_i} \tag{2.2}$$

**Turnover of RBCs** The first event at the end of the day ($t = 1$), is clearance and replenishment of RBCs. In the absence of infection, we assumed that RBCs are subjected to background RBC mortality, $\mu_R$. The host replaces RBCs lost to baseline cell mortality by producing $R_c(1 - e^{-\mu_R})$ new RBCs, where $R_c$ is the RBC density at homeostatic equilibrium, assumed equal to the RBC density measured per mouse before parasite administration (i.e., $\text{RBC}_{(t=0)}$). While we have strong prior information on baseline mortality and replenishment in the absence of infection (i.e., $\mu_R$; Van Putten and Croon, 1958; Foster et al., 2014), we fitted two new parameters ($\mu'_R$ and $\mu''_R$, respectively) that allow these processes to be qualitatively different during infection. Our motivation for this was the following. First, during malaria infection experiments, RBCs are lost to daily blood sampling and perhaps handling related stress. Second, fitting $\mu'_R$ allows for the possibility that some indiscriminate clearance of RBCs is independent of iRBC dynamics (unlike in equation 2.2). Third, there is evidence that erythropoiesis is downregulated

during malaria infection (Wale et al., 2019), and fitting $\mu''_R$ allowed us to capture this possibility.

Indiscriminate RBC clearance, due to the action of the immune response, occurs at a daily rate $N_{1(t=1)}$. In addition to baseline replenishment of RBCs (governed by $\mu''_R$ as described above), RBCs are produced in a density-dependent manner during infection to restore the RBC population (Chang et al., 2004) with a time-lag of two to three days before the newly produced RBCs are released in the bloodstream (Savill et al., 2009). Here assuming a two-day lag (indicated by $d-2$), the host produces a fraction $\rho$ of the deviation from RBC density at $R_c$. Infected cells incur an additional rate of mortality, $N_{2(t=1)}$ through targeted killing. Together, the turnover of RBCs is expressed as:

$$R_{(t=1)} = R_{(t=0)}\, e^{-(\mu'_R + N_{1(t=1)})} + R_c(1 - e^{-\mu''_R}) + \rho(R_c - (R_{(d-2)} + I_{(d-2)})) \quad (2.3)$$

$$I_{(t=1)} = I_{(t=0)}\, e^{-(\mu'_R + N_{1(t=1)} + N_{2(t=1)})}. \quad (2.4)$$

where $R_{(t=1)}$ and $I_{(t=1)}$ are the post-turnover densities.

**iRBC bursting** Given synchronous iRBC bursting and the short lifespan of merozoites relative to the length of a day, we modelled iRBC bursting and merozoite invasion as instantaneous events. As iRBCs rupture and release merozoites into the bloodstream at midnight (t=1), the density of merozoites, $M$ equals $\beta\, I_{(t=1)}$ where $\beta$ is the parasite burst size per iRBC.

**RBC invasion by merozoites** Upon release, a merozoite either invades an uninfected red blood cell (uRBC), $R_{(t=1)}$, at rate $p\, R_{(t=1)}$ where $p$ is the per capita merozoite invasion rate, or it gets cleared before invasion, with a short halflife of $1/\mu_M$ ($\sim$ 30 minutes (McAlister, 1977)). For simplicity, we ignore infections of RBCs by multiple merozoites. Thus, the probability that a given merozoite successfully invades an uRBC is:

$$\frac{p\, R_{(t=1)}}{p\, R_{(t=1)} + \mu_M}. \quad (2.5)$$

Multiplying the probability by the density of merozoites, and dividing by $R_{(t=1)}$, the average number of invading merozoites per uRBC, $\lambda$ is:

$$\lambda = \frac{M}{R_{(t=1)} + \omega}. \quad (2.6)$$

where $\omega = \frac{\mu_M}{p}$. Since the parameters $\mu_M$ and $p$ are mutually non-identifiable, we instead estimated $\omega$, the ratio of merozoite mortality to invasion rate. We assumed that the probability of RBC invasion by merozoites is Poisson-distributed with parameter $\lambda$, i.e., Prob(invasion by $k$ mezoroites) $= \frac{\lambda^k\, e^{-\lambda}}{k!}$ (Miller et al., 2010; Mideo et al., 2011). Thus, the probability that a given uRBC gets invaded by a merozoite (i.e., $k = 1$) is $\lambda\, e^{-\lambda}$ and the probability that an uRBC escapes merozoite invasion altogether (i.e., $k = 0$) is $e^{-\lambda}$. Ignoring infections of RBCs by multiple merozoites, it follows that the numbers of uRBCs and iRBCs after merozoite invasion (i.e., $R^*_{(t=1)}$ and $I^*_{(t=1)}$ with the asterisk denoting the post-invasion densities) are:

$$R^*_{(t=1)} = R_{(t=1)}\, e^{-\lambda} \quad (2.7)$$

$$I^*_{(t=1)} = R_{(t=1)} \lambda\, e^{-\lambda}. \quad (2.8)$$

Table 2.1: Description of model parameters and their fixed values, or prior distributions used in Bayesian statistical inference. Where parameters were estimated (indicated by an asterisk on the description), we assigned a generic, weakly informative prior for immune parameters ($\psi_{N_1}$, $\psi_{N_2}$, $\phi_{N_1}$ and $\phi_{N_2}$) and informative priors for the rest based on specific prior information from previous studies.

| Symbol | Description | Fixed value or prior | Source |
|---|---|---|---|
| Host responses | | | |
| $\rho$ | *Proportion of deviation from $R_c$ restored per day | $0.25 \times \exp(\mathcal{N}(0, 0.25))$ | (Miller et al., 2010) |
| $\psi_{N_1}$ | *Activation strength of indiscriminate RBC clearance | $\exp(\mathcal{N}(ln(1) + 2.5, \sqrt{2.5})$ | |
| $\psi_{N_2}$ | *Activation strength of targeted RBC clearance | $\exp(\mathcal{N}(ln(1) + 2.5, \sqrt{2.5})$ | |
| $\phi_{N_1}$ | *Daily decay rate of indiscriminate RBC clearance | $\exp(\mathcal{N}(ln(1) + 2.5, \sqrt{2.5})$ | |
| $\phi_{N_2}$ | *Daily decay rate of targeted RBC clearance | $\exp(\mathcal{N}(ln(1) + 2.5, \sqrt{2.5})$ | |
| Within-host infection dynamics | | | |
| $R_c$ | RBC density at homeostatic equilibrium | $\text{RBC}_{(t=0)}$ | data |
| $I_{\max}$ | Maximum iRBC density observed | $2.65 \times 10^6$ per microliter | data |
| $\mu_R$ | Daily background RBC mortality rate | 0.025 | (Miller et al., 2010) |
| $\mu'_R$ | *Daily background RBC mortality rate (during infection) | $0.025 \times \exp(\mathcal{N}(0, 0.25))$ | (Miller et al., 2010) |
| $\mu''_R$ | *Density-independent RBC replenishment rate (during infection) | $0.025 \times \exp(\mathcal{N}(0, 0.25))$ | (Miller et al., 2010) |
| $\beta$ | *Parasite burst size | $7 \times \exp(\mathcal{N}(0, 0.25))$ | (Miller et al., 2010) |
| $p$ | Merozoite invasion rate | $1.5 \times 10^{-5}$ per day | (Mideo et al., 2011) |
| $\mu_M$ | Merozoite mortality rate | 48 per day | (McAlister, 1977) |
| $\omega$ | *Ratio of merozoite mortality to invasion rate | $\frac{\mu_M}{p} \times \exp(\mathcal{N}(0, 0.25))$ | |
| Measurement errors | | | |
| $\sigma_{\text{RBC}}$ | *Standard deviations for total RBC density | $\mathcal{N}(5 \times 10^5, 5 \times 10^5/10)$ | (Miller et al., 2010) |
| $\sigma_{\text{iRBC}}$ | *Standard deviations for $\log_{10}$ iRBC count | $\mathcal{N}(0.2, 0.2/10)$ | (Mideo et al., 2008*b*) |

### 2.3.3 Bayesian hierarchical inference

We fitted the above within-host infection model to the corresponding longitudinal data of 80 mice using a Bayesian statistical approach, which allows for parameter estimation in high dimensional spaces, for example, in hierarchical models where observations are organised in multiple levels of sampling units (Mugglin et al., 2002; Cressie et al., 2009). In this study, there are two levels of sampling units: mouse strains and subjects (i.e., individual mice).

**Strain-specific and individual variation** We estimated host strain- and individual-specific effects ($s$ and $u$, respectively) in a set of nine fitted parameters describing within-host ecological processes. Below, we collectively refer to the parameter set as $\theta$ ($\theta \ni \mu'_R, \mu''_R, \rho, \psi_{N_1}, \psi_{N_2}, \phi_{N_1}, \phi_{N_2}$, $\beta$, $\omega$). The prior distributions for these parameters are provided in Table 2.1.

**Likelihood** A Bayesian approach requires a likelihood function to assess the probability of observing the data given model parameters and associated predictions. Our log-likelihood function assumed that the measurement error for the total density of RBCs (i.e., sum of uRBCs and iRBCs), and iRBCs is distributed normally and $\log_{10}$-normally, respectively (Mideo et al., 2008*b*, 2011):

$$\begin{aligned} \ln L \;=\; & \sum_{i}^{n_{\text{mice}}} \left\{ \sum_{d}^{n_{\text{days}}} \ln\left\{ \frac{1}{\sigma_{\text{RBC}}\sqrt{2\pi}} exp\left[ -\frac{(D_{i,d}^{\text{RBC}} - M_{i,d}^{\text{RBC}})^2}{2(\sigma_{\text{RBC}})^2} \right] \right\} \right. \\ + \; & \left. \sum_{d}^{n_{\text{days}}} \ln\left\{ \frac{1}{\sigma_{\text{iRBC}}\sqrt{2\pi}} exp\left[ -\frac{(\log_{10}(D_{i,d}^{\text{iRBC}} + 1) - \log_{10}(M_{i,d}^{\text{iRBC}} + 1))^2}{2(\sigma_{\text{iRBC}})^2} \right] \right\} \right\} \end{aligned} \tag{2.9}$$

where $D_{i,d}^{\text{RBC}}$ and $D_{i,d}^{\text{iRBC}}$ are the observed count of total RBCs and iRBCs, $M_{i,d}^{\text{RBC}}$ and $M_{i,d}^{\text{iRBC}}$ are the model predictions of total RBCs and iRBCs for individual $i$ at day $d$. We estimated standard deviations, $\sigma_{\text{RBC}}$ and $\sigma_{\text{iRBC}}$ for the total RBC and iRBC count, respectively, with specific informative priors (Mideo et al., 2008*b*; Miller et al., 2010) (Table 2.1). Our modelling focused on the first wave of infection, thus we fitted data up to two weeks post-infection ($n_{\text{days}} = 14$ at maximum). In mice that succumbed to infection, we fitted the model to data until the last sampling prior to death.

**MCMC sampling** Estimating the posterior probability density of parameters of a complex model requires a Markov Chain Monte Carlo (MCMC) sampling algorithm, which can be computationally intensive for large hierarchical models. Our model was written in Stan 2.18.2 and fitted through the RStan interface (Carpenter et al., 2017; Stan Development Team, 2019), which provides an efficient, general-purpose MCMC sampler (No-U-Turn Hamiltonian Monte Carlo) and a Bayesian inference environment. The model was fitted in parallel in four independent chains, each with 5000 sampled iterations and 5000 warmup iterations. For diagnostics, we confirmed over 400 effective samples and ensured convergence of independent chains using the $\hat{R}$ metric (values below 1.1 are considered an indication of multi-chain convergence) for all parameters (Gelman et al., 2013; Stan Development Team, 2018).

## 2.4 Results and Discussion

### 2.4.1 Functional mechanisms underlying resilience to malaria

Our fitted model accurately described the time-course of RBCs and iRBCs during the acute phase of malaria infection in all mouse strains (Appendix 2.6.1), indicating that our model represents a useful abstraction of the true within-host malaria ecology. Several estimated model parameters varied with mouse strains (Fig. 2.3). To characterise these multivariate, ecological differences, we carried out principal component analysis (PCA) on the estimated parameter set, $\theta$. We found several clusters that distinguished mouse strains revealing functional diversity of host resilience to malaria infection (Fig. 2.4).

First, we identified C57BL/6 (90% survival; Fig. 2.1) as the most "functionally average" of the eight strains, indicated by the most central position in the PCA biplot (Fig. 2.4a) and near-zero estimates for strain-specificity, $s$ (Fig. 2.3a). Two fully resilient (100% survival) strains, 129S1/SvImJ and NZO/HILtJ, were functionally similar to C57BL/6, but these strains showed a slower decay of host responses (lower $\phi_{N_1}$ and $\phi_{N_2}$) and smaller parasite burst sizes, $\beta$ (Fig. 2.3). These differences suggest that 129S1/SvImJ and NZO/HILtJ are subtly better able to resist malaria infection than C57BL/6, agreeing with the slightly better survival outcome (Fig. 2.1). Overall, we found larger strain-specific variability, $s$ in the rates of activation (i.e., $\psi_{N1}$ and $\psi_{N2}$) than decay of responses (i.e., $\phi_{N1}$ and $\phi_{N2}$) (Fig. 2.3a), suggesting that immunogenic differences between strains is largely due to differences in the speed and strength with which responses are turned on, rather than how long those responses last.

In addition to having the highest propensity to activate targeted clearance of iRBCs (highest $\psi_{N_2}$), WSB/Eij, another fully resilient strain, demonstrated the smallest $\beta$, meaning that the same malaria parasite infecting this host strain produced the fewest merozoites per iRBC (Fig. 2.3). Previous studies have demonstrated variation in the number of merozoites released per iRBC (i.e., parasite burst size, $\beta$) and the ratio of merozoite mortality to invasion rate (i.e., $\omega$) across parasite strains (Miller et al., 2010; Mideo et al., 2011; Santhanam et al., 2014). As $\beta$ was more variable than $\omega$ among host strains (Fig.

2.3a), the host's contribution to variation in parasite proliferation is likely mediated through differences in the number of merozoite released per iRBC, rather than merozoite clearance or invasion of new RBCs. To our knowledge, however, little is documented on the host's contribution to iRBC bursting. One host factor that could affect parasite burst size is intrinsic differences in RBC properties among mouse strains. For example, the flow cytometry marker, TER119, standard for counting mouse RBCs, works poorly with WSB/Eij, hinting at a possible difference in RBC surface proteins (personal observation). In addition, WSB/Eij showed the highest capacity to increase background RBC mortality, $\mu_R'$, and downregulate constant background RBC replenishment during infection, $\mu_R''$, both of which contribute to limiting parasite growth through lowered resource availability. Consistent with this reduced RBC replenishment is the fact that WSB/Eij is known to have an elevated level of the von Willebrand factor (VWF) (Shavit et al., 2009): VWF deficiency has been linked to increased production of young RBCs (Kraisin et al., 2019). Overall, WSB/Eij excelled in every facet of resilience against (at least the AJ strain of) *P. chabaudi* and maintained relatively low iRBC densities (Fig. 2.2). Infection resilience in this mouse strain may generalize to other malaria parasites, including *P. berghei* (Bopp et al., 2010), yet interestingly these mice are highly vulnerable to *Salmonella* infections (Zhang et al., 2019).

Three less resilient strains (CAST/EiJ, NOD/ShiLtJ and PWK/PhJ) clustered together in the PCA biplot (Fig. 2.4a), indicating that these strains are functionally similar to each other. In comparison to the "functionally average" C57BL/6, these strains that succumb more easily to infection (69%, 40% and 5% survival to day 15, respectively, Fig. 2.1) were estimated to more weakly trigger immune responses, both targeted (lower $\psi_{N_2}$) and indiscriminate (lower $\psi_{N_1}$) (Fig. 2.3, Fig. 2.4a). A closer inspection with a subset PCA analysis (Fig. 2.4b) revealed that better survival among these three strains was associated with higher activation of targeted iRBC clearance (higher $\psi_{N_2}$) and lower activation of general RBC clearance (lower $\psi_{N_1}$), distinguishing between moderately poor surviving strains (CAST/EiJ and NOD/ShiLtJ; 69% and 40% survival, respectively) from an extremely fragile strain (PWK/PhJ; 5% survival) along PC2 (Fig. 2.4b). The contrasting impacts of targeted and general responses hint at a possible harmful effect of general RBC clearance under some circumstances. Specifically, our results suggest that indiscriminate clearance of RBCs may be deleterious without sufficient activation of targeted mechanisms to suppress the parasite population.

Finally, the A/J mouse strain showed the strongest activation of general RBC clearance (highest $\psi_{N_1}$; 2.3b). Given the poor resilience of these mice (20% survival; Fig. 2.1), the general RBC clearance is likely mostly deleterious, at least in this strain of mice. Taken together, while the host potentially stands to benefit from destroying RBCs by removing some iRBCs and taking the resource away from malaria parasites, this "scorched-earth tactic" (Wale et al., 2019) could remove healthy RBCs in excess and trigger severe anaemia that causes host mortality. The significant role of indiscriminate RBC clearance on severe anaemia is empirically supported by a study that demonstrated a high turnover of transfused RBCs in BALB/c mice infected with *P. berghei* (Evans et al., 2006). The clearance was likely immune-mediated as severe anaemia was alleviated by depletion of immune cells (Evans et al., 2006). Another study observed lower young RBC (i.e., reticulocyte) counts in A/J mice and postulated that these mice are defective in the production of new RBCs during malaria infection (Chang et al., 2004). However, their observation is also consistent with our model prediction that the A/J host excessively clears RBCs because indiscriminate RBC clearance is another mechanism that would reduce the reticulocyte density.

The potentially negative impact of RBC clearance highlights vital implications for clinical interventions against malaria. First, blood transfusion or erythropoietin (EPO) injection to treat severe anaemia

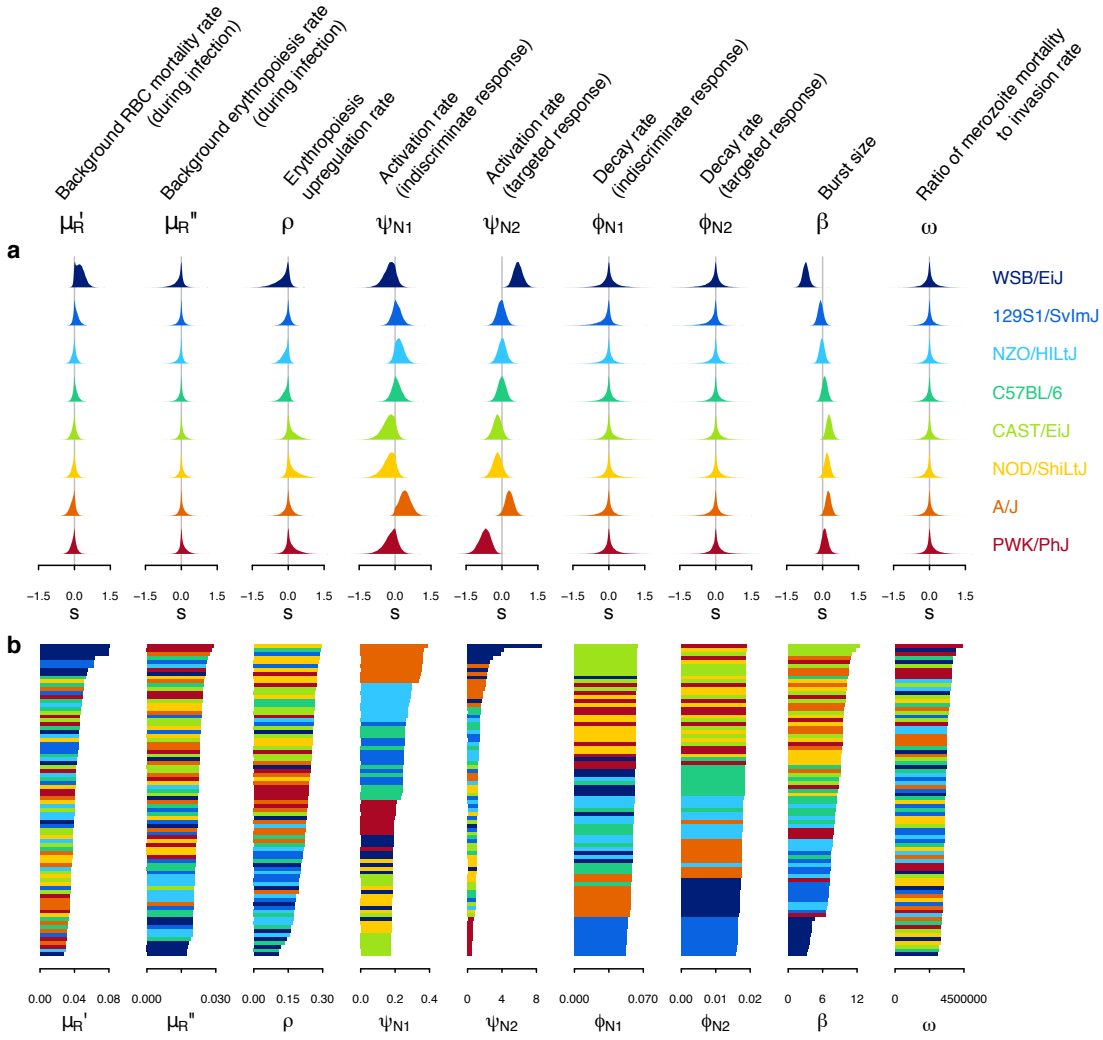


Figure 2.3: Differences in within-host ecology parameters reveal functional diversity linked to resilience to malaria infection. a) Strain-specific variation, $s$, in each parameter of the set $\theta \ni (\mu_R', \mu_R'', \rho, \psi_{N_1}, \psi_{N_2}, \phi_{N_1}, \phi_{N_2}, \beta, \omega)$. The eight strains are ordered according to survival percentage from the top (see Fig. 2.1). The average parameter value across the eight strains is indicated by $s = 0$. b) Ordered parameter stacks show functional similarities and differences between individual mice of different strains (indicated by colours). Each slice of a stack represents the median estimate for an individual mouse.

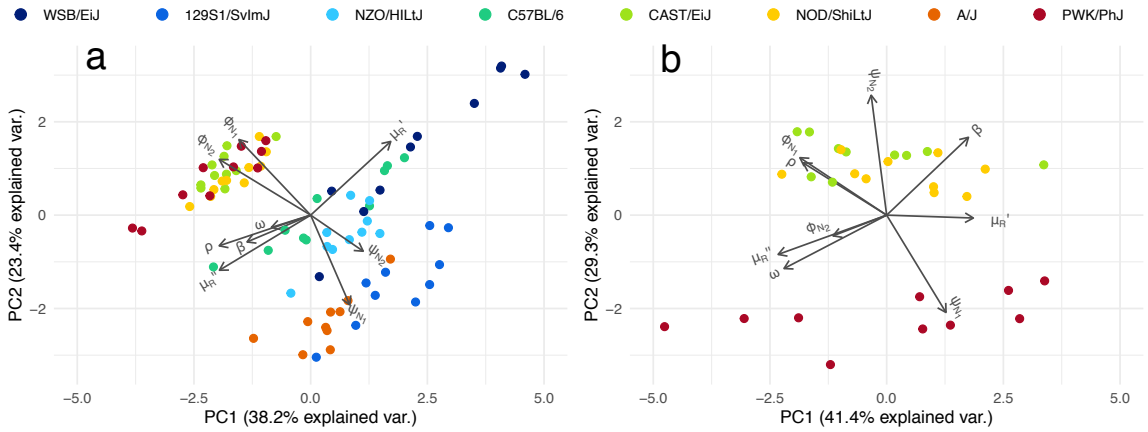


Figure 2.4: Within-host ecological parameters differentiate mouse strains with varying degrees of resilience to malaria infection. The PCA biplots display the relationship between individual mice in the first two principal components, which collectively account for 61.6% (panel a) and 70.7% (panel b) of the total variance in parameters describing within-host malaria ecology, $\theta \ni (\mu'_R, \mu''_R, \rho, \psi_{N_1}, \psi_{N_2}, \phi_{N_1}, \phi_{N_2}, \beta, \omega)$. The direction and length of the grey arrows indicate the contribution of each parameter to the principal components. a) A full dataset with 80 mice from eight strains and b) a subset of poorly resilient mouse strains (CAST/EiJ, NOD/ShiLtJ and PWK/PhJ; 69%, 40% and 5% survival, respectively) that cluster together in panel a, thus are functionally similar to each other. Parameter descriptions are found in Table 1.

may be most effective against patients that are particularly prone to indiscriminate RBC clearance. In fact, timely EPO injection alleviates anaemia and improves survival in A/J mice (Chang et al., 2004). However, the same treatment may be less effective against other poorly resilient strains (CAST/EiJ, NOD/ShiLtJ and PWK/PhJ) whose mortality is attributed to insufficient immune responses (Fig. 2.3, Fig. 2.4). Second, the potentially pathological consequence of indiscriminate RBC clearance should be considered during the development of a blood-stage malaria vaccine. It is pertinent to ensure that vaccine-triggered immunity that helps clear malaria parasites also avoid immunopathology, including severe anaemia. Therefore, a better understanding of signalling pathways that trigger general RBC clearance is desired. In summary, model predicted that mouse strains with immune activation that was too weak (in CAST/EiJ, NOD/ShiLtJ and PWK/PhJ) or too strong (in A/J) was associated with high host mortality. Thus, the host's ability to maintain a healthy balance between protection and immunopathology is likely a major determinant of host survival.

### 2.4.2 Cytokine assay supports model predictions

Pro- and anti-inflammatory cytokines play a pivotal role in regulating immune responses. Notably, pro-inflammatory cytokines such as TNF-$\alpha$ and IFN-$\gamma$ impact malaria parasite clearance, while anti-inflammatory cytokines like IL-10 and TGF-$\beta$ are crucial for regulating immune responses (Artavanis-Tsakonas et al., 2003). We assayed the expression patterns of these four cytokines throughout the course of infection to compare between host strains (Fig. 2.5).

First, the model predicted that the highly resilient mouse strains 129S1/SvImJ, NZO/HILtJ and to a large extent C57BL/6, activate the targeted response more strongly. This prediction is in agreement with the higher expression of pro-inflammatory cytokines in these strains (Fig. 2.5), in comparison to

two of the lesser resilient strains (CAST/EiJ and PWK/PhJ) for which we predicted weak immune responses (Fig. 2.3 and 2.4). Importantly, in the three strains that show higher survival (129S1/SvImJ, NZO/HILtJ, and C57BL/6), the robust expression of TNF-$\alpha$ and IFN-$\gamma$ was counterbalanced by equally robust expression of IL-10 and TGF-$\beta$, which inhibits overproduction of immune effectors (Artavanis-Tsakonas et al., 2003). It is worth noting that in these highly resilient strains, the balanced cytokine expression was reached early (by day 3 to 5), and observed even in the absence of infection (especially in 129S1/SvIm). In contrast, the less resilient NOD/ShiLtJ strain achieved a similarly balanced cytokine expression, but not until later in infections. In fact, the balance is observed only on day 8 or 9, while individuals of this strain typically succumb to infection by day 10. Thus, these responses may have been too late for controlling parasites effectively.

In less resilient CAST/EiJ and PWK/PhJ, which were estimated to weakly activate responses (Fig. 2.3), we observed a reduction in the expression of anti-inflammatory cytokines during infection (black; Fig. 2.5) compared to the baseline (pink; Fig. 2.5). Since excess TGF-$\beta$ hinders parasite clearance through oversuppression of pro-inflammatory cytokines (Tsutsui and Kamiyama, 1999), lowering anti-inflammatory pathways could potentially be beneficial. However, our results demonstrated that reducing the expression of anti-inflammatory cytokines alone does not boost pro-inflammatory pathways (Fig. 2.5), nor does it facilitate adequate parasite clearance.

We found clear signs of pro-inflammatory bias in the cytokine expressions of NOD/ShiLtJ and A/J (Fig. 2.5), both of which are poorly resilient at 40 and 20% survival, respectively (Fig. 2.1). In these strains, we observed elevated expression of pro-inflammatory cytokines (TNF-$\alpha$ and IFN-$\gamma$) during infection without a corresponding change in anti-inflammatory responses, as was observed for better-surviving strains (Fig. 2.5). For the A/J mice, our model predicted strong immune responses, both indiscriminate and targeted (high $\psi_{N_1}$ and $\psi_{N_2}$; Fig. 2.3), matching the expectation that a pro-inflammatory bias leads to robust anti-parasite responses (King and Lamb, 2015). However, immunoregulatory imbalance is also associated with immunopathology during malaria infections (King and Lamb, 2015). In particular, overproduction of immune effectors could cause collateral host tissue damage and excessive indiscriminate RBC clearance may lead to severe anaemia. In contrast to the A/J strain, our model predicted NOD/ShiLtJ mice to trigger weaker than average indiscriminate and targeted responses (low $\psi_{N_1}$ and $\psi_{N_2}$; Fig. 2.3). This is despite the relatively strong expression of pro-inflammatory cytokines (Fig. 2.5). Thus, our model prediction and cytokine assay together indicate that inflammatory responses at the molecular level somehow failed to translate functionally to protection against malaria infection. This is likely due to immunodeficiencies downstream of pro-inflammatory cytokines: e.g., NOD mice show severely reduced natural killer cell activity (Kataoka et al., 1983), defective development of macrophages (Serreze et al., 1993) and antigen-presenting dendritic cells (Pearson et al., 2003).

We observed low expression of both pro- and anti-inflammatory cytokines in WSB/Eij (Fig. 2.5), for which our model predicted exceptional parasite control (through small parasite burst size and high parasite clearance, low $\beta$ and high $\psi_{N_2}$) and resource suppression (heightened RBC mortality and lowered erythropoiesis; high $\mu_R'$ and low $\mu_R''$) (Fig. 2.3 & 2.4). One interpretation is that mechanisms other than inflammation are responsible for this strain's resilience. This notion is supported by the relatively low baseline cytokine expressions, compared to other resilient strains such as 129S1/SvImJ, NZO/HILtJ, and C57BL/6 (Fig. 2.5). It is also possible that the effective, rapid parasite control in WSB/Eij means that iRBC density (Fig. 2.2) and hence the cue for triggering cytokine production remains low.

Overall, our cytokine assay confirm that that host resilience to malaria infection is linked to a balanced

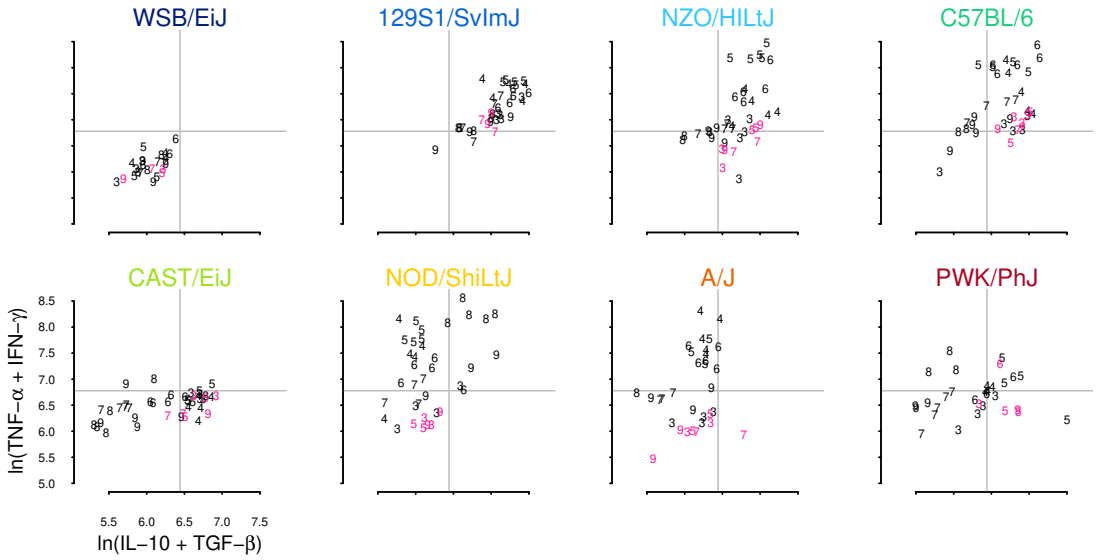


Figure 2.5: Eight mouse strains show distinct expression patterns of pro- (TNF-$\alpha$ and IFN-$\gamma$) and anti-inflammatory cytokines (IL-10 and TGF-$\beta$) that correspond to our model prediction that the balance between immune protection and immunopathology impacts survival during malaria infection. The grey lines represent the median expression value across available data for the respective cytokine pair. The day post-infection is indicated by the numbers. The pink and black numbers indicate control and infected mice, respectively. Shown are additive expressions (i.e., TNF-$\alpha$ + IFN-$\gamma$ and IL-10 + TGF-$\beta$), but multiplicative expression patterns (i.e., TNF-$\alpha \times$ IFN-$\gamma$ and IL-10 $\times$ TGF-$\beta$) were qualitatively identical (results not shown).

expression of pro- and anti-inflammatory cytokines, corroborating the importance of balanced immune responses predicted by the mathematical model. Poorly resilient strains either showed stunted activation of pro-inflammatory cytokines associated with insufficient parasite control, or pro-inflammatory bias that has been implicated in immunopathology (Artavanis-Tsakonas et al., 2003).

## 2.5 Conclusion

Immune responses are a key host factor influencing protection from malaria infections (López et al., 2010). However, it is difficult to relate health outcomes to the underlying variation in host immunity because parasite load, immune regulation and host health are intertwined and are variable over time. In other words, infections present complex and dynamic systems that demand rigorous quantitative investigations. Also, the highly dimensional nature of immune systems demands quantitative mapping of what is empirically measurable (e.g., immune molecules and cells) to what is functionally relevant to infection dynamics (e.g., net effect of parasite clearance). Over the past two decades, several dynamical models have inferred mechanisms of complex within-host ecological interactions from longitudinal data of parasite load and host health in the rodent malaria system (e.g. (Haydon et al., 2003; Mideo et al., 2008*b*; Miller et al., 2010; Kochin et al., 2010; Mideo et al., 2011; Santhanam et al., 2014; Wale et al., 2019)). However, it remained difficult to apply the knowledge of molecular and cellular immunity to predict clinically relevant infection phenotypes, in part because few models that quantitatively described infection dynamics incorporated (semi-)mechanistic immune regulation (but see Chapter 1).

By combining, dynamical modelling of infection and immunity with cross-sectional cytokine assays in a rodent malaria system, the present study demonstrated that robust, and well-regulated immune responses — more so than differences in RBC production or parasite-RBC interactions — are the primary functional motif of inbred mouse strains that survive malaria infections. The next progression in mechanistic modelling of within-host ecology may be to incorporate explicit molecular mechanisms and interactions that have been implicit in current modelling studies of malaria infection. In so doing, empirical measurements of molecular and cellular components may be used directly for outcome prediction.

## 2.6 Appendix

### 2.6.1 Assessment of model fit

Our fitted model accurately describes the daily time course of RBCs and iRBCs during the acute phase of malaria infection in mice (Fig. 2.6).

To provide a rigorous assessment of the model fit, we examined the standardised residuals for RBC and iRBC densities following Miller et al. (2010). By integrating over the probability density of each parameter, $\Phi$, the marginal standardised residual of each data point $i$ was defined as:

$$r_{x,i} = \frac{1}{\sigma_x} \int_{\Phi} (x_{data,i} - x_{model,i}(\Phi)) d\Phi \tag{2.10}$$

where $\sigma_x$ is standard deviation of $x$, which is either RBC or iRBC density. The fit of the dynamical model to RBC and iRBC density was accurate without a significant sign of bias (Fig. 2.7).


Figure 2.6: The fit of the dynamical model to the density of RBCs (red) and iRBCs (blue). Each column corresponds to a mouse strain. The crosses indicate data and grey bands correspond to 95% predictive intervals of the model, incorporating uncertainty in parameter estimation and sampling.

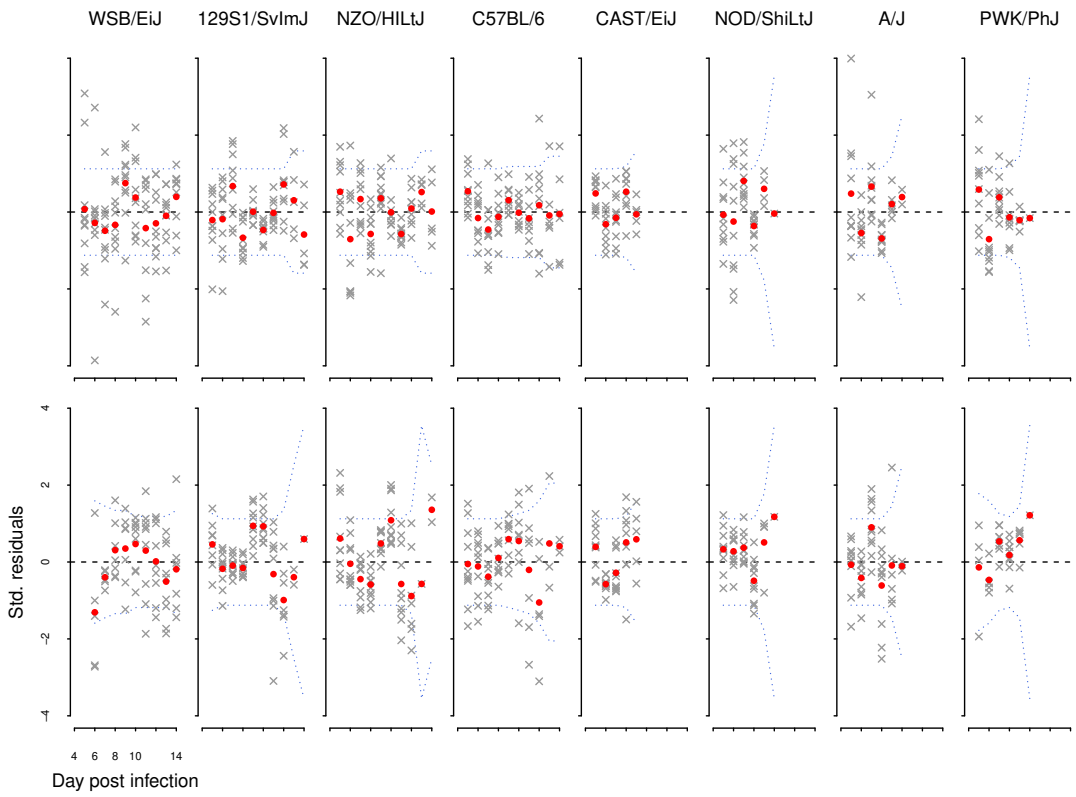


Figure 2.7: Standardised model residuals of the dynamical model. Poor fits are indicated by the mean residuals deviating from confidence intervals. Blue dotted lines indicated the Bonferroni-corrected 95% intervals.

# Chapter 3

# Epidemiological consequences of immune sensitisation by pre-exposure to vector saliva.

This work was carried out in collaboration with Megan Greischar (University of Toronto) and Nicole Mideo (University of Toronto).

Contents of this chapter have been published in Kamiya et al.,. Epidemiological consequences of immune sensitisation by pre-exposure to vector saliva. *PLOS Neglected Tropical Diseases*. 2017, 11 (10), e0005956.

## 3.1 Abstract

Blood-feeding arthropods — like mosquitoes, sand flies, and ticks — transmit many diseases that impose serious public health and economic burdens. When a blood-feeding arthropod bites a mammal, it injects saliva containing immunogenic compounds that facilitate feeding. Evidence from *Leishmania*, *Plasmodium* and arboviral infections suggests that the immune responses elicited by pre-exposure to arthropod saliva can alter disease progression if the host later becomes infected. Such pre-sensitisation of host immunity has been reported to both exacerbate and limit infection symptoms, depending on the system in question, with potential implications for recovery. To explore if and how immune pre-sensitisation alters the effects of vector control, we develop a general model of vector-borne disease. We show that the abundance of pre-sensitised infected hosts should increase when control efforts moderately increase vector mortality rates. If immune pre-sensitisation leads to more rapid clearance of infection, increasing vector mortality rates may achieve greater than expected disease control. However, when immune pre-sensitisation prolongs the duration of infection, e.g., through mildly symptomatic cases for which treatment is unlikely to be sought, vector control can actually increase the total number of infected hosts. The rising case burden may go unnoticed unless active surveillance methods are used to detect such sub-clinical individuals, who could provide long-lasting reservoirs for transmission and suffer long-term health consequences of those sub-clinical infections. Sensitivity analysis suggests that these negative consequences could be mitigated through integrated vector management. While the effect of saliva pre-exposure on acute symptoms is well-studied for leishmaniasis, the immunological and clinical consequences are largely uncharted for other vector-parasite-host combinations. We find a large range of plausible epidemiological outcomes, positive and negative for public health, underscoring the need to quantify how immune pre-sensitisation modulates recovery and transmission rates in vector-borne diseases.

## 3.2 Introduction

When a mammal is bitten by a blood feeding arthropod, it is injected with vasodilatory and immunomodulatory compounds in the arthropod's saliva that facilitate feeding (Charlab et al., 1999; Ribeiro and Francischetti, 2003; Oliveira et al., 2013*a*; Chagas et al., 2014). The mammalian host is not a passive recipient in this interaction, but rather mounts a variety of immune responses (Gomes and Oliveira, 2012). Local immune responses to an arthropod bite include inflammation, production of anti-salivary protein antibody and recruitment of immune cells to the skin. These same arthropods can be vectors of important parasites and a recent focus of research has been elucidating the influence of salivary proteins on transmission of a wide array of diseases, including those caused by protozoan parasites such as *Plasmodium* and *Leishmania* and arboviruses such as dengue and West Nile virus (Titus and Ribeiro, 1988; Schneider et al., 2004; Brodie et al., 2007; Kebaier et al., 2010; Gomes and Oliveira, 2012; Machain-Williams et al., 2013). In a majority of lab experiments, parasites that are co-inoculated with vector saliva or salivary proteins show higher infection success than when parasites are injected alone (Ockenfels et al., 2014; Pingen et al., 2017). Co-inoculation can benefit parasite establishment through saliva proteins that modulate host immune responses (e.g., downregulating particularly harmful pathways or upregulating pathways that will inhibit parasite-specific responses) and can lead to the recruitment of immune cells that those parasites exploit for replication (Schneider et al., 2004; Brodie et al., 2007;

Gomes and Oliveira, 2012; Pingen et al., 2017).

In contrast, immune responses elicited by the bite of an uninfected vector appear to have diverse effects on the outcome of disease manifestation if a host later becomes infected. In *Leishmania*, from which the majority of empirical evidence is available, experimental rodent infections have demonstrated that prior exposure to sand fly saliva partially protects against the symptoms of a subsequent infection (Belkaid et al., 1998; Kamhawi et al., 2000; Thiakaki et al., 2005; Ahmed et al., 2010; Gomes et al., 2012). A recent meta-analysis found a significant reduction in *Leishmania* lesion development and a marginally significant reduction in parasite load due to pre-exposure to sand fly saliva (Ockenfels et al., 2014). Such protective properties of exposure to uninfected saliva ("pre-sensitisation") have garnered enthusiasm for the development of anti-leishmaniasis vaccines using sand fly saliva proteins (Kamhawi et al., 2014). For malaria, prior exposure to mosquito saliva has been shown to reduce *Plasmodium* burden in the liver- and blood-stage (Donovan et al., 2007) while no pre-sensitisation effect was found for the infectivity of sporozoites (i.e., the stage that is transferred from vector to host, Kebaier et al., 2010). In West Nile virus, empirical evidence for the role of pre-exposure to mosquito saliva is mixed (Schneider et al., 2007; Machain-Williams et al., 2013). The immunological mechanisms behind any protective effects remain an open question (Oliveira et al., 2013*a*), but may include direct effects on parasites (e.g., polarisation of the immune response towards microbial killing, Gomes and Oliveira, 2012) or indirect effects, like neutralising saliva proteins that would otherwise facilitate parasite proliferation (Gomes and Oliveira, 2012).

Classic epidemiological models tend to ignore the effects of immune pre-sensitisation. These models (e.g., Ross, 1911*a*; Macdonald, 1957; Anderson and May, 1991) predict that heightened adult vector mortality can effectively control a vector-borne disease by reducing vector abundance, the number of bites per vector, and the probability of surviving the extrinsic incubation period (i.e., the time it takes for an exposed vector to become infectious; reviewed in Smith and McKenzie, 2004; Mandal et al., 2011). These theoretical predictions encouraged the World Health Organization (WHO) to carry out a world-wide insecticide spraying campaign against the mosquito vectors of malaria parasites, with successful elimination of the disease reported in many countries by the late 1970s (Mendis et al., 2009). Insecticide spraying remains a frontline prevention and control strategy against malaria and many other vector-borne diseases, including dengue and leishmaniasis (Mendis et al., 2009; World Health Organization, 2012*a*; Bates et al., 2015). While insecticides have generally proven effective in reducing the incidence of malaria (Kim et al., 2012), there is considerable heterogeneity in the efficacy of spraying reported: interventions that target adult vector survival have failed to reduce the number of infections in some host populations (Pluess et al., 2010; Corbel et al., 2012; Stockdale and Newton, 2013). These outcomes have been attributed to a number of factors ranging from insecticide resistance, sublethal exposure, behavioural alterations by arthropod vectors to avoid insecticides, the presence of a non-human reservoir, heterogeneity in vector life-history traits, and spatial and temporal variation in host and vector populations (Corbel et al., 2012; Stockdale and Newton, 2013; Bellan, 2010; Hemingway, 2014; Brady et al., 2016), though the relative role of each of these factors is unknown.

Here we develop mathematical models to determine the potential for pre-exposure to vector saliva to affect between-host infection dynamics and modulate the consequences of interventions that target vectors. Where vector-borne diseases are endemic, a significant proportion of individuals are likely pre-sensitised by vector saliva; in one sample of individuals from Mali, 23% demonstrated a robust immune response against sand fly salivary molecules (Oliveira et al., 2013*b*). Our work shows that the interplay

between vector saliva and host immunity can produce a variety of epidemiological outcomes, depending of the effect of pre-sensitisation on the duration of infection.

## 3.3 Methods

### 3.3.1 Model

We modelled vector-borne disease dynamics as a set of ordinary differential equations (ODE), and alternatively, as a set of delay differential equations (DDE) that track the change in the abundance of three vector (susceptible, exposed and infectious) and five host (naïve susceptible, pre-sensitised susceptible, naïve infected, pre-sensitised infected and recovered) classes. We first describe the ODE formulation as follows (Fig. 3.1; Eq. 3.1–3.8):

$$\frac{dV_S(t)}{dt} = \phi_V - (\mu_V + r(T_{VH}H_I(t) + T_{VH'}H'_I(t)))V_S(t) \tag{3.1}$$

$$\frac{dV_E(t)}{dt} = r(T_{VH}H_I(t) + T_{VH'}H'_I(t))V_S(t) - (\mu_V + \sigma_V)V_E(t) \tag{3.2}$$

$$\frac{dV_I(t)}{dt} = \sigma_V V_E(t) - \mu_V V_I(t) \tag{3.3}$$

$$\begin{aligned}\frac{dH_S(t)}{dt} = &-(rP_{HV}(V_S(t) + V_E(t) + (1 - T_{HV})V_I(t)) + rT_{HV}V_I(t))H_S(t) \\ &+\theta_{H'}H'_S(t) + \tau_H H_R(t)\end{aligned} \tag{3.4}$$

$$\begin{aligned}\frac{dH'_S(t)}{dt} = &(rP_{HV}(V_S(t) + V_E(t) + (1 - T_{HV})V_I(t)))H_S(t) \\ &-(rT_{H'V}V_I(t) + \theta_{H'})H'_S(t)\end{aligned} \tag{3.5}$$

$$\frac{dH_I(t)}{dt} = rT_{HV}V_I(t)H_S(t) - \gamma_H H_I(t) \tag{3.6}$$

$$\frac{dH'_I(t)}{dt} = rT_{H'V}V_I(t)H'_S(t) - \gamma_{H'}H'_I(t) \tag{3.7}$$

$$\frac{dH_R(t)}{dt} = \gamma_H H_I(t) + \gamma_{H'}H'_I(t) - \tau_H H_R(t). \tag{3.8}$$

While the process of vector input into the population is complex and likely important for predicting disease dynamics, data on the potentially density-dependent processes in vector population dynamics are scarce (Beck-Johnson et al., 2013). Therefore, we assumed that susceptible vectors ($V_S$) are born at a constant rate, $\phi_V$. We also assumed that all vectors experience the same mortality rate, $\mu_V$, regardless of their infection status. In our model, vectors are equally likely to bite a host of any class, so hosts get bitten by a given vector at the rate $r$, which is calculated as the per vector biting rate, $b$, divided by the total host population size, $H_T$ (where $H_T = H_S + H'_S + H_I + H'_I + H_R$). This formalisation makes transmission frequency-dependent (Keeling and Rohani, 2008). A susceptible vector becomes exposed ($V_E$) to parasites when it bites a naïve infected host ($H_I$) or a pre-sensitised infected host ($H'_I$) with the probability $T_{VH}$ or $T_{VH'}$, respectively. In this ODE model, exposed vectors are assumed to become infectious ($V_I$) at a constant incubation rate, $\sigma_V$, which is the inverse of the mean extrinsic incubation period (EIP, $1/\sigma_V$). Thus, EIP follows an exponential distribution with large variance ($\sigma_V^{-2}$), leading to an implicit assumption that the parasite can complete development in the vector at any time, even immediately after a vector becomes exposed. Empirical estimates of the variability in the EIP are rare, but it is known to vary on the order of days in dengue (approx. 5-33 days at 25C, Chan and Johansson,

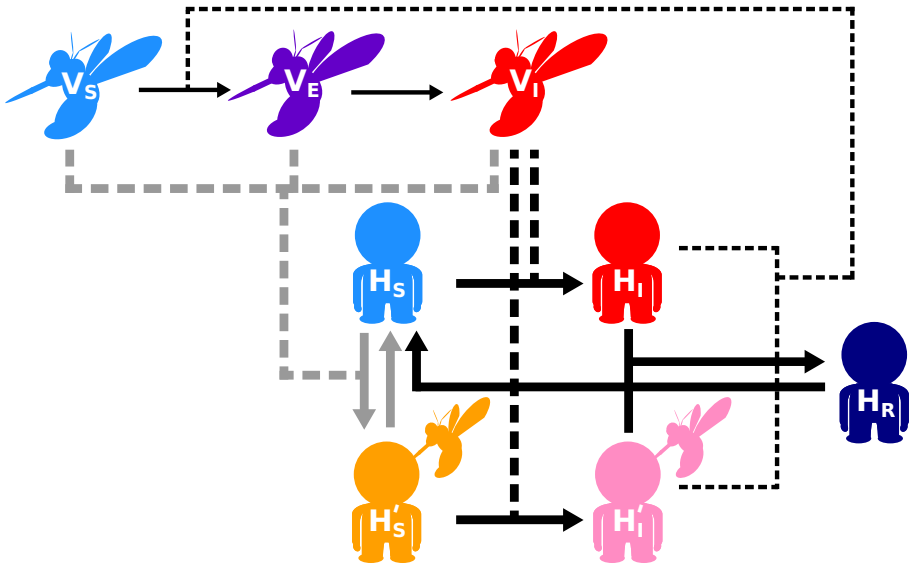


Figure 3.1: Schematic of vector-borne disease dynamics model when host immunity can be pre-sensitised through vector saliva pre-exposure. Susceptible hosts ($H_S$) may become pre-sensitised ($H'_S$) when bitten by either a susceptible vector ($V_S$), an exposed but non-infectious vector ($V_E$), or an infectious vector ($V_I$) if parasite transmission is unsuccessful. Susceptible hosts that are pre-exposed to vector saliva remain sensitised until the protective status is lost over time. Susceptible pre-sensitised and naïve hosts ($H'_S$ and $H_S$ respectively) can become infected ($H'_I$ and $H_I$ respectively) when bitten by an infectious vector. Upon recovering from infection, the host gains immunity against future infections ($H_R$), but that immunity wanes over time. Further details can be found in Methods. Infection routes of hosts are shown in thick black; pre-sensitisation routes in grey; infection of vectors in thin black. The movement between classes is shown in solid lines and the interactions that lead to that movement are shown by dashed lines.

2012) and malaria (approx. 5-14 days at 24C, Paaijmans et al., 2011) and that variation is thought to influence disease transmission (Paaijmans et al., 2011). To examine whether our results are sensitive to the assumption of large variability in the duration of the EIP, we also formulated the model as a system of delay differential equations (DDEs), which assumes the opposite extreme of no variation in EIP: all exposed vectors require exactly the length of the mean EIP, or $1/\sigma_V$ days to become infectious, though some vectors may not survive that period.

The DDE formulation differs from the ODE counterpart in two equations (ODE: Eq. 3.2 & 3.3; DDE: Eq. 3.9 & 3.10), which describe the dynamics of exposed and infectious vectors, respectively:

$$\begin{aligned}\frac{dV_E(t)}{dt} &= r(T_{VH}H_I(t) + T_{VH'}H'_I(t))V_S(t) - \mu_V V_E(t) \\ &\quad -r(T_{VH}H_I(t-EIP) + T_{VH'}H'_I(t-EIP))V_S(t-EIP)\mathrm{e}^{-\mu_V EIP} \qquad (3.9)\\ \frac{dV_I(t)}{dt} &= r(T_{VH}H_I(t-EIP) + T_{VH'}H'_I(t-EIP))V_S(t-EIP)\mathrm{e}^{-\mu_V EIP} \\ &\quad -\mu_V V_I(t) \qquad (3.10)\end{aligned}$$

where $\mathrm{e}^{-\mu_V EIP}$ is the probability that an exposed vector survives the length of the extrinsic incubation period (EIP, i.e., $1/\sigma$) to become infectious. The simulation starts with a population of susceptible vectors and one infectious vector; there are no exposed vectors initially, so $\mathrm{e}^{-\mu_V EIP}$ needs only be defined

for $t > 0$. Note that this DDE system can be written in terms of only $dV_S$ and $dV_I$, but we retain an exposed vector equation for clarity and ease of comparison with the ODE model.

As in most models of vector-borne diseases (reviewed in Mandal et al., 2011), we kept the host population size constant by ignoring host birth and death. The assumption of constant population size is reasonable over the time scale of vector control. Note that our analyses focus on equilibrium conditions of the model (see below). As such, we refer to the equilibrium quantity of a given host class as abundance, number, or cases throughout the manuscript (e.g., abundance of pre-sensitised infected hosts); however, changes in these quantities are concomitant with changes in the proportion or prevalence of the host class as the total host population size is held constant. A susceptible host becomes pre-exposed to vector saliva and pre-sensitised ($H'_S$) when bitten by a susceptible or an exposed vector ($V_S$ and $V_E$, respectively) with the probability $P_{HV}$, or by an infectious vector ($V_I$) with the probability $P_{HV}(1-T_{HV})$, i.e., when parasite transmission fails upon contact but pre-sensitisation is successful. Alternatively, a susceptible host becomes infected ($H_I$) when bitten by an infectious vector with the probability $T_{HV}$. Pre-sensitised susceptible hosts lose their protected status at a rate $\theta_{H'}$. Once infected, naïve infected hosts recover from infection at a rate $\gamma_H$. After a host is pre-sensitised, a bite from an infectious vector creates a pre-sensitised infected host, $H'_I$ with the probability $T_{H'V}$. As a host recovers from infection ($H_R$), it becomes temporarily immune to future infections until acquired immunity wanes, which occurs at a rate $\tau_H$.

We focus primarily on the effect of vector saliva pre-exposure on the duration of infection by assuming that pre-sensitised infected hosts recover at a unique rate, $\gamma_{H'}$. The available data indicate that immune pre-sensitisation through pre-exposure to vector saliva has a likely role in altering parasite growth and density (Donovan et al., 2007; Schneider et al., 2007; Oliveira et al., 2008; Machain-Williams et al., 2013; Ockenfels et al., 2014). This could lead, respectively, to reduced or amplified symptoms during a future infection, with knock on consequences for the duration of that infection. For example, if patients with more severe symptoms are more likely to seek treatment, their infections may be shortened by clinical interventions. Therefore, if pre-sensitisation to vector saliva leads to exacerbation of disease symptoms, then this could lead to shorter infections. A similar outcome might be expected if pre-sensitisation leads to increased resistance of the host. Alternatively, disease mitigation through pre-sensitisation may increase the duration of infection if pre-exposure to vector saliva only provides partial resistance, i.e., parasite growth is hindered, but infections are not cleared — a scenario that is consistent with a meta-analysis on *Leishmania* (Ockenfels et al., 2014) and some studies on *Plasmodium* (Donovan et al., 2007) and West Nile virus (Machain-Williams et al., 2013). If pre-sensitised infected patients experience less severe symptoms due to lower parasite burdens, they may also be less likely to seek clinical treatment, thereby prolonging the time to recovery. We also investigated the effect of vector saliva pre-exposure on susceptibility, $T_{H'V}$, and infectiousness, $T_{VH'}$ as part of a sensitivity analysis (see Analysis for details). While a reduction in infection-induced host mortality is another potential consequence of immune pre-sensitisation, a meaningful interpretation of such an effect would rely on understanding how host death affects the recruitment of susceptible hosts, a complication outside the scope of the present study.

### 3.3.2 Analysis

First, using the ODE model, we derived the abundance of each vector class at quasi-equilibrium to examine the effect of control measures on vector demography. The quasi-equilibrium approach assumes that the lifespan of a vector is much shorter than that of a host so that the vector population quickly

reaches a steady state (Keeling and Rohani, 2008). Mathematically, this means that the rates of change of vector populations, i.e., $\frac{dV_S(t)}{dt}$, $\frac{dV_E(t)}{dt}$ and $\frac{dV_I(t)}{dt}$ (Eq. 3.1–3.3), are set to zero and by solving for $V_S$, $V_E$ and $V_I$, we find the quasi-equilibrium vector abundances:

$$\widehat{V_S} = \frac{\phi_V}{r(H_I T_{VH} + H'_I T_{VH'}) + \mu_V}, \tag{3.11}$$

$$\widehat{V_E} = \widehat{V_S}\frac{r(H_I T_{VH} + H'_I T_{VH'})}{\mu_V + \sigma_V}, \tag{3.12}$$

$$\widehat{V_I} = \widehat{V_E}\frac{\sigma_V}{\mu_V}. \tag{3.13}$$

Second, we numerically simulated both the ODE and DDE model (Eq. 3.1–3.8 & 3.9 & 3.10) to a stable equilibrium and investigated how the demographic shift in the vector population driven by increased vector mortality affects the abundance of hosts in different classes, in the presence and absence of pre-sensitisation effects of pre-exposure to vector saliva. We performed numerical simulations in *R* Version 3.2.4 (R Core Team, 2018), using the package *deSolve* (Soetaert et al., 2010) to solve for a steady state. The stability of steady states in the ODE model was assessed using the package *rootSolve* (Soetaert, 2009) while we simulated the DDE model forward in time until the derivatives approached zero with a threshold of $10^{-4}$. The simulations were initialised with disease-free equilibrium conditions for susceptible vectors and hosts (Appendix 3.7.1) and one infected vector ($V_I(0) = 1$). Whenever we simulated the dynamics in the presence of an intervention targeting vector survival, vector mortality was elevated from the onset of a disease outbreak, mimicking, for example, indoor residual spraying regimes. Parameter values used in our simulations are listed in Table 1. Where possible, default parameter values were chosen from within the range of parameters explored in previous iterations of the Ross-McDonald model of leishmaniasis and malaria dynamics (reviewed in Rock et al., 2015; Mandal et al., 2011); a wider range of values were explored for parameters describing the process of saliva immune pre-sensitisation due to a paucity of estimates. We also investigated the short term infection dynamics by analysing the effect of saliva pre-exposure on $R_0$, which characteristically describes the early infection dynamics (Appendix 3.7.1) and by simulating the transient infection dynamics in the presence and absence of a control (Appendix 3.7.2). Finally, using the ODE model, we graphically explored parameter sensitivity of the key findings to identify factors that influence the interaction between vector saliva pre-sensitisation and interventions targeting vector survival (Appendix 3.7.3).

## 3.4 Results

### 3.4.1 Interventions targeting vector survival facilitate immune pre-sensitisation through pre-exposure to vector saliva

Before making any assumptions about the immunological consequences of pre-sensitisation through pre-exposure to vector saliva, we first assume that there are none: pre-sensitised and naïve infected hosts are assumed to have the same rates of recovery and probabilities of onward transmission. From quasi-equilibrium conditions (Eq. 3.11–3.13), we can infer the effect of increased vector mortality on the abundance of vectors in different classes, and the subsequent influence on the abundance of infected hosts that are pre-exposed to vector saliva. As expected from the classical Ross-MacDonald model

Table 3.1: Model parameters and their values (defaults and ranges explored for parameter sensitivity are listed). Rates are in units of per day unless otherwise indicated.

| Symbol | Description | Default (Range) |
|---|---|---|
| $\phi_V$ | Vector birth rate | 1500 (100, 5000) |
| $\mu_V$ | Vector mortality rate | $14^{-1}$ ($14^{-1}$, $14^{-1} + 2.5^{-1}$) |
| $r$ | Rate at which a host gets bitten by a vector | $\frac{b}{H_T}$ |
| $b$ | Biting rate per vector | 0.15 (0.05, 0.5) |
| $\sigma_V$ | Parasite incubation rate in vector (1/EIP) | $14^{-1}$ ($30^{-1}$, $2^{-1}$) |
| $P_{HV}$ | Pre-sensitisation probability upon contact | 0.1 (0, 1) |
| $H_T$ | Total number of hosts | $H_S + H'_S + H_I + H'_I + H_R$, 1000 |
| $\theta_{H'}$ | Rate of loss of immune pre-sensitisation through saliva pre-exposure effect | 0 (0, $14^{-1}$) |
| $T_{HV}$ | Transmission probability from vector to naïve host | 0.5 |
| $T_{H'V}$ | Transmission probability from vector to pre-sensitised host | 0.5 (0.05, 0.5) |
| $T_{VH}$ | Transmission probability from naïve host to vector | 0.5 |
| $T_{VH'}$ | Transmission probability from pre-sensitised host to vector | 0.5 (0.05, 0.5) |
| $\gamma_H$ | Recovery rate with acquired immunity of naïve hosts | $60^{-1}$ ($150^{-1}$ , $20^{-1}$ ) |
| $\gamma_{H'}$ | Recovery rate with acquired immunity of pre-sensitised hosts | $\frac{\gamma_H}{5}$ ($\frac{\gamma_H}{5}$, $2\gamma_H$) |
| $\tau_H$ | Rate of loss of acquired immunity | 2 years$^{-1}$ (10 years$^{-1}$, $\frac{1}{2}$ year$^{-1}$) |

(reviewed in Smith and McKenzie, 2004; Mandal et al., 2011), our model shows that heightened vector mortality incurs multiplicative effects on parasite transmission in the vector population. First, vector abundance declines with vector mortality (Eq. 3.11). Second, the number of times a vector bites during its lifetime is a function of its lifespan, so increased vector mortality reduces the likelihood that a vector bites an infected host and becomes exposed to a parasite (Eq. 3.11). Third, a parasite must survive the extrinsic incubation period in the vector in order for the exposed vector to become infectious and as vector mortality increases, exposed vectors are less likely to survive that period (Eq. 3.12). Additionally, once becoming infectious, vectors are shorter living (Eq. 3.13). Taken together, an increase in vector mortality reduces the total vector abundance, and increases the ratio of non-infectious to infectious vectors by disproportionately reducing the abundance of infectious vectors (Fig. 3.2a).

The impact of control measures on the host population is more nuanced. First, as expected, the reduction in the total vector abundance reduces the rate of contact between hosts and vectors, leaving more hosts in the naïve susceptible class. Second, the processes of infection and saliva pre-sensitisation 'compete' for the common resource, naïve susceptible hosts. Thus, the increased ratio of non-infectious to infectious vectors increases the likelihood of vector saliva pre-sensitisation over that of infection. Together with the increase in the number of susceptible hosts, the increasing likelihood of pre-sensitisation increases the abundance of pre-sensitised susceptible hosts as control reduces vector survival. As intuition would suggest, the force of infection from vectors monotonically decreases with the intensity of vector control (Fig. 3.2a). However, over a range of vector mortality values, the increasing availability of pre-sensitised susceptible hosts outweighs the decreasing force of infection from vectors. Consequently, when the increase in vector mortality is moderate, the number of pre-sensitised infected hosts can actually increase ($H'_I$, Fig. 3.2b; pink). More generally, vector control increases the number of hosts that become pre-exposed to vector saliva prior to an infectious bite. Thus, the proportion of infected hosts that are pre-sensitised always increases with heightened vector mortality (Fig. 3.2b), assuming that the probability of transmission from the vector to host is unaffected by the saliva pre-exposure. In summary, without assuming any effect of vector-saliva pre-exposure on host recovery rate, the overall infection abundance ($H_I + H'_I$) always declines with increasing vector mortality when facing vector control. Importantly, even while the total abundance of infected hosts declines, the number and proportion

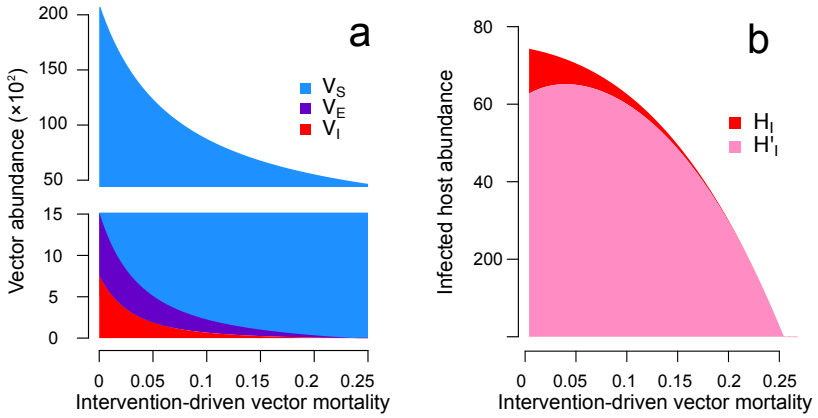


Figure 3.2: Interventions targeting vector survival, such as insecticide spraying, increase the likelihood of immune pre-sensitisation through pre-exposure to vector saliva. Shown are the equilibrium abundances in the ODE model of (a) susceptible ($V_S$; blue), exposed ($V_E$; purple) and infectious ($V_I$; red) vectors, and (b) infected hosts that are not pre-exposed ($H_I$; red) and that are pre-exposed ($H'_I$; pink) to vector saliva. Here, the x-axis is the daily rate of vector mortality imposed by vector control. Pre-sensitised and naïve infected hosts are assumed to have the identical recovery rates ($\gamma_H = \gamma_{H'} = 60^{-1}$ per day) and transmission probabilities ($T_{HV} = T_{H'V} = T_{VH} = T_{VH'} = 0.5$). Note that the force of infection from vectors, $rT_{HV}V_I$, is proportional to the abundance of infectious vectors, and the rate of immune pre-sensitisation through vector saliva pre-exposure, $rP_{HV}(V_S + V_E + (1 - T_{HV})V_I)$, is roughly proportional to the abundance of susceptible vectors (notice that $V_S$ is at least one order of magnitude larger than $V_E$ or $V_I$

of infected hosts that are pre-exposed to vector saliva can increase due to the increased availability of susceptible hosts that are pre-exposed to vector saliva.

### 3.4.2 A moderate increase in vector mortality can elevate infection cases

When pre-exposure to vector saliva mitigates disease manifestation and prolongs the time until recovery through clinical intervention, we find that, in the short term, vector control suppresses the peak number of infections in both host and vector populations and slows the spread of infection (Appendix 3.7.2). At equilibrium, increased vector mortality reduces the abundance of infectious vectors (Fig. 3.3a) and the abundance of naïve infected hosts (i.e., those assumed to show clinical symptoms, Fig. 3.3b). The previous section demonstrated that vector control can increase the abundance of pre-sensitised infected hosts (Fig. 3.2b), an increase that is amplified when pre-sensitisation results in longer durations of infection (Fig. 3.3c; cool colours).

This scenario presents a dilemma where vector control can successfully decrease the abundance of infectious vectors and symptomatic hosts (Fig. 3.3a & b) while counterintuitively — and counterproductively — increasing the number of pre-sensitised infections and even the total abundance of infectious hosts (in both ODE and DDE models; Fig. 3.4a & b, respectively). Further increases to vector mortality eventually outweigh the increase in the availability of pre-sensitised susceptible hosts, reducing the total number of infected hosts. If we assume the opposite effect of pre-exposure to vector saliva, i.e., pre-sensitisation increases the recovery rate either by promoting natural recovery or by exacerbating disease symptoms and ensuring earlier treatment, then the efficacy of vector control is enhanced by the pre-sensitisation effect (Fig. 3.3 warm colours).

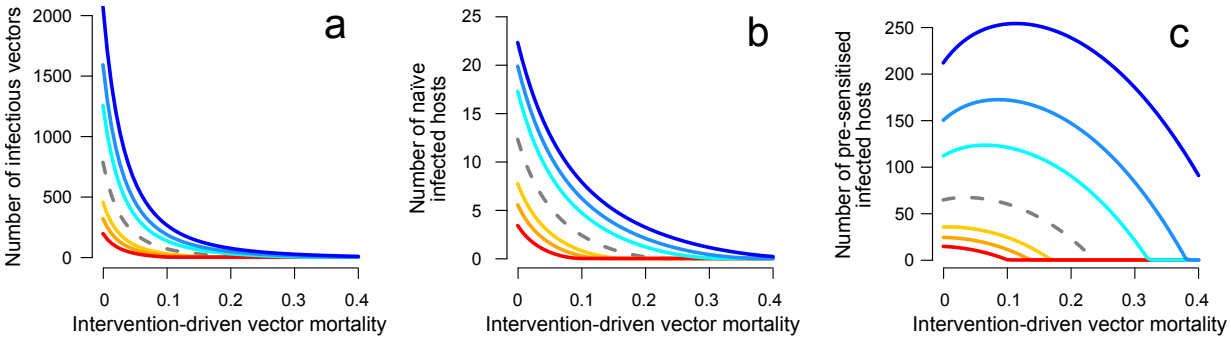


Figure 3.3: Increasing vector mortality can elevate pre-sensitised and total infection cases when pre-exposure to vector saliva prolongs the time to recovery. Shown are (a) the abundance of infectious vectors, (b) naïve infected hosts, and (c) pre-sensitised infected hosts in the ODE model. The total infection cases in the host population (the sum of b and c) can increase with vector mortality, since pre-sensitised infections are more abundant (note the difference in scale between b and c). The dashed grey line shows the result when pre-exposure has no effect (i.e. $\gamma_{H'} = \gamma_H$). Shown in cool colours are the results when pre-sensitisation causes decreased recovery rates with the strength of pre-sensitisation reflected in the intensity of blue: recovery rates of pre-sensitised infected hosts equaling $\frac{1}{2}$, $\frac{1}{3}$, and $\frac{1}{5}th$ of the recovery rate of naïve infected hosts. Conversely, the effects of pre-exposure as increased recovery rate are shown in warm colours reflecting 2, 3, and 5 times the recovery rate of naïve infected hosts.

### 3.4.3 Sensitivity to modelling assumptions and parameters

Our model predicts that a moderate increase in vector mortality can elevate infection cases due to the change in the ratio of non-infectious to infectious vectors. Because large variability in the EIP assumed by the ODE model is expected to support a higher level of parasite transmission (because more vectors will survive the EIP when it is sometimes short), the severity of the adverse effect might be influenced by the assumption about the distribution of the EIP. Thus, we simulated the DDE model in which we expect fewer infectious vectors because the EIP is assumed to be fixed in duration. We find that both models predict the same qualitative outcome that a moderate increase in vector mortality can lead to an increase in infection cases when pre-sensitisation prolongs the time to recovery (Fig. 3.4). However, eliminating the variation in the EIP reduces the parameter space over which control might be expected to increase the total number of infected hosts. Furthermore, the DDE model predicts that a lower intensity of control is needed than in the ODE model to achieve a 90% reduction in the number of infected hosts — a global target by 2030 set by WHO in the fight against malaria (World Health Organization, 2015) (Fig. 3.5a). Both models, nonetheless, predict that the intervention-driven vector mortality required to achieve this goal increases steeply if saliva pre-sensitisation decreases the rate of host recovery. It is noteworthy that the DDE model predicts that the initial response to vector control (e.g., the number of infected hosts after a small reduction in vector lifespan) can be exaggerated compared to the ODE model depending on how strongly saliva pre-sensitisation reduces the recovery rate (Fig. 3.5b). Therefore, the adverse effect may occur regardless of the assumption about variability in parasite development, but the severity of the effect will likely change depending on the variability in the EIP.

Returning to the ODE model, we explored the parameter sensitivity in order to identify factors that influence the adverse interaction between vector saliva pre-sensitisation and interventions targeting vector survival. First, the unintended increase in pre-sensitised infected hosts is augmented when parameters

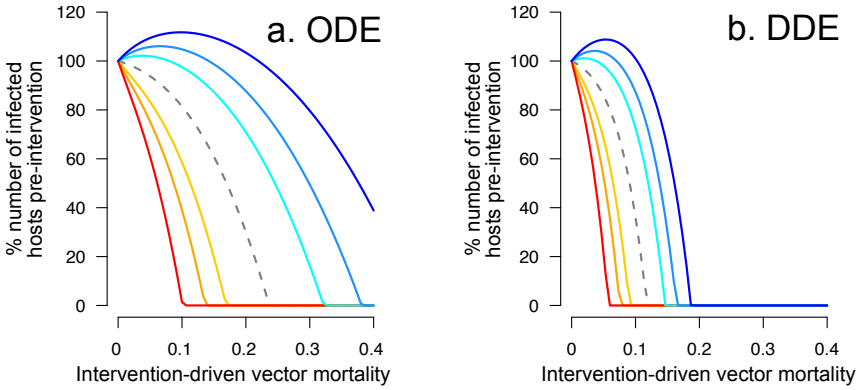


Figure 3.4: Both ordinary (ODE) and delay (DDE) differential equation models point to the possibility of an adverse consequence of moderate vector control interventions. Shown are the percentage of infection cases relative to the pre-intervention level predicted by (a) the ODE model and (b) the DDE model plotted against the intensity of intervention-driven vector mortality. The colour keys are as described in Fig. 3.3.

associated with the vector population are favourable for parasite transmission, i.e., when vectors are born at a high rate, parasite incubation in the vector is fast, or the vector biting rate is high ($b$, $\sigma_V$ and $\phi_V$, respectively; Appendix 3.7.3). Second, experimental evidence from a rodent model of leishmaniasis suggests that the immunological effects of pre-exposure to vector saliva wane over time (Rohoušová et al., 2011); we find that if immune pre-sensitisation wanes fast enough, vector control is not predicted to increase the abundance of infected hosts (Fig. 3.7, $\theta_{H'}$). Third, and counterintuitively, the vector control-driven increase in pre-sensitised infection is most pronounced when the probability of pre-sensitisation upon contact is low (but non-zero; Fig. 3.7, $P_{HV}$). At high probability, the number of pre-sensitised hosts is already high in the absence of vector control interventions, and increasing vector mortality through control decreases the force of infection more than it increases the likelihood of pre-exposure to vector saliva. Whereas at low probability, the increasing availability of susceptible pre-sensitised hosts due to control can outweigh the decreasing force of infection. Fourth, the increase in the pre-sensitised infections can be minimised by increasing the recovery rate of naïve, infected hosts, which in turn limits the overall parasite transmission (Fig. 3.7, $\gamma_H$). In addition, the vector control-mediated increase in pre-sensitised infections is minimal when immune memory is long lasting, because immune-waning provides a source of susceptible hosts that helps sustain parasite transmission (Fig. 3.7, $\tau_H$). Finally, understanding the contribution of pre-sensitised hosts to parasite transmission is the key to estimating the impact of saliva pre-sensitisation on epidemiology: our model predicts that the adverse consequence of vector control can be avoided if the probability of transmission to and from pre-sensitised hosts is considerably smaller than for naïve hosts (Fig. 3.7, $T_{H'V}$ and $T_{VH'}$).

## 3.5 Discussion

Prior exposure of mammalian hosts to uninfected vector bites can alter host immune responses against a variety of parasites (Ockenfels et al., 2014). While this three-way interaction between hosts, vectors, and parasites has been shown to influence progression of a wide range of vector-borne diseases (Ockenfels et al., 2014; Pingen et al., 2017), the detailed biology of this interaction remains an active area of research and the epidemiological consequences are not obvious. Therefore, mapping the possible epidemiological

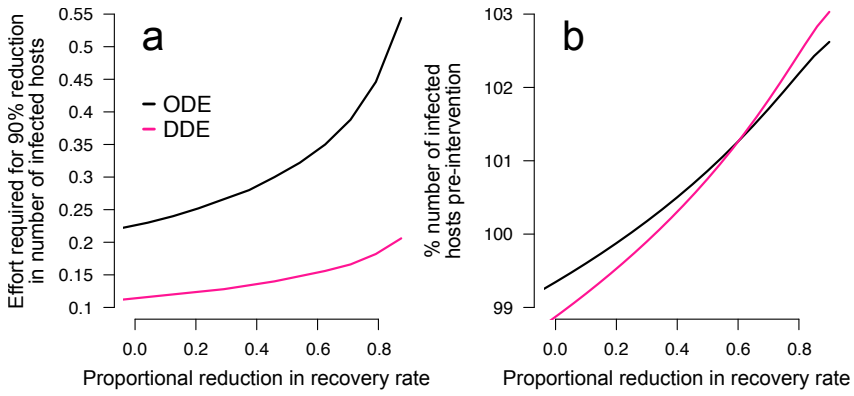


Figure 3.5: The severity and detectable signs of the adverse interaction between vector saliva pre-exposure and increased vector mortality are likely to be influenced by the effect of saliva pre-sensitisation in reducing the rate of recovery and the assumption about the variability in parasite development. Shown are (a) the level of intervention-driven vector mortality ("effort") required to achieve a 90% reduction in the number of infected hosts and (b) the percentage of the pre-intervention number of infected hosts after a small reduction (25%) in vector lifespan due to vector control. The x-axis denotes the assumed effect of saliva pre-exposure on recovery as the proportional reduction in recovery rate.

implications relies on mathematical models (Lee and Bartsch, 2017). Using a generic model of vector-borne diseases, we have shown that interventions targeting adult vector survival may increase the number of hosts that are pre-exposed to vector saliva. When pre-sensitisation mitigates disease symptoms as reported for *Leishmania*, *Plasmodium* and West Nile virus (Donovan et al., 2007; Machain-Williams et al., 2013; Ockenfels et al., 2014) and, as a consequence, prolongs the time to recovery through clinical interventions, we predict that a moderate increase in vector mortality can increase the infection cases in the host population. Alternatively, if immune pre-sensitisation leads to more rapid clearance of infection, we find that increasing vector mortality rates may achieve greater than expected disease control.

If the sole effect of a disease intervention is a modest increase in vector mortality, then our model predicts it could actually increase the public health burden when pre-sensitisation leads to milder and, ultimately, untreated infections. One might ask if an increase in sub-clinical infections is truly a concern for public health. The answer depends on patient health and transmission potential of those hosts. Evidence from a range of vector-borne diseases suggests that asymptomatic or sub-clinical patients suffer substantial viability and reproductive costs associated with carrying parasites (Guzman and Vazquez, 2010; Rassi and Marin-Neto, 2010; Michel et al., 2011; Scott et al., 2011; Cunnington et al., 2012). From a population perspective, sub-clinical infections maintain a reservoir of active transmission, which may seed periodic outbreaks (Stauch et al., 2011; Babiker et al., 2013). Indeed, our analysis of $R_0$ confirms that vector saliva pre-exposure can facilitate disease outbreaks under the assumption that the immunological effect of pre-exposure prolongs the duration of infection (Appendix 3.7.1).

Immune sensitisation triggered by pre-exposure to vector saliva has been hypothesised to involve both antibody-based and cell-mediated immunity (Gomes and Oliveira, 2012) with the two arms of immunity exhibiting distinct functional roles. For example, the suggested role of anti-salivary antibodies is to neutralise salivary proteins (Gomes and Oliveira, 2012), which would otherwise facilitate parasite infection (Ockenfels et al., 2014). In contrast, cell-mediated responses at the site of an uninfectious bite are thought to hinder future nearby parasite infection as collateral damage (Gomes and Oliveira, 2012). The relative importance of different arms of immunity, and whether they lead to different disease

outcomes and parasite transmission remain open questions (Andrade and Teixeira, 2012; Gomes and Oliveira, 2012). However, with the majority of experimental studies reporting quantitative effects (e.g., changes in parasite density and lesion size), it is unclear whether pre-sensitisation affects the probability of initial parasite establishment. Therefore, there is little direct evidence to suggest that immune sensitisation triggered by pre-exposure to vector saliva is powerful enough to offer complete protection from infection. On the other hand, the consensus finding from leishmaniasis, that pre-exposure leads to disease mitigation (Ockenfels et al., 2014), is consistent with the notion that pre-exposed patients are more likely to remain sub-clinical (Andrade and Teixeira, 2012). Further understanding of the immunological pathways involved in pre-sensitisation, as well as the success of parasites in pre-sensitised hosts (e.g., probability of establishment and transmitted parasite density) and the clinical outcome for the host (e.g., recovery and mortality) will open possibilities for predictions of epidemiological patterns.

Theories on vaccination and immune priming predict that mechanisms that improve host health (and hence prolong infection), but do not block transmission can increase disease prevalence in host populations (Vale et al., 2014; Tate, 2017). Supporting the theory, a recent experimental study demonstrated that vaccination of chickens against Marek's disease virus leads to increased cumulative transmission of highly virulent viral strains because vaccination prolongs infection without preventing transmission (Read et al., 2015). These previous findings as well as the results presented here invite careful examination of clinical consequences associated with saliva-derived vaccines (reviewed in Kamhawi et al., 2014) so that vaccination achieves a desired goal both clinically and epidemiologically over a long timescale.

Our study suggests that caution is warranted in interpreting empirical estimates regarding the impact of interventions. First, the efficacy of vector control is rarely reported at the human population level (Stockdale and Newton, 2013); instead, studies often rely on signals from vector populations. Our model shows that an optimistic signal from the vector population – reduced vector abundance and reduced proportion of infected individuals in the vector population – can coincide with increasing sub-clinical cases and an overall increase in infection cases in the host population. Therefore, estimates of infection cases in the host population are crucial for assessing intervention efficacy. Second, parasite prevalence in a population is often inferred from the number of clinical cases, which is inevitably limited to symptomatic patients who seek treatment. Our results demonstrate that even when vector control decreases the force of infection, it may simultaneously increase the abundance of infected hosts pre-sensitised by vector saliva whose infections may go undetected due to milder symptoms. In light of growing evidence that sub-clinical hosts are infectious to arthropod vectors (Duong et al., 2015; Molina et al., 1994), our results reinforce the need for active surveillance in order to accurately estimate parasite transmission in a given population.

Our findings highlight the importance of both thorough spraying programmes and integrated vector management approaches, especially when control is expected to achieve only moderate increases in vector mortality. Fortunately, vector control tools are rarely used in isolation; rather, multiple intervention approaches are integrated to target different components of the parasite transmission cycle (World Health Organization, 2012*b*). Our parameter sensitivity analysis underscores the importance of integrated vector management by showing that parameters associated with conventional methods for combatting vector-borne diseases – reduced vector birth rate (e.g., removing standing water where female vectors lay their eggs), reduced vector-biting rate (e.g., use of bednets), and increased recovery of symptomatic hosts (e.g., treatment efficacy) – all help limit the risk that increased vector mortality will elevate the number of pre-sensitised infections. Finally, predictions about the consequences of integrated control

might require better quantitative knowledge about the underlying density-dependent processes in the vector population. For example, increased adult mortality should lead to reduced egg laying, which may ultimately reduce adult recruitment (Brady et al., 2016). However, increased adult mortality could also relax larval competition, leading to greater subsequent adult recruitment (Beck-Johnson et al., 2013). Which of these effects prevails will likely be system- (and possibly environment-) specific, but will likely impact epidemiological outcomes.

## 3.6 Conclusion

We demonstrated that pre-exposure to vector saliva alters epidemiological outcomes in a manner that could be positive or negative to public health. It is currently not possible to make precise epidemiological predictions due to the gaps of detailed knowledge about the effect of pre-sensitisation on clinical outcomes and parasite transmission, and more generally in vector ecology. Filling in these gaps will be crucial for delineating the potentially negative interaction between pre-exposure to saliva and vector control, and for deploying saliva-based vaccines effectively in the future. Our work underscores the importance of considering the interplay among vector biology, host immunity, and control measures so that the combined effect of interventions yield desirable disease control outcomes.

## 3.7 Appendices

### 3.7.1 Disease-free equilibrium and calculating $R_0$

In the ODE model, when a vector population is free of parasites, the change in the number of vectors, $V_S$, is described simply by:

$$\frac{dV_S(t)}{dt} = \phi_V - \mu_V V_S(t)$$

where $\phi_V$ and $\mu_V$ are the rates of vector birth and death respectively. By setting $\frac{dV_S(t)}{dt}$ equal to zero, we obtain the disease-free vector equilibrium, i.e. $\widehat{V_S} = \frac{\phi_V}{\mu_V}$.

Similarly, in the absence of parasites, the change in the number of naïve susceptible, $H_S$, susceptible hosts is described as

$$\frac{dH_S(t)}{dt} = -rP_{HV}V_S(t)H_S(t) + \theta_{H'}(H_T - H_S(t))$$

where $r$ is the rate at which a host gets bitten by a vector (defined as $\frac{b}{H_T}$ where $b$ is the biting rate per vector and $H_T$ is the constant total host population size), $P_{HV}$ is the probability of pre-sensitisation per biting event, and $\theta_{H'}$ is the rate of loss of the saliva pre-exposure effect. Note that $H_T - H_S(t)$ is the number of susceptible hosts that are pre-exposed to vector saliva. By setting $\frac{dH_S(t)}{dt}$ equal to zero, we obtain the disease-free susceptible host equilibrium,

$$\widehat{H_S} = \frac{\theta_{H'}{H_T}^2}{bP_{HV}\widehat{V_S} + \theta_{H'}H_T},$$

and the equilibrium number of pre-sensitised susceptible hosts, $\widehat{H'_S}$, is simply $H_T - \widehat{H_S}$.

The risk of an epidemic outbreak is conventionally expressed as the basic reproductive number, $R_0$, which is the number of secondary infections produced when one infected individual is introduced to an entirely susceptible population of hosts. Here we calculate $R_0$ using the next generation method (Diekmann et al., 1990), which is a general approach to calculate $R_0$ for infection cycles involving multiple infected compartments as the dominant eigenvalue of the next generation matrix (refer to Heffernan et al. (2005) for an accessible overview of this approach). Following the notation of Heffernan et al. Heffernan et al. (2005), the infection matrix, $F$ and the transition matrix, $V$ for our ODE model (Eq. 3.1–3.8) are described as follows:

$$F = \begin{Bmatrix} 0 & 0 & rT_{VH}V_S & rT_{VH'}V_S \\ 0 & 0 & 0 & 0 \\ 0 & rT_{HV}H_S & 0 & 0 \\ 0 & rT_{H'V}H'_S & 0 & 0 \end{Bmatrix},$$

$$V = \begin{Bmatrix} \mu_V + \sigma_V & 0 & 0 & 0 \\ -\sigma_V & \mu_V & 0 & 0 \\ 0 & 0 & \gamma_H & 0 \\ 0 & 0 & 0 & \gamma_{H'} \end{Bmatrix}.$$

The next generation matrix is then calculated as the product of the infection matrix and the inverse of the transition matrix, $FV^{-1}$ as follows:

$$FV^{-1} = \begin{Bmatrix} 0 & 0 & \frac{rT_{VH}V_S}{\gamma_H} & \frac{rT_{VH'}V_S}{\gamma_{H'}} \\ 0 & 0 & 0 & 0 \\ \frac{\sigma_V rT_{HV}H_S}{\mu_V^2+\mu_V\sigma_V} & \frac{rT_{HV}H_S}{\mu_V} & 0 & 0 \\ \frac{\sigma_V rT_{H'V}H'_S}{\mu_V^2+\mu_V\sigma_V} & \frac{rT_{H'V}H'_S}{\mu_V} & 0 & 0 \end{Bmatrix}.$$

Then the dominant eigenvalue of the matrix $FV^{-1}$ gives $R_0$:

$$R_0 = \frac{r\sqrt{V_S}\sqrt{\sigma_V}\sqrt{H_S T_{HV} T_{VH}\gamma_{H'} + H'_S T_{H'V} T_{VH'}\gamma_{H'}}}{\sqrt{\gamma_H}\sqrt{\gamma_{H'}}\sqrt{\mu_V(\mu_V+\sigma_V)}}.$$

The effect of saliva-induced pre-sensitisation on the chance of a disease outbreak can be assessed by taking the partial derivative of $R_0$ with respect to the probability of successful pre-sensitisation upon contact, i.e., $P_{HV}$. While the full expression of $\frac{\partial R_0}{\partial P_{HV}}$ is rather large and not shown here, we find the following proportional relationship:

$$\frac{\partial R_0}{\partial P_{HV}} \propto T_{H'V}T_{VH'}\gamma_H - T_{HV}T_{VH}\gamma_{H'}.$$

The sign of this expression determines the directional influence of saliva pre-sensitisation probability on $R_0$: when positive, pre-sensitisation increases the chance of an outbreak and when negative it decreases the same chance. This term can be rearranged to give a condition for when pre-sensitisation increases $R_0$:

$$\frac{T_{H'V}T_{VH'}}{T_{HV}T_{VH}} > \frac{\gamma_{H'}}{\gamma_H}.$$

This expression simply tells us that pre-sensitisation facilitates disease outbreaks if the ratio of the product of the transmission probabilities (i.e., vector to host and host to vector transmission) of pre-sensitised hosts to naïve hosts is greater than the relative recovery rate of pre-sensitised hosts to naïve hosts. Such a scenario is foreseeable if pre-exposure to saliva leads to milder infections that are rarely treated, and susceptibility and infectivity of pre-sensitised hosts remain sufficiently high.

### 3.7.2 Transient dynamics with and without control

We simulated the transient infection dynamics of the ODE model to investigate the short term consequences of vector control in the presence of saliva pre-sensitisation (Fig. 3.6). In the short term, vector control suppresses the peak number of infections for both naïve and pre-sensitised hosts (i.e., Fig. 3.6a & b) and the proportion of vectors that are infectious (Fig. 3.6d). However, vector control can increase the equilibrium abundance of pre-sensitised infected hosts and even the overall infection cases when pre-exposure to vector saliva prolongs the time to recovery (Fig. 3.6b & c).

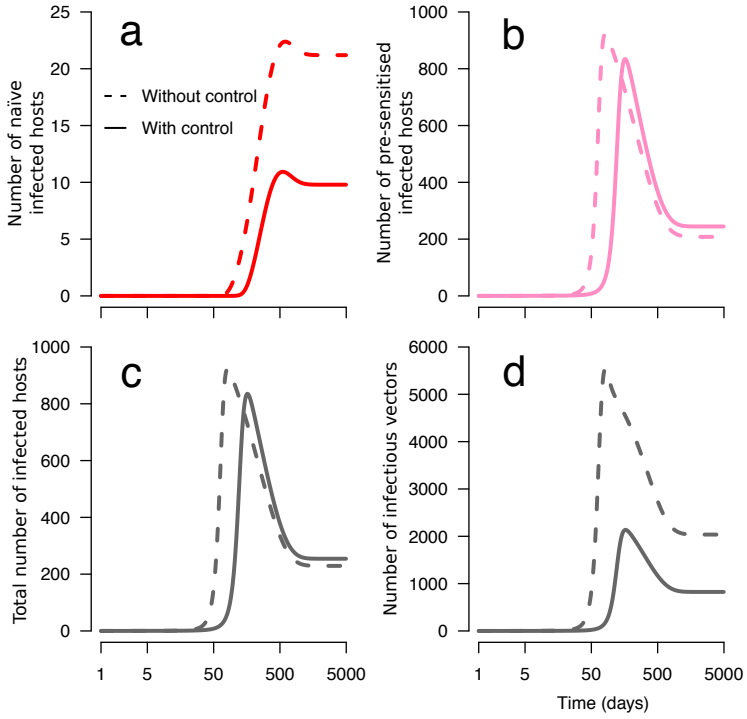


Figure 3.6: A moderate increase in vector mortality reduces the peak, but can increase the equilibrium, number of infections in hosts. The solid lines represent a moderate increase in vector mortality through control efforts ($\mu_V = 7^{-1}$ per day compared to the baseline mortality of $14^{-1}$ presented as dashed lines). Shown are (a) the number of naïve infected hosts ($H_I$) and (b) pre-sensitised infected hosts ($H_I'$), (c) number of all hosts that are infected, regardless of pre-sensitisation status and (d) number of infectious vectors. The x-axes are on a $\log_{10}$ scale. Disease introduction and an intervention targeting vector survival take place simultaneously at the beginning of the simulations. The recovery rate of the pre-sensitised hosts is set to be $\frac{1}{5}th$ that of naïve hosts, who recover at a rate of $60^{-1}$ per day.

### 3.7.3 Parameter sensitivity

We explored the parameter sensitivity of the result that pre-sensitised infections can increase in response to vector control targeting vector survival using the ODE model (Fig. 3.7). The change in the number of pre-sensitised infections due to control is driven by the change in 1) the availability of pre-sensitised susceptible hosts, and 2) the force of infection. Therefore, the increase in the number of pre-sensitised infections is most pronounced in parameter spaces where the change in the availability of pre-sensitised susceptible hosts due to control is large (e.g., low rate of loss of saliva pre-exposure effect, $\theta_{H'}$) and the force of infection is high (e.g., high vector biting rate, $b$).

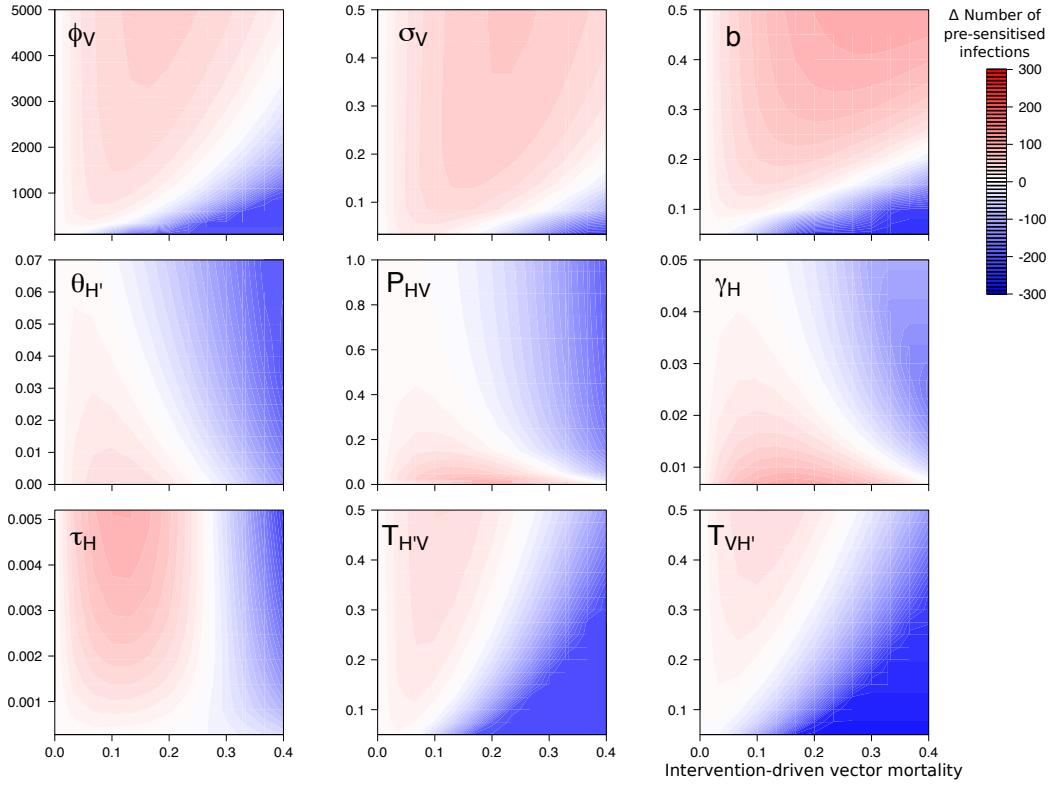


Figure 3.7: Parameter sensitivity. Contour plots show the change of the number of pre-sensitised infections as a function of the rate of intervention-driven vector mortality ($\mu_V$; x-axis) and a parameter of interest labelled on each y-axis. Parameters explored in the ODE model are vector birth rate ($\phi_V$), parasite incubation rate in the vector ($\sigma_V$), vector biting rate ($b$), rate of loss of saliva pre-exposure effect ($\theta_{H'}$), pre-sensitisation probability upon contact ($P_{HV}$), recovery rate of naïve hosts ($\gamma_H$), rate of loss of acquired immunity ($\tau_H$), transmission probability from naïve host to vector ($T_{VH}$) and transmission probability from pre-sensitised host to vector ($T_{VH'}$). Areas in red show increasing number of pre-sensitised infections in response to vector control, while areas in blue decreasing pre-sensitised infections. (The y-axes delineates the baseline conditions of no vector control and only natural vector mortality). The parameter ranges explored are given in Table 3.1. Parameters that are not explicitly varied in each panel are set as defaults in Table 3.1 .

# Chapter 4

# Temperature-dependent variation in the extrinsic incubation period elevates the risk of vector-borne disease emergence

This work was carried out in collaboration with Megan Greischar (University of Toronto), Kiran Wadhawan (University of Toronto), Benjamin Gilbert (University of Toronto), Krijn Paaijmans (Arizona State University) and Nicole Mideo (University of Toronto).

Contents of this chapter have been published in Kamiya et al.,. Temperature-dependent variation in the extrinsic incubation period elevates the risk of vector-borne disease emergence. *Epidemics*. 2020, 30, 100382.

## 4.1 Abstract

Identifying ecological drivers of disease transmission is central to understanding disease risks. For vector-borne diseases, temperature is a major determinant of transmission because vital parameters determining the fitness of parasites and vectors are highly temperature-sensitive, including the extrinsic incubation period required for parasites to develop within the vector. Temperature also underlies dramatic differences in the individual-level variation in the extrinsic incubation period, yet the influence of this variation in disease transmission is largely unexplored. We incorporate empirical estimates of dengue virus extrinsic incubation period and its variation across a range of temperatures into a stochastic model to examine the consequences for disease emergence. We find that such variation impacts the probability of disease emergence because exceptionally rapid, but empirically observed incubation — typically ignored by modelling only the average — increases the chance of disease emergence even at the limits of the temperature range for dengue transmission. We show that variation in the extrinsic incubation period causes the greatest proportional increase in the risk of disease emergence at cooler temperatures where the mean incubation period is long, and associated variation is large. Thus, ignoring EIP variation will likely lead to underestimation of the risk of vector-borne disease emergence in temperate climates.

## 4.2 Introduction

Temperature is a key climatic feature driving the risk of vector-borne diseases, impacting the vital performance of arthropod vector species (Dell et al., 2011) as well as the development of parasites within those vectors (Paaijmans et al., 2011; Liu et al., 2017). Many traits of vectors and parasites exhibit unimodal thermal performance curves, with the peak performance observed at some intermediate temperature (Mordecai et al., 2013). Mathematical models taking into account these relationships have predicted that the estimates of disease risks are highly temperature-sensitive (Mordecai et al., 2013; Johnson et al., 2015; Mordecai et al., 2017*a*), and their predictions have been instrumental in understanding the expanding threat of vector-borne diseases in the context of climate change.

A growing body of experimental studies documents the time-course of pathogen incubation and maturation in arthropod vectors, showing considerable variation in the time it takes for a vector to become infectious following exposure, known as the extrinsic incubation period (EIP) (e.g., West Nile virus (Reisen et al., 2006; Johansson et al., 2010); malaria (Paaijmans et al., 2011); bluetongue virus (Carpenter et al., 2011); dengue (Carrington et al., 2013; Chan and Johansson, 2012)). The process of extrinsic incubation involves a journey through several vector tissues and organs. For example, in dengue virus, the mosquito stage of the virus's lifecycle starts when the mosquito ingests a blood meal from an infectious host. After the virus spreads and multiplies in the midgut, viral particles migrate to various tissues before reaching the salivary gland, from where the virus can be transmitted, and the vector thus becomes infectious (Guzman et al., 2016). For many vector-borne parasites, the timing of incubation is crucial for their success because the average adult lifespan of a female mosquito is comparable to the average EIP. Empirical data for dengue show that the timing is particularly tight at both temperature extremes, where the expected EIP is the same or longer than the expected lifespan (Fig. 4.1a). Under these conditions, the odds are stacked against a "typical" parasite in a "typical" vector (i.e., infection with the expected EIP duration) to successfully complete incubation before the vector dies due to extrinsic causes. The probability of successfully completing incubation, and the vector

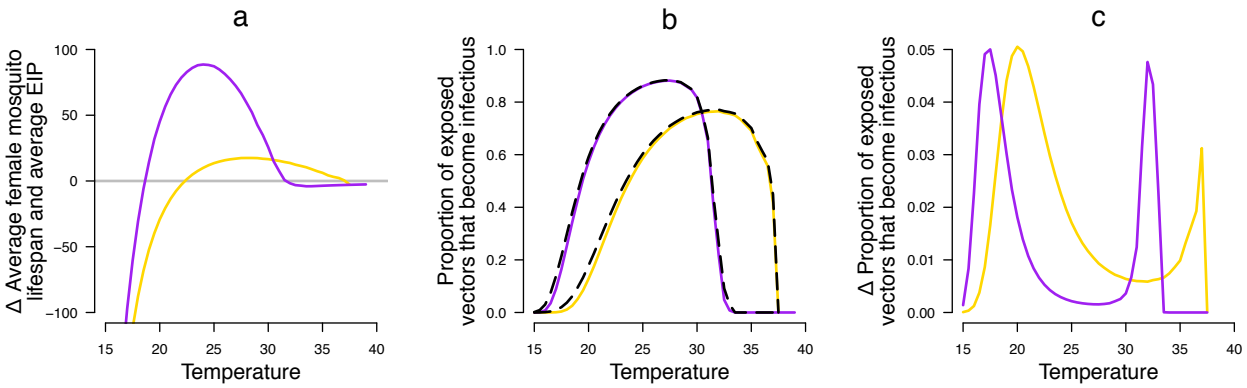


Figure 4.1: At low and high temperatures, dengue viruses face a tight race against time to complete incubation before the vector dies. a) The difference between the expected lifespan of female adult mosquitoes and the expected duration of EIP. Below the grey line, the average incubation period exceeds the average vector lifespan. b) The proportion of exposed vectors that become infectious calculated based on the population average EIP, $e^{-\mu\,\mathrm{E[EIP]}}$ (solid lines), and the proportion calculated with realistic distribution of EIP duration, $\mathrm{E}[e^{-\mu\,\mathrm{EIP}}] = \int_0^\infty e^{-\mu\,\mathrm{EIP}} PDF(\mathrm{EIP}) d\mathrm{EIP}$ where $PDF(\mathrm{EIP})$ refers to the probability density function of the EIP distribution. For dengue virus, $PDF(\mathrm{EIP})$ is best described by the log-normal distribution for a given temperature (Chan and Johansson, 2012) (black dashed lines). c) The elevated proportion of exposed vectors that become infectious due to incubation variation peaks at both ends of the temperature range suitable for dengue transmission. The colours, yellow and purple, indicate the two primary mosquito vectors of dengue, *Aedes aegypti* and *A. albopictus*, respectively. The estimates for mosquito mortality and EIP distributions were adopted from Mordecai et al. (2017*a*) and Chan and Johansson (2012), respectively.

becoming infectious to the next vertebrate host, diminishes exponentially with every passing moment after infecting a mosquito because the vector is expected to suffer extrinsic mortality due to, for example, pollutants, solar radiation, and predation. As a result, there is an accelerating benefit in reducing EIP, and hence parasites with a short EIP enjoy a disproportionate fitness advantage through increased incubation success.

Crucially for understanding temperature-dependent disease risks, temperature affects both the mean and variability of the duration of EIP: in dengue virus, it has been shown that both the expected duration of EIP and the variation around that expectation decrease with increasing temperature (Fig. 4.2, Chan and Johansson, 2012). The understanding of how temperature mediates EIP variation is important for its impact on the proportion of exposed vectors that survive to become infectious (i.e., probability of successful incubation), an effect that can be explained mathematically by Jensen's Inequality (reviewed in Denny, 2017). Assuming a constant rate of extrinsic mortality, $\mu$, the probability that an exposed vector survives a period of time, $e^{-\mu\,t}$, decays exponentially with time, $t$. Therefore, the probability that an exposed vector survives to become infectious, $e^{-\mu\,\mathrm{EIP}}$, is a convex function of time, as supported by mark-recapture data of female *Aedes aegypti* in the field (Harrington et al., 2014). Due to this convex relationship, Jensen's Inequality implies that the expected proportion of exposed vectors that become infectious for a distribution of EIP values, $\mathrm{E}[e^{-\mu\,\mathrm{EIP}}]$, is greater than, or equal to, the conventional estimate, $e^{-\mu\,\mathrm{E[EIP]}}$, which is the same proportion calculated based on the population average EIP (Fig. 4.1b). Failing to incorporate realistic EIP variation (Chan and Johansson, 2012) will, therefore, lead to underestimating the proportion of vectors that survive to become infectious. Focusing on two primary mosquito vectors of dengue, Figure 4.1c shows that the maximum difference between $\mathrm{E}[e^{-\mu\,\mathrm{EIP}}]$

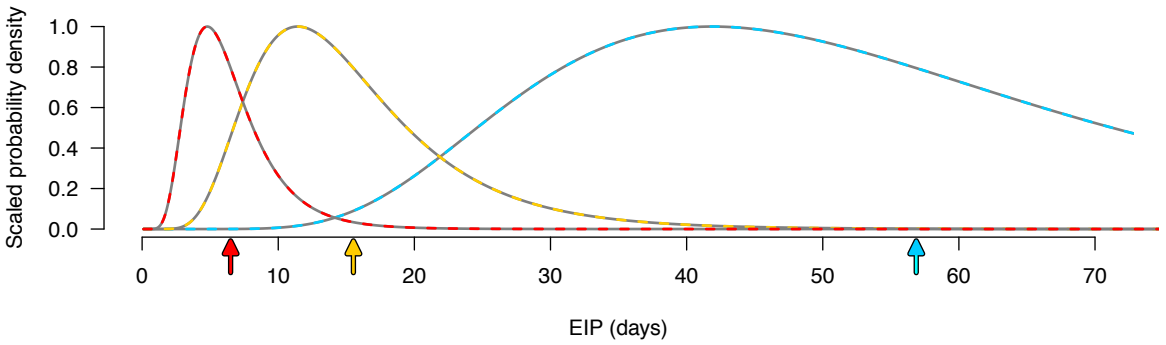


Figure 4.2: Both the mean and variation of the duration of dengue extrinsic incubation period (EIP) are temperature-sensitive. The lines indicate the log-normally distributed duration of EIP estimated in *Aedes* mosquitoes by Chan and Johansson (2012) with colours (blue, yellow, and red) representing temperatures (20C, 25C, 30C, respectively). The arrows indicate the average EIP at the corresponding temperature. The dataset used to estimate the temperature-dependent probability distributions contained both *Aedes aegypti* and *A. albopictus*, though *A. aegypti* was overrepresented in the data (140 versus 6 observations, Chan and Johansson, 2012).

and $e^{-\mu\,\mathrm{E[EIP]}}$ is estimated at approximately 5%. The biological intuition behind this increase is that exceptional cases completing incubation faster than the population average have greater odds of surviving the duration of EIP.

Despite being a key component of the vector-borne disease lifecycle, a large fraction (∼38%) of epidemiological models ignore extrinsic incubation altogether (Reiner et al., 2013). Furthermore, even models that consider the process often opt for mathematically convenient simplifications of the biology, for example by ignoring variation (i.e., assuming EIP follows a Dirac delta distribution, e.g., Paaijmans et al., 2009), or assuming that EIP is exponentially distributed (e.g., Carvalho et al., 2019). Importantly, these contrasting assumptions about EIP variation can quantitatively alter the estimation of disease risks (Chapter 3; Kamiya et al., 2017). With growing attention to the causes and consequences of variability in extrinsic incubation (Rudolph et al., 2014; Christofferson et al., 2016; Ohm et al., 2018), several recent epidemiological models have relaxed conventional assumptions of EIP distribution to reflect empirical evidence. For example, realistic EIP variation has been shown analytically to elevate conventional disease risk estimates (Brand et al., 2016), and variation has been incorporated into differential equation models of disease dynamics by assuming a Gamma distribution (i.e., using a linear chain trick, Robert et al., 2019). An increasing number of studies make use of the distributions of viral and vector traits to estimate uncertainty in epidemiological properties such as the basic reproductive number, vectorial capacity, generation interval and epidemic growth (Karl et al., 2014; Perkins et al., 2016; Siraj et al., 2017; Codeço et al., 2018). Furthermore, empirically measured EIP variability has been incorporated into individual-based simulations to reveal variation in disease risks among dengue genotypes (Fontaine et al., 2018).

Here, we use dengue virus as a case study to illustrate the impact of temperature-dependent EIP variation on disease emergence using a stochastic individual-based simulation approach. We take advantage of the meta-analytic estimates of empirical EIP distributions published by Chan and Johansson (2012) who compiled EIP data for dengue virus from 35 studies to determine that the variation in EIP is best described by the log-normal distribution (Fig. 4.2). We predict the probability of dengue virus

emergence and epidemic size in a human population given the introduction of a single infected human across a range of temperatures and mosquito-to-human ratios. We find that variation in the EIP elevates the disease risk because exceptionally rapid incubation — which would be ignored by modelling only the average — increases the chance of disease emergence, even outside the temperature range where dengue transmission is commonly expected. We show that the proportional increase in the risk of disease emergence due to EIP variation is greater at cooler temperatures where the mean EIP is long, and its variation is large. This finding has implications for predicting the geographical distribution and the transmission season of dengue virus.

## 4.3 Methods

We used a stochastic algorithm to simulate a classic Ross-Macdonald model as a system of delay differential equations that mirror the epidemiology of dengue virus in a human population (reviewed in Smith et al., 2012). Following Barrio et al. (2006), we implemented a fixed duration process (viral incubation within mosquitoes) in an otherwise standard method for stochastically simulating ordinary differential equations (i.e., Gillespie algorithm). The dynamics of the mosquito population are governed by:

$$\frac{dM_S(t)}{dt} = \lambda M_T(t) - (\mu + rT_{MH}H_I(t))M_S(t) \tag{4.1a}$$

$$\frac{dM_E(t)}{dt} = rT_{MH}H_I(t)M_S(t) - \mu M_E(t) - r(T_{MH}H_I(t-\mathrm{EIP})M_S(t-\mathrm{EIP})\mathrm{e}^{-\mu\,\mathrm{EIP}} \tag{4.1b}$$

$$\frac{dM_I(t)}{dt} = r(T_{MH}H_I(t-\mathrm{EIP}))M_S(t-\mathrm{EIP})\mathrm{e}^{-\mu\,\mathrm{EIP}} - \mu M_I(t). \tag{4.1c}$$

In this model, susceptible mosquitoes, $M_S$, were born at a per-capita rate, $\lambda$. We kept the mosquito population size constant (so, $\lambda = \mu M_T$, where $M_T$ and $\mu$ are the total population size and the rate of mosquito extrinsic mortality, respectively), in order to forgo the vast complexity of processes governing the larval mosquito dynamics (Beck-Johnson et al., 2013), for which there is a dearth of data on *Aedes* mosquitoes. We assumed that all mosquitoes experience the same mortality rate, $\mu$, regardless of their infection status. In our model, mosquitoes were equally likely to bite a host of any class, so hosts get bitten by a given mosquito at the rate $r$, calculated as the per mosquito biting rate, $b$, divided by the total host population size, $H_T$, making disease transmission frequency-dependent (Keeling and Rohani, 2008). A susceptible mosquito becomes exposed, $M_E$, to the virus when it bites an infected host, $H_I$, with the probability $T_{MH}$. If a mosquito gets exposed to the virus, the process of viral incubation — i.e., transition from exposed, $M_E$, to infectious, $M_I$ (Eq. 4.1b & c) — takes the exact duration of EIP. In the stochastic simulation, the duration of EIP was assigned to each mosquito at birth, making the model individual-based with respect to the duration of EIP. An exposed mosquito survives the duration of EIP with probability $\mathrm{e}^{-\mu\,\mathrm{EIP}}$. The individual EIP value in a polymorphic population (with realistic EIP variation) was determined by randomly sampling from the empirically derived lognormal distribution estimated by Chan and Johansson (2012) who compiled EIP data for dengue virus from 35 studies. From their model (their Eq. 1 and Table 1; Chan and Johansson, 2012) and parameter estimates (their Table 2, 4th row; Chan and Johansson, 2012), we obtained the distribution of EIP across a range of temperatures (Fig. 4.2). In a mosquito population monomorphic for the duration of EIP (i.e., ignoring EIP variation), the average duration of EIP (often referred to as $\mathrm{EIP}_{50}$, Christofferson et al., 2016) at

the appropriate temperature was assigned to every mosquito at birth.

The host population was modelled as a compartmental susceptible-exposed-infected-recovered (SEIR) model,

$$\frac{dH_S(t)}{dt} = -rT_{HM}M_I(t)H_S(t) \quad (4.2a)$$

$$\frac{dH_E(t)}{dt} = rT_{HM}M_I(t)H_S(t) - \theta H_E(t) \quad (4.2b)$$

$$\frac{dH_I(t)}{dt} = \theta H_E(t) - \gamma H_I(t) \quad (4.2c)$$

$$\frac{dH_R(t)}{dt} = \gamma H_I(t), \quad (4.2d)$$

where $T_{HM}$, $\theta$ and $\gamma$ are the probability of mosquito-to-human viral transmission, viral incubation rate in humans and human recovery rate, respectively. The average latent period of dengue virus in humans has been estimated at 5.9 days (Chan and Johansson, 2012, i.e., $\theta = 5.9^{-1}$ per day) and patients typically recover from dengue fever after a week (Guzman et al., 2016, i.e., $\gamma = 7^{-1}$ per day). Robust immune responses against dengue confer life-long protection for a given serotype (Guzman et al., 2016); thus we did not consider waning immunity in this model. The human population size was set to 1000 and we explored a range of values for the total mosquito density, $M_T$, as reliable estimates of the mosquito-to-human ratio are rare. We parameterised the rest of the model with temperature-dependent empirical estimates published by Mordecai et al. (2017*a*). Specifically, we used GraphClick (Arizona-Software, 2010) to extract the estimated dengue virus trait values from their Fig. 1 and Fig. A in Supporting information 1 for *A. aegypti* and *A. albopictus*, respectively (Mordecai et al., 2017*a*). We list the parameter values used in the simulations in Supplementary Information 1. The complete collection of data by Mordecai et al. (2017*a*) are available online (Mordecai et al., 2017*b*).

We estimated the probability of disease emergence as the fraction of runs (of 10000 replicates) for which the introduction of a single infected human to the entirely susceptible population led to at least one secondary human infection. We quantified the relative effect of EIP variation as the log risk ratio ($lnRR$, also known as relative risk) of the probability of disease emergence in simulations with realistic EIP variation to the probability of disease emergence in simulations only considering the population average EIP, keeping all other parameters constant.

## 4.4 Results & Discussion

Using a stochastic simulation model parameterised for dengue virus, we found that realistic variation in EIP across exposed mosquitoes elevates disease emergence risks in human populations (Fig. 4.3). Specifically, our results demonstrate that EIP variation in either of the primary dengue vector species, *Aedes aegypti* or *A. albopictus*, increases the chance that the introduction of a single infected host causes secondary human infections in a fully susceptible population, at a given temperature. As a consequence, EIP variation extends the temperature range over which disease emergence can occur, particularly at the lower extreme. These effects are amplified with increasing mosquito-to-human ratios (Fig. 4.3).

The relative impact of EIP variation was most pronounced at the fringe of the temperature range that allows for dengue emergence (Fig. 4.4), meaning that assuming a constant, average EIP will underestimate the risk. When the climatic conditions are sub-optimal for dengue transmission — for

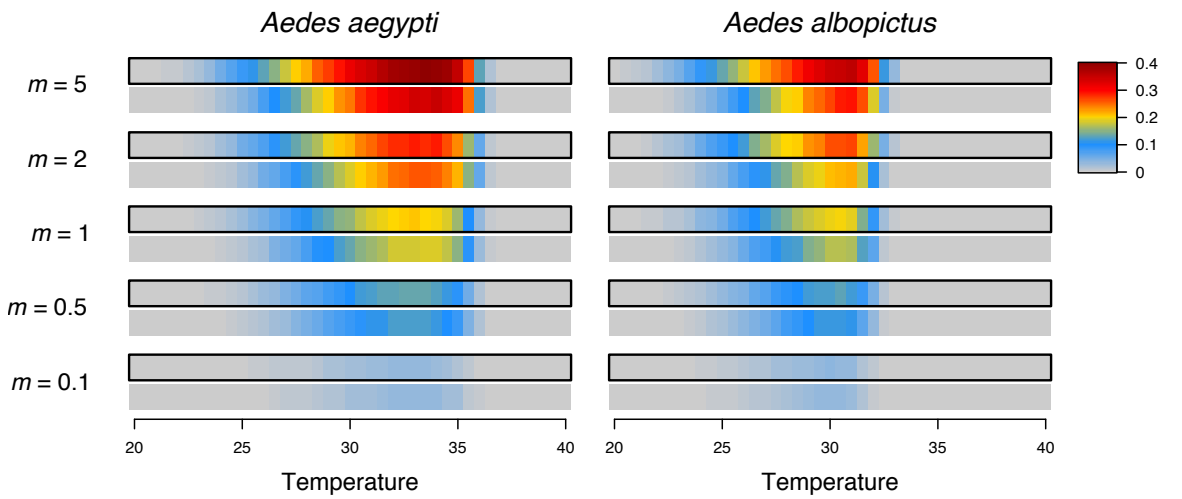


Figure 4.3: Variation in viral EIP elevates the risk of dengue emergence in human populations. The model that incorporates realistic incubation variation (outlined in black) predicts elevated risk of disease emergence for human populations assuming dengue is vectored by either *Aedes aegypti* or *A. albopictus*, compared to the conventional approach that ignores variation (no outline). The probability of disease emergence (indicated by colours) given the introduction of a single infected host (i.e., production of one or more secondary human infection(s)) was calculated assuming a mosquito population comprised solely of either *A. aegypti* and *A. albopictus* across a range of temperatures (x-axis) and mosquito-to-human ratios, $m$ (y-axis).

example, when the race between incubation and mosquito mortality is tight — disease transmission is largely carried out by a small fraction of exceptional vectors that complete EIP faster than the population average. This phenomenon is ignored in a conventional fixed-EIP approach. The finding that variation in EIP has a stronger impact at low temperatures is due to the interplay between the distribution of EIP and other temperature-dependent vital parameters. First, the distribution of dengue EIP for a given temperature is best explained by the log-normal distribution, for which the variance increases with the mean (Chan and Johansson, 2012). Therefore the variation in EIP is larger at lower temperatures where the mean duration in EIP is also long. Second, a number of other factors governing the interaction between dengue virus and mosquitoes are temperature-dependent, and so they also shape the temperature range suitable for disease emergence. For example, the spike in the proportion of exposed vectors that become infectious due to variation in *A. aegypti* at the high temperature range (Fig. 4.1c ∼37C) has little effect since the probability of an exposed mosquito becoming infectious tends towards zero beyond 35C for this species (Mordecai et al., 2017*a*, Fig. 4.1b ∼37C). Thus, the influence of incubation variation at the high-temperature end, in particular, is buffered by a sharp decline in other vital parameters of the mosquito and virus.

Our model was parameterised with the most comprehensive estimates of temperature-dependent dengue EIP variation and mosquito vital parameters published by Chan and Johansson (2012) and Mordecai et al. (2017*a*), respectively. While primary observations are rather sparse at high temperatures in these studies, our finding that the relative impact of EIP variation is largest at lower temperatures is likely robust as parameter estimates were based on relatively more data at the lower temperature range (Mordecai et al., 2017*a*; Chan and Johansson, 2012). Because the relationship between mosquito and human densities is highly complex (Romeo-Aznar et al., 2018), we explored the impact of EIP variation

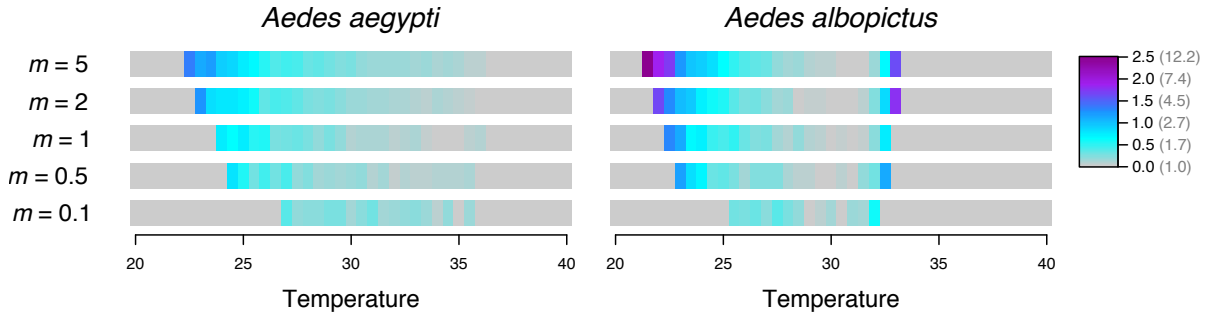


Figure 4.4: The impact of EIP variation on dengue emergence is strongest at the lower fringe of the temperature range that allows for dengue transmission. The log risk ratio ($lnRR$, shown in colours) was calculated as the natural logarithm of the ratio between the probabilities of disease emergence when taking EIP variation into account versus not, i.e., the values presented in Fig. 4.3 with and without the black outline, respectively. The colour legend shows $lnRR$ (in black) with the corresponding linear-transformed risk ratio in parentheses (in grey): for example, $lnRR = 2$ indicates a 7.4-fold increase in the probability of disease emergence. In calculating $lnRR$, we focused on simulations where the probability of disease emergence with EIP variation exceeded 1% to disregard extremely rare events.

across a range of mosquito-to-human ratios. We find that the impact of EIP variation increases with the mosquito-to-human ratio, indicating that incorporating EIP variation is most important for accurate prediction of disease risk in areas of high relative mosquito density (Fig. 4.4).

We next explored the size of additional epidemics expected due to EIP variation. We found an over-representation of minor epidemics — defined as those in which less than 10% of the human population becomes infected — under sub-optimal conditions for dengue transmission (e.g., low mosquito-to-human ratio and fringe temperatures, Fig. 4.5). This result suggests that EIP variation — and the few exceptionally rapidly incubating infections that result from it — increases the chance of short transmission chains involving a small handful of humans even when the deterministic force of infection is too weak to sustain transmission. These epidemics, which are small and rare, yet still concerning from a public health perspective, would be overlooked by the conventional approach that ignores EIP variation. Put another way, EIP variation reduces the chance of disease extinction due to demographic stochasticity. As a consequence, the model that takes into account EIP variation predicts the more frequent occurrence of epidemics across the entire temperature range (Fig. 4.5).

To highlight the impact of temperature-dependent EIP variation in a geographical context, we predicted the probability of disease emergence across the continental United States, using average temperature in July (Matsuura and Willmott, 2018), the warmest month in North America. We note that our projection here offer insight about relative (rather than absolute) risk: while we allow temperature to determine EIP variation and other virus and vector traits, we assume all else is equal across this geographic range. Figure 4.6 shows that ignoring the variation would lead to underestimation of dengue risk in its entire geographical range, but particularly at the expanding northern edge, for example in cities like Indianapolis (IN) and Philadelphia (PH), but less so in Austin (AU) — three US cities within the range of *A. albopictus* predicted by the Center for Disease Control (CDC, 2017). Furthermore, since EIP variation increases the risk at low temperatures and never reduces it (Fig. 4.4), the standard approach is likely to underestimate the duration of dengue transmission seasons. Again, the predicted pattern demonstrates that the impact of EIP variation increases with the mosquito-to-human ratio, indicating that ignoring EIP variation also leads to a severe underestimation of disease risk in areas with high

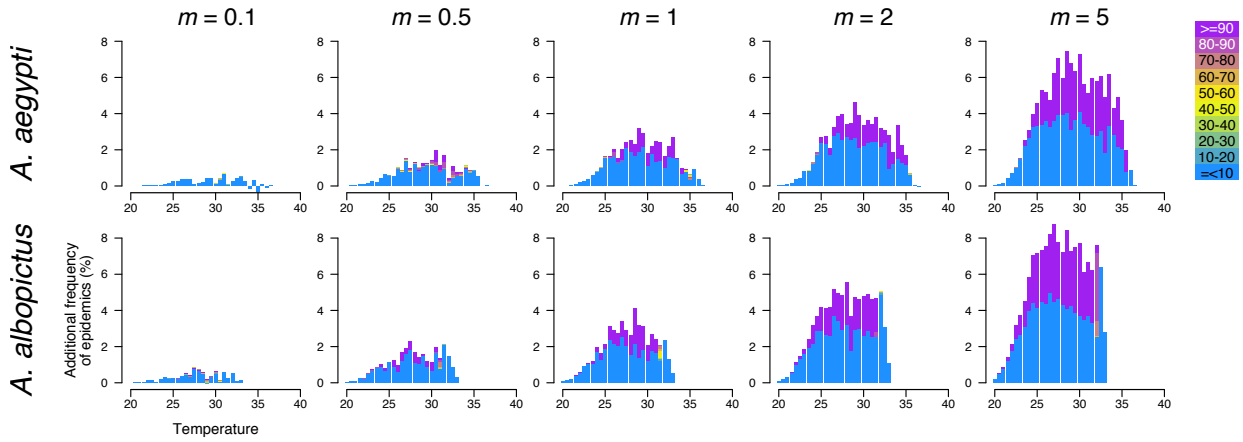


Figure 4.5: Realistic EIP variation uncovers epidemics unaccounted for by the conventional approach that ignores EIP variation. Plotted in stacked histograms is the difference in the frequency of epidemics between simulations with and without EIP variation across a range of temperatures and mosquito-to-human ratios, $m$, for *Aedes aegypti* and *A. albopictus*. The colours indicate the epidemic size measured as the proportion of the human population cumulatively infected during an epidemic, with blue and purple indicating minor ($\leq 10\%$) and major ($\geq 90\%$) epidemics, respectively.

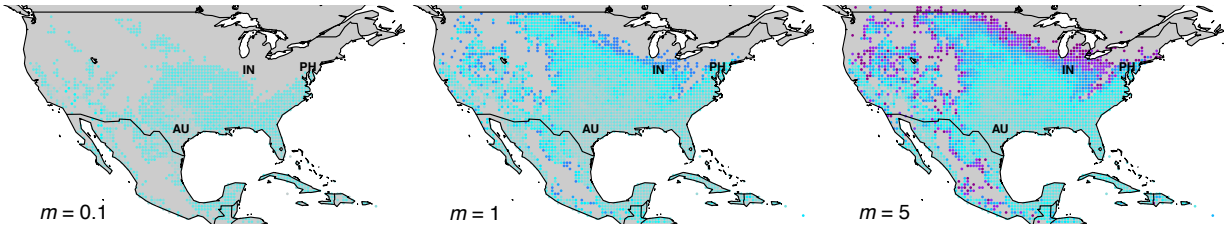


Figure 4.6: Ignoring EIP variation underestimates the disease risk in its entire geographical range, but particularly at the temperate edge, for example in cities like Indianapolis (IN) and Philadelphia (PH), but less so in Austin (AU) where the climate is warmer. The colour indicates the impact of EIP variation (measured as $lnRR$ of the probability of disease emergence with and without realistic EIP variation; as shown in Fig. 4.4, which uses the same scale) on the probability of disease emergence by *A. albopictus* in July. In calculating $lnRR$, we focused on simulations where the probability of disease emergence with EIP variation exceeded 1% to disregard extremely rare events.

relative mosquito density (Fig. 4.4 & 4.6). However, since mosquito abundance is climate-driven and generally lower in the fringes of the species' ranges (Li et al., 2019), the actual elevated risk may not be as exaggerated as our most extreme predictions indicate (Fig. 4.6, right panel). Nonetheless, accurate prediction of the risk of dengue emergence locally will rely on a fine-scale understanding of local mosquito abundance, and ultimately, the mosquito-to-human ratio.

In the present study, we assumed that female adult mosquitoes experience constant mortality due to extrinsic causes, as assumed by the standard approach in vector-borne disease modelling. In reality, extrinsic sources of mortality most likely operate alongside intrinsic causes, which leads to senescence and age-dependent mosquito survival (Harrington et al., 2014). Per Jensen's Inequality, the impact of EIP variation would differ qualitatively if young adult female mosquitoes rarely experience mortality such that mosquito survival is a concave function of time. However, we believe such a situation is unlikely because field mark-recapture data support a convex relationship between mosquito survival and time (Harrington et al., 2014), and the finding that estimated mosquito survival is lower in mark-recapture

experiments carried out in the wild compared to laboratory experiments also supports the role of extrinsic mortality in wild mosquito populations (Ryan et al., 2015). Little is known about the relative importance of different sources of mortality in the wild and it appears context-dependent (e.g., with respect to the climate, Hugo et al., 2014). Future predictive models will benefit from an understanding of mosquito survival in the wild with respect to both temperature and age, information that, to our knowledge, is currently only available for malaria vectors in a laboratory setting (Shapiro et al., 2017).

Recent years have seen sporadic re-emergence of vector-borne diseases in temperate regions where they had been absent for decades (Bouri et al., 2012; Tomasello and Schlagenhauf, 2013; Schaffner and Mathis, 2014; Lai et al., 2015). Because major dengue epidemics are unlikely to occur in these areas (Mordecai et al., 2017*a*), our primary focus was to better understand the impact of temperature-dependent individual heterogeneity on stochastic occurrences of small disease outbreaks that would be overlooked by deterministic modelling. Our individual-based simulations demonstrated that failing to incorporate variability in the duration of EIP across individual vectors can lead to a severe underestimation of the risk of minor epidemics and duration of potential dengue exposure in cooler climates. Although researchers should also consider more analytically tractable modelling approaches (e.g., branching process theory and Kolmogorov equations, Lloyd et al., 2007), stochastic individual simulations are appealing for studying the impact of heterogeneities in vector-borne diseases due to their ability to accommodate comprehensive empirical knowledge (Perkins et al., 2019).

Dengue virus offers the most comprehensive documentation on temperature-sensitive measures of mosquito and pathogen traits and EIP variation to date. Nonetheless, we expect that the basic mathematical principle underlying the inflation of disease risk due to variation — Jensen's Inequality due to the convex relationship between the duration of EIP and extrinsic incubation success — applies widely across vector-borne diseases. Thus, variation in EIP is likely to elevate disease risks in other vector-borne diseases, though the exact quantitative impact is likely to vary across diseases and vector species, as we found in our comparisons of *A. albopictus* and *A. aegypti*. Furthermore, while we here focused solely on temperature-dependent variability in EIP, a future challenge is to characterise and integrate the knowledge of variability in multiple vector and parasite life-history traits and their covariation across a range of temperatures (Vazquez-Prokopec et al., 2016). Individual-based simulations, together with a growing body of experimental data, will offer further opportunities to achieve a more comprehensive understanding of the role of individual heterogeneity in vector-borne disease epidemiology.

# Thesis conclusion

The research presented in this thesis uncovered within-host origins, and explored the between-host consequences, of heterogeneities in vector-borne diseases. In the first half, I examined how differences in within-host ecological processes generate variation in the parasite dynamics and health outcomes of malaria infection across an environmental gradient (Chapter 1) and host genetic backgrounds (Chapter 2). In the latter half, I presented host population-level consequences of variation generated by tri-trophic interactions between parasites, hosts, and arthropod disease vectors (Chapter 3), and of temperature-dependent heterogeneity in within-vector processes that govern the timing of infectivity (Chapter 4).

Each chapter of this thesis highlighted the benefits of an exchange of ideas and methodologies across study disciplines. For instance, in Chapter 1, I formulated parameters of a dynamical model as reaction norms — a classic concept in evolutionary ecology — to infer patterns of host and parasite phenotypic expression across an environmental gradient, i.e., initial infection dose. I demonstrated that a quantitative genetics framework to analyse reaction norms is a powerful tool to study processes of within-host infection, which are usually influenced by environmental variables. In Chapter 2, I adopted a hierarchical Bayesian approach to fit a mechanistic within-host infection model to experimental infection data. Hierarchical modelling integrates multiple levels of variation; for example, in this case, variation among mouse strains, and nested within it was variation among individuals of the same mouse strain. By modelling individual heterogeneity as samples from a distribution, and estimating properties of the distribution under a Bayesian framework that incorporates prior knowledge, a hierarchical Bayesian approach excels at explaining complex datasets. While many of the cutting-edge concepts and methodologies of this approach have been developed in social sciences (Gelman, 2006, 2011; Gelman et al., 2013; Carpenter et al., 2017), applications in biological sciences are growing in recent years. The work presented in Chapter 2 demonstrated that it is an ideal approach for modelling experimental within-host infection data. Throughout this thesis, I approached infectious disease systems with the lens of an ecologist. In Chapter 3, I explored the epidemiological consequence of non-infectious bites of arthropod vectors that "prime" or pre-sensitise host immunity. Although every vector-borne disease system involves at least three species (i.e., vectors, hosts and parasites), interactions between vectors and hosts are relatively overlooked in the epidemiology literature. In contrast, other areas of ecology have paid a more equal attention to each interaction of tri-trophic relationships (e.g., plant-herbivore-predator interactions (Turlings and Erb, 2018)). Having a broader ecological perspective, therefore, was a valuable asset for discovering lines of questions previously unexplored. Finally, in Chapter 4, I adopted a modified Gillespie algorithm of biochemical reactions (Barrio et al., 2006) to develop an individual-based model that simulates infection events with an exact waiting time. This approach is more flexible than the conventional stochastic simulation used in epidemiology because it can simulate samples from any probability distribution and direct empirical measurements of modelled parameters. Also, since the approach is individual-based, it is likely more accessible to biologists and epidemiologists, who may be less familiar with derivations of analytical stochastic models.

To a large extent, clinical and public health applications guide research questions asked by infectious disease scientists. Yet, the ability to find applied solutions — for better treatment, control and prevention — stems from the foundation of basic knowledge about the biology of parasites and their hosts. The work presented in this thesis sought fundamental understandings of within- and between-host ecology of vector-borne diseases, keeping in mind implications for clinical and public health. For example, I found that the host clears malaria parasites most effectively at an intermediate infection dose due to a non-monotonic impact of the infection dose on immune responses (Chapter 1). This finding

has potential implications for optimal dosing of anti-malaria vaccines, as the maximum possible antigen dose may not result in optimal protection. In Chapter 2, I uncovered the functional diversity of host resilience to malaria infections, finding that malaria-induced mortality in mice is associated with insufficient or excessive immune responses depending on the host genetic background. My work, therefore, suggests that immunotherapy and symptom mitigation treatments ought to be individually tailored to maximise safety and efficacy. In Chapter 3, I demonstrated that moderate-intensity insecticide spraying could inadvertently increase vector-borne disease transmission when uninfected vector bites mitigate disease symptoms. Finally, the epidemiological model presented in Chapter 4 cautioned that ignoring temperature-dependent variation in parasite development within vectors likely underestimates the risk of vector-borne disease emergence in temperate climates.

The work carried out during my PhD inspired new avenues of research. Below I discuss two potential extensions of the work presented in this thesis:

**Identifying the genetic basis of host responses** Host defences shape within-host parasite dynamics. Therefore, characterising the genetic markers of interactions between host responses and parasites is likely key to better understanding why some hosts suffer more than others from the same infectious agent. I am currently working on characterising the functional diversity of host responses by fitting dynamical models developed in this thesis (Chapters 1 & 2) to a large panel of laboratory mice, whose chromosomes are fully mapped. By conducting quantitative trait locus (QTL) analysis, I plan to identify regions of the mouse genome that are linked to variation in host functional responses against malaria infection.

**Measuring and incorporating realistic trait distributions in all parameters of an epidemiological model** The quest for a fuller understanding of heterogeneity is not unique to epidemiology, but universal to population ecology. In Chapter 4, I have demonstrated the epidemiological consequence of empirically informed temperature-dependent variation in one parameter (i.e., extrinsic incubation period) of an epidemiological model of vector-borne diseases. However, realistic distributions in multiple, let alone all parameters, of an epidemiological system are rarely considered simultaneously. Given that the spread of clinically relevant diseases is impacted by specific assumptions about trait variation (e.g., infectiousness; Lloyd-Smith et al., 2005), a better understanding of the extent and impact of realistic heterogeneity in multiple traits (e.g., time to encounter, recovery and death) is warranted in more disease systems. It is important to obtain a multi-dimensional understanding of trait heterogeneity also because trait heterogeneities are often coupled (Vazquez-Prokopec et al., 2016). Thus, ignoring heterogeneity in one trait could bias the estimation of others. From a modelling perspective, it is straightforward to extend the flexible individual-based modelling approach that I developed in Chapter 4 to incorporate the exact waiting time sampled from multiple empirical distributions. A major challenge, however, lies currently in the dearth of detailed data of multiple trait heterogeneities. A promising avenue is to measure trait variation and epidemiological dynamics in a tractable laboratory system (e.g., *Daphnia*; Kirk et al., 2018) where distributions of individual traits and the time course of an epidemic can be measured experimentally. Using such data, one could study the relative importance of heterogeneity in different traits.

A retelling of human history would be incomplete without mentioning infectious diseases. They are a significant part of the present, and will probably be of the future. Perhaps that is not particularly surprising considering half of all life forms adopt a parasitic lifestyle (Poulin and Morand, 2014). Yet, one cannot be blamed for feeling anxious about a future riddled with microscopic creatures that are sometimes deadly. An optimist may instead highlight major innovations in infectious disease sciences that led to the vaccine that eradicated smallpox and the anti-viral therapy that prevents HIV positivity from being a death sentence. With the growing availability of large datasets and computational resources, I have no doubt that data-driven modelling — including approaches presented in this thesis — will be an integral part of future innovations to manage, if not eradicate, infectious diseases.

# Bibliography

Aderem, A., J. N. Adkins, C. Ansong, J. Galagan, S. Kaiser, M. J. Korth, G. L. Law, J. G. McDermott, S. C. Proll, C. Rosenberger, et al. 2011. A systems biology approach to infectious disease research: innovating the pathogen-host research paradigm. MBio 2:e00325–10.

Afrough, S., S. Rhodes, T. Evans, R. White, and J. Benest. 2020. Immunologic dose-response to adenovirus-vectored vaccines in animals and humans: a systematic review of dose-response studies of replication incompetent adenoviral vaccine vectors when given via an intramuscular or subcutaneous route. Vaccines 8:131.

Ahmed, S. B. H., I. Chelbi, B. Kaabi, S. Cherni, M. Derbali, and E. Zhioua. 2010. Differences in the salivary effects of wild-caught versus colonized *Phlebotomus papatasi* (Diptera: Psychodidae) on the development of zoonotic cutaneous leishmaniasis in BALB/c mice. Journal of Medical Entomology 47:74–79.

Anderson, R., R. May, and S. Gupta. 1989. Non-linear phenomena in host—parasite interactions. Parasitology 99:S59–S79.

Anderson, R. M., and R. M. May. 1991. Infectious diseases of humans: dynamics and control. Oxford University Press, Oxford.

Andrade, B. B., and C. R. Teixeira. 2012. Biomarkers for exposure to sand flies bites as tools to aid control of leishmaniasis. Frontiers in Immunology 3:121.

Arizona-Software. 2010. Graphclick. `http://www.arizona-software.ch`.

Artavanis-Tsakonas, K., J. Tongren, and E. Riley. 2003. The war between the malaria parasite and the immune system: immunity, immunoregulation and immunopathology. Clinical & Experimental Immunology 133:145–152.

Ashworth, S., C. Kennedy, and G. Blanc. 1996. Density-dependent effects of *Anguillicola crassus* (nematoda) within and on its copepod intermediate hosts. Parasitology 113:303–309.

Babiker, H. A., A. A. Gadalla, and L. C. Ranford-Cartwright. 2013. The role of asymptomatic *P. falciparum* parasitaemia in the evolution of antimalarial drug resistance in areas of seasonal transmission. Drug Resistance Updates 16:1–9.

Barrio, M., K. Burrage, A. Leier, and T. Tian. 2006. Oscillatory regulation of Hes1: discrete stochastic delay modelling and simulation. PLOS Computational Biology 2:e117.

Bates, P. A., J. Depaquit, E. A. Galati, S. Kamhawi, M. Maroli, M. A. McDowell, A. Picado, P. D. Ready, O. D. Salomón, J. J. Shaw, et al. 2015. Recent advances in phlebotomine sand fly research related to leishmaniasis control. Parasites and Vectors 8:131.

Beck-Johnson, L. M., W. A. Nelson, K. P. Paaijmans, A. F. Read, M. B. Thomas, and O. N. Bjørnstad. 2013. The effect of temperature on anopheles mosquito population dynamics and the potential for malaria transmission. PLOS One 8:e79276.

Beier, J. 1993. Malaria sporozoites: survival, transmission and disease control. Parasitology Today 9:210–215.

Beier, J., F. Onyango, J. Koros, M. Ramadhan, R. Ogwang, R. Wirtz, D. Koech, and C. Roberts. 1991. Quantitation of malaria sporozoites transmitted in vitro during salivation by wild afrotropical *Anopheles*. Medical and Veterinary Entomology 5:71–79.

Belkaid, Y., S. Kamhawi, G. Modi, J. Valenzuela, N. Noben-Trauth, E. Rowton, J. Ribeiro, and D. L. Sacks. 1998. Development of a natural model of cutaneous leishmaniasis: powerful effects of vector saliva and saliva preexposure on the long-term outcome of *Leishmania major* infection in the mouse ear dermis. Journal of Experimental Medicine 188:1941–1953.

Bellan, S. E. 2010. The importance of age dependent mortality and the extrinsic incubation period in models of mosquito-borne disease transmission and control. PLOS One 5:e10165.

Ben-Ami, F., R. R. Regoes, and D. Ebert. 2008. A quantitative test of the relationship between parasite dose and infection probability across different host–parasite combinations. Proceedings of the Royal Society B: Biological Sciences 275:853–859.

Bennett, A. 1987. Interindividual variability: an underutilized resource. Pages 147–169 *in* M. Feder, A. Bennett, W. Burggren, and R. Huey, eds. New Directions in Ecological Physiology. Cambridge University Press, Cambridge.

Bjørnstad, O. N. 2015. Nonlinearity and chaos in ecological dynamics revisited. Proceedings of the National Academy of Sciences of the United States of America 112:6252–6253.

Bogdan, C., M. Röllinghoff, and A. Diefenbach. 2000. Reactive oxygen and reactive nitrogen intermediates in innate and specific immunity. Current Opinion in Immunology 12:64–76.

Bopp, S. E., V. Ramachandran, K. Henson, A. Luzader, M. Lindstrom, M. Spooner, B. M. Steffy, O. Suzuki, C. Janse, A. P. Waters, et al. 2010. Genome wide analysis of inbred mouse lines identifies a locus containing Ppar-$\gamma$ as contributing to enhanced malaria survival. PLOS One 5.

Bouharoun-Tayoun, H., C. Oeuvray, F. Lunel, and P. Druilhe. 1995. Mechanisms underlying the monocyte-mediated antibody-dependent killing of *Plasmodium falciparum* asexual blood stages. Journal of Experimental Medicine 182:409–418.

Bouri, N., T. K. Sell, C. Franco, A. A. Adalja, D. Henderson, and N. A. Hynes. 2012. Return of epidemic dengue in the United States: implications for the public health practitioner. Public Health Reports 127:259–266.

Brady, O. J., H. C. J. Godfray, A. J. Tatem, P. W. Gething, J. M. Cohen, F. E. McKenzie, T. A. Perkins, R. C. Reiner, L. S. Tusting, M. E. Sinka, et al. 2016. Vectorial capacity and vector control: reconsidering sensitivity to parameters for malaria elimination. Transactions of the Royal Society of Tropical Medicine and Hygiene 110:107–117.

Brand, S. P., K. S. Rock, and M. J. Keeling. 2016. The interaction between vector life history and short vector life in vector-borne disease transmission and control. PLOS Computational Biology 12:e1004837.

Brodie, T. M., M. C. Smith, R. V. Morris, and R. G. Titus. 2007. Immunomodulatory effects of the *Lutzomyia longipalpis* salivary gland protein maxadilan on mouse macrophages. Infection and Immunity 75:2359–2365.

Brunner, J. L., K. Richards, and J. P. Collins. 2005. Dose and host characteristics influence virulence of ranavirus infections. Oecologia 144:399–406.

Bunn, H. F. 2013. Erythropoietin. Cold Spring Harbor Perspectives in Medicine 3:a011619.

Cabrera, D., L. Colosi, and C. Lobdell. 2008. Systems thinking. Evaluation and Program Planning 31:299–310.

Carpenter, B., A. Gelman, M. D. Hoffman, D. Lee, B. Goodrich, M. Betancourt, M. Brubaker, J. Guo, P. Li, and A. Riddell. 2017. Stan: A probabilistic programming language. Journal of Statistical Software 76.

Carpenter, S., A. Wilson, J. Barber, E. Veronesi, P. Mellor, G. Venter, and S. Gubbins. 2011. Temperature dependence of the extrinsic incubation period of orbiviruses in *Culicoides* biting midges. PLOS One 6:e27987.

Carrington, L. B., M. V. Armijos, L. Lambrechts, and T. W. Scott. 2013. Fluctuations at a low mean temperature accelerate dengue virus transmission by *Aedes aegypti*. PLOS Neglected Tropical Diseases 7:e2190.

Carvalho, S. A., S. O. da Silva, and I. da Cunha Charret. 2019. Mathematical modeling of dengue epidemic: control methods and vaccination strategies. Theory in Biosciences 138:223–239.

Castro-Gomes, T., L. C. Mourão, G. C. Melo, W. M. Monteiro, M. V. Lacerda, and É. M. Braga. 2014. Potential immune mechanisms associated with anemia in *Plasmodium vivax* malaria: a puzzling question. Infection and Immunity 82:3990–4000.

CDC. 2017. Estimated potential range of *Aedes aegypti* and *Aedes albopictus* in the United States. `https://www.cdc.gov/zika/vector/range.html`. Accessed: 2019-01-16.

Chagas, A. C., F. Oliveira, A. Debrabant, J. G. Valenzuela, J. M. Ribeiro, and E. Calvo. 2014. Lundep, a sand fly salivary endonuclease increases *Leishmania* parasite survival in neutrophils and inhibits XIIa contact activation in human plasma. PLOS Pathogens 10.

Chan, M., and M. A. Johansson. 2012. The incubation periods of dengue viruses. PLOS One 7:e50972.

Chang, K.-H., M. Tam, and M. M. Stevenson. 2004. Modulation of the course and outcome of blood-stage malaria by erythropoietin-induced reticulocytosis. Journal of Infectious Diseases 189:735–743.

Charlab, R., J. G. Valenzuela, E. D. Rowton, and J. M. Ribeiro. 1999. Toward an understanding of the biochemical and pharmacological complexity of the saliva of a hematophagous sand fly *Lutzomyia longipalpis*. Proceedings of the National Academy of Sciences of the United States of America 96:15155–15160.

Chong, K. K. L., W. H. Tay, B. Janela, A. M. H. Yong, T. H. Liew, L. Madden, D. Keogh, T. M. S. Barkham, F. Ginhoux, D. L. Becker, et al. 2017. *Enterococcus faecalis* modulates immune activation and slows healing during wound infection. Journal of Infectious Diseases 216:1644–1654.

Christofferson, R. C., C. N. Mores, and H. J. Wearing. 2016. Bridging the gap between experimental data and model parameterization for chikungunya virus transmission predictions. Journal of Infectious Diseases 214:S466–S470.

Chua, C. L. L., G. Brown, J. A. Hamilton, S. Rogerson, and P. Boeuf. 2013. Monocytes and macrophages in malaria: protection or pathology? Trends in Parasitology 29:26–34.

Clark, I., K. Rockett, and W. Cowden. 1991. Proposed link between cytokines, nitric oxide and human cerebral malaria. Parasitology Today 7:205–207.

Codeço, C. T., D. A. Villela, and F. C. Coelho. 2018. Estimating the effective reproduction number of dengue considering temperature-dependent generation intervals. Epidemics 25:101–111.

Corbel, V., M. Akogbeto, G. B. Damien, A. Djenontin, F. Chandre, C. Rogier, N. Moiroux, J. Chabi, G. G. Padonou, and M.-C. Henry. 2012. Combination of malaria vector control interventions in pyrethroid resistance area in Benin: a cluster randomised controlled trial. Lancet Infectious Diseases 12:617–626.

Cressie, N., C. A. Calder, J. S. Clark, J. M. V. Hoef, and C. K. Wikle. 2009. Accounting for uncertainty in ecological analysis: the strengths and limitations of hierarchical statistical modeling. Ecological Applications 19:553–570.

Cromer, D., J. Stark, and M. P. Davenport. 2009. Low red cell production may protect against severe anemia during a malaria infection—insights from modeling. Journal of Theoretical Biology 257:533–542.

Crooks, L. 2008. Problems with continuous-time malaria models in describing gametocytogenesis. Parasitology 135:881–896.

Cunnington, A. J., J. B. de Souza, M. Walther, and E. M. Riley. 2012. Malaria impairs resistance to *Salmonella* through heme-and heme oxygenase-dependent dysfunctional granulocyte mobilization. Nature Medicine 18:120–127.

Dell, A. I., S. Pawar, and V. M. Savage. 2011. Systematic variation in the temperature dependence of physiological and ecological traits. Proceedings of the National Academy of Sciences of the United States of America 108:10591–10596.

Denny, M. 2017. The fallacy of the average: on the ubiquity, utility and continuing novelty of Jensen's inequality. Journal of Experimental Biology 220:139–146.

Diekmann, O., J. A. P. Heesterbeek, and J. A. Metz. 1990. On the definition and the computation of the basic reproduction ratio R0 in models for infectious diseases in heterogeneous populations. Journal of Mathematical Biology 28:365–382.

Dingemanse, N. J., and N. A. Dochtermann. 2013. Quantifying individual variation in behaviour: mixed-effect modelling approaches. Journal of Animal Ecology 82:39–54.

Donovan, M. J., A. S. Messmore, D. A. Scrafford, D. L. Sacks, S. Kamhawi, and M. A. McDowell. 2007. Uninfected mosquito bites confer protection against infection with malaria parasites. Infection and Immunity 75:2523–2530.

Duong, V., L. Lambrechts, R. E. Paul, S. Ly, R. S. Lay, K. C. Long, R. Huy, A. Tarantola, T. W. Scott, A. Sakuntabhai, et al. 2015. Asymptomatic humans transmit dengue virus to mosquitoes. Proceedings of the National Academy of Sciences of the United States of America 112:14688–14693.

Dwyer, G., J. S. Elkinton, and J. P. Buonaccorsi. 1997. Host heterogeneity in susceptibility and disease dynamics: tests of a mathematical model. American Naturalist 150:685–707.

Ebert, D., C. D. Zschokke-Rohringer, and H. J. Carius. 2000. Dose effects and density-dependent regulation of two microparasites of *Daphnia magna*. Oecologia 122:200–209.

Eckhardt, M., J. F. Hultquist, R. M. Kaake, R. Hüttenhain, and N. J. Krogan. 2020. A systems approach to infectious disease. Nature Reviews Genetics 21:339–354.

Evans, K. J., D. S. Hansen, N. van Rooijen, L. A. Buckingham, and L. Schofield. 2006. Severe malarial anemia of low parasite burden in rodent models results from accelerated clearance of uninfected erythrocytes. Blood 107:1192–1199.

Fonseca, L. L., H. S. Alezi, A. Moreno, J. W. Barnwell, M. R. Galinski, and E. O. Voit. 2016. Quantifying the removal of red blood cells in *Macaca mulatta* during a *Plasmodium coatneyi* infection. Malaria Journal 15:410.

Fontaine, A., S. Lequime, I. Moltini-Conclois, D. Jiolle, I. Leparc-Goffart, R. C. Reiner Jr, and L. Lambrechts. 2018. Epidemiological significance of dengue virus genetic variation in mosquito infection dynamics. PLOS Pathogens 14:e1007187.

Foster, H. L., J. D. Small, and J. G. Fox. 2014. The mouse in biomedical research: normative biology, immunology, and husbandry. Academic Press, Cambridge, Massachusetts.

Franklin, B. S., S. O. Rodrigues, L. R. Antonelli, R. V. Oliveira, A. M. Goncalves, P. A. Sales-Junior, E. P. Valente, J. I. Alvarez-Leite, C. Ropert, D. T. Golenbock, et al. 2007. MyD88-dependent activation of dendritic cells and CD4+ T lymphocytes mediates symptoms, but is not required for the immunological control of parasites during rodent malaria. Microbes and Infection 9:881–890.

Galatas, B., Q. Bassat, and A. Mayor. 2015. Malaria parasites in the asymptomatic: looking for the hay in the haystack. Trends in Parasitology 32:296–308.

Garnham, P. 1966. Malaria parasites and other haemosporidia. Blackwell Scientific, Hoboken, New Jersey.

Gazzinelli, R. T., P. Kalantari, K. A. Fitzgerald, and D. T. Golenbock. 2014. Innate sensing of malaria parasites. Nature Reviews Immunology 14:744.

Gelman, A. 2006. Prior distributions for variance parameters in hierarchical models (comment on article by browne and draper). Bayesian Analysis 1:515–534.

———. 2011. Bayesian statistical pragmatism. Statistical Science 26:10–11.

Gelman, A., H. S. Stern, J. B. Carlin, D. B. Dunson, A. Vehtari, and D. B. Rubin. 2013. Bayesian data analysis. Chapman and Hall/CRC, London.

Gomes, R., and F. Oliveira. 2012. The immune response to sand fly salivary proteins and its influence on *Leishmania* immunity. Frontiers in Immunology 3:110.

Gomes, R., F. Oliveira, C. Teixeira, C. Meneses, D. C. Gilmore, D.-E. Elnaiem, S. Kamhawi, and J. G. Valenzuela. 2012. Immunity to sand fly salivary protein LJM11 modulates host response to vector-transmitted *Leishmania* conferring ulcer-free protection. Journal of Investigative Dermatology 132:2735–2743.

Graham, A. L., J. E. Allen, and A. F. Read. 2005. Evolutionary causes and consequences of immunopathology. Annual Review of Ecology, Evolution, and Systematics 36:373–397.

Gravenor, M. B., A. L. Lloyd, P. G. Kremsner, M. A. Missinou, M. English, K. Marsh, and D. Kwiatkowski. 2002. A model for estimating total parasite load in falciparum malaria patients. Journal of Theoretical Biology 217:137–148.

Greischar, M. A., N. Mideo, A. F. Read, and O. N. Bjørnstad. 2016*a*. Quantifying transmission investment in malaria parasites. PLOS Computational Biology 12.

Greischar, M. A., A. F. Read, and O. N. Bjørnstad. 2013. Synchrony in malaria infections: how intensifying within-host competition can be adaptive. American Naturalist 183:E36–E49.

Greischar, M. A., S. E. Reece, and N. Mideo. 2016*b*. The role of models in translating within-host dynamics to parasite evolution. Parasitology 143:905–914.

Guzman, M. G., D. J. Gubler, A. Izquierdo, E. Martinez, and S. B. Halstead. 2016. Dengue infection. Nature Reviews. Disease Primers 2:16055–16055.

Guzman, M. G., and S. Vazquez. 2010. The complexity of antibody-dependent enhancement of dengue virus infection. Viruses 2:2649–2662.

Handel, A., Y. Li, B. McKay, K. A. Pawelek, V. Zarnitsyna, and R. Antia. 2018. Exploring the impact of inoculum dose on host immunity and morbidity to inform model-based vaccine design. PLOS Computational Biology 14:e1006505.

Harrington, L. C., Françoisevermeylen, J. J. Jones, S. Kitthawee, R. Sithiprasasna, J. D. Edman, and T. W. Scott. 2014. Age-dependent survival of the dengue vector *Aedes aegypti* (diptera: Culicidae) demonstrated by simultaneous release–recapture of different age cohorts. Journal of Medical Entomology 45:307–313.

Hatta, Y., K. Hershberger, K. Shinya, S. C. Proll, R. R. Dubielzig, M. Hatta, M. G. Katze, Y. Kawaoka, and M. Suresh. 2010. Viral replication rate regulates clinical outcome and CD8 T cell responses during highly pathogenic H5N1 influenza virus infection in mice. PLOS Pathogens 6:e1001139.

Haydon, D. T., L. Matthews, R. Timms, and N. Colegrave. 2003. Topndash; down or bottom–up regulation of intra–host blood–stage malaria: do malaria parasites most resemble the dynamics of prey or predator? Proceedings of the Royal Society B: Biological Sciences 270:289–298.

Hedrick, P. W. 2011. Population genetics of malaria resistance in humans. Heredity 107:283–304.

Heffernan, J., R. Smith, and L. Wahl. 2005. Perspectives on the basic reproductive ratio. Journal of The Royal Society Interface 2:281–293.

Hellriegel, B. 1992. Modelling the immune response to malaria with ecological concepts: short-term behaviour against long-term equilibrium. Proceedings of the Royal Society of London. Series B: Biological Sciences 250:249–256.

Hemingway, J. 2014. The role of vector control in stopping the transmission of malaria: threats and opportunities. Philosophical Transactions of the Royal Society B 369:20130431.

Hempelmann, E., and K. Krafts. 2013. Bad air, amulets and mosquitoes: 2,000 years of changing perspectives on malaria. Malaria Journal 12:232.

Hernandez-Valladares, M., J. Naessens, and F. A. Iraqi. 2005. Genetic resistance to malaria in mouse models. Trends in Parasitology 21:352–355.

Hernandez-Valladares, M., J. Naessens, A. Musoke, K. Sekikawa, P. Rihet, P. Busher, F. Iraqi, et al. 2006. Pathology of TNF-deficient mice infected with *Plasmodium chabaudi adami* 408XZ. Experimental Parasitology 114:271–278.

Herzfeld, D. J., and R. Shadmehr. 2014. Motor variability is not noise, but grist for the learning mill. Nature Neuroscience 17:149–150.

Hochman, S., and K. Kim. 2009. The impact of HIV and malaria coinfection: what is known and suggested venues for further study. Interdisciplinary Perspectives on Infectious Diseases 2009.

Hughes, G., R. Kitching, and M. Woolhouse. 2002. Dose-dependent responses of sheep inoculated intranasally with a type O foot-and-mouth disease virus. Journal of Comparative Pathology 127:22–29.

Hugo, L. E., J. A. Jeffery, B. J. Trewin, L. F. Wockner, N. T. Yen, N. H. Le, E. Hine, P. A. Ryan, B. H. Kay, et al. 2014. Adult survivorship of the dengue mosquito *Aedes aegypti* varies seasonally in central vietnam. PLOS Neglected Tropical Diseases 8:e2669.

Jakeman, G., A. Saul, W. Hogarth, and W. Collins. 1999. Anaemia of acute malaria infections in non-immune patients primarily results from destruction of uninfected erythrocytes. Parasitology 119:127–133.

Johansson, M. A., N. Arana-Vizcarrondo, B. J. Biggerstaff, and J. E. Staples. 2010. Incubation periods of yellow fever virus. American Journal of Tropical Medicine and Hygiene 83:183–188.

Johnson, L. R., T. Ben-Horin, K. D. Lafferty, A. McNally, E. Mordecai, K. P. Paaijmans, S. Pawar, and S. J. Ryan. 2015. Understanding uncertainty in temperature effects on vector-borne disease: a Bayesian approach. Ecology 96:203–213.

Kamhawi, S., H. Aslan, and J. G. Valenzuela. 2014. Vector saliva in vaccines for visceral leishmaniasis: a brief encounter of high consequence? Frontiers in Public Health 2:99.

Kamhawi, S., Y. Belkaid, G. Modi, E. Rowton, and D. Sacks. 2000. Protection against cutaneous leishmaniasis resulting from bites of uninfected sand flies. Science 290:1351–1354.

Kamiya, T., M. A. Greischar, and N. Mideo. 2017. Epidemiological consequences of immune sensitisation by pre-exposure to vector saliva. PLOS Neglected Tropical Diseases 11:1–19.

Kamiya, T., M. A. Greischar, K. Wadhawan, B. Gilbert, K. Paaijmans, and N. Mideo. 2020. Temperature-dependent variation in the extrinsic incubation period elevates the risk of vector-borne disease emergence. Epidemics 30:100382.

Karl, S., N. Halder, J. K. Kelso, S. A. Ritchie, and G. J. Milne. 2014. A spatial simulation model for dengue virus infection in urban areas. BMC Infectious Diseases 14:447.

Kataoka, S., J. Satoh, H. Fujiya, T. Toyota, R. Suzuki, K. Itoh, and K. Kumagai. 1983. Immunologic aspects of the nonobese diabetic (nod) mouse: abnormalities of cellular immunity. Diabetes 32:247–253.

Kebaier, C., T. Voza, and J. Vanderberg. 2010. Neither mosquito saliva nor immunity to saliva has a detectable effect on the infectivity of *Plasmodium* sporozoites injected into mice. Infection and Immunity 78:545–551.

Keeling, M. J., and P. Rohani. 2008. Modeling infectious diseases in humans and animals. Princeton University Press, Princeton.

Kim, D., K. Fedak, and R. Kramer. 2012. Reduction of malaria prevalence by indoor residual spraying: a meta-regression analysis. American Society of Tropical Medicine and Hygiene 87:117–124.

King, T., and T. Lamb. 2015. Interferon-$\gamma$: the Jekyll and Hyde of malaria. PLOS Pathogen 11:e1005118.

Kirk, D., N. Jones, S. Peacock, J. Phillips, P. K. Molnár, M. Krkošek, and P. Luijckx. 2018. Empirical evidence that metabolic theory describes the temperature dependency of within-host parasite dynamics. PLOS Biology 16:e2004608.

Kochin, B. F., A. J. Yates, J. C. De Roode, and R. Antia. 2010. On the control of acute rodent malaria infections by innate immunity. PLOS One 5:e10444.

Kraisin, S., S. Verhenne, T.-T. Pham, K. Martinod, C. Tersteeg, N. Vandeputte, H. Deckmyn, K. Vanhoorelbeke, P. E. Van den Steen, and S. F. De Meyer. 2019. von Willebrand factor in experimental malaria-associated acute respiratory distress syndrome. Journal of Thrombosis and Haemostasis 17:1372–1383.

Kremsner, P. G., S. Winkler, C. Brandts, E. Wildling, L. Jenne, W. Graninger, J. Prada, U. Bienzle, P. Juillard, and G. E. Grau. 1995. Prediction of accelerated cure in *Plasmodium falciparum* malaria by the elevated capacity of tumor necrosis factor production. American Journal of Tropical Medicine and Hygiene 53:532–538.

Lai, S., Z. Huang, H. Zhou, K. L. Anders, T. A. Perkins, W. Yin, Y. Li, D. Mu, Q. Chen, Z. Zhang, et al. 2015. The changing epidemiology of dengue in China, 1990-2014: a descriptive analysis of 25 years of nationwide surveillance data. BMC Medicine 13:100.

Lamb, T. J., D. E. Brown, A. J. Potocnik, and J. Langhorne. 2006. Insights into the immunopathogenesis of malaria using mouse models. Expert Reviews in Molecular Medicine 8:1–22.

Last, J. 2007. A Dictionary of Public Health. Oxford reference online premium. Oxford University Press, Oxford.

Lazzaro, B. P., and T. J. Little. 2008. Immunity in a variable world. Philosophical Transactions of the Royal Society B: Biological Sciences 364:15–26.

Lee, B. Y., and S. M. Bartsch. 2017. How to determine if a model is right for neglected tropical disease decision making. PLOS Neglected Tropical Diseases 11:e0005457.

Leggett, H. C., C. K. Cornwallis, and S. A. West. 2012. Mechanisms of pathogenesis, infective dose and virulence in human parasites. PLOS Pathogens 8:e1002512.

Li, C., L. A. Sanni, F. Omer, E. Riley, and J. Langhorne. 2003. Pathology of *Plasmodium chabaudi chabaudi* infection and mortality in interleukin-10-deficient mice are ameliorated by anti-tumor necrosis factor alpha and exacerbated by anti-transforming growth factor $\beta$ antibodies. Infection and Immunity 71:4850–4856.

Li, R., L. Xu, O. N. Bjørnstad, K. Liu, T. Song, A. Chen, B. Xu, Q. Liu, and N. C. Stenseth. 2019. Climate-driven variation in mosquito density predicts the spatiotemporal dynamics of dengue. Proceedings of the National Academy of Sciences of the United States of America 116:3624–3629.

Li, Y., and A. Handel. 2014. Modeling inoculum dose dependent patterns of acute virus infections. Journal of Theoretical Biology 347:63–73.

Lines, J., and J. Armstrong. 1992. For a few parasites more: inoculum size, vector control and strain-specific immunity to malaria. Parasitology Today 8:381–383.

Liu, Z., Z. Zhang, Z. Lai, T. Zhou, Z. Jia, J. Gu, K. Wu, and X.-G. Chen. 2017. Temperature increase enhances *Aedes albopictus* competence to transmit dengue virus. Frontiers in Microbiology 8:2337.

Lloyd, A. L., J. Zhang, and A. M. Root. 2007. Stochasticity and heterogeneity in host–vector models. Journal of The Royal Society Interface 4:851–863.

Lloyd-Smith, J. O., S. J. Schreiber, P. E. Kopp, and W. M. Getz. 2005. Superspreading and the effect of individual variation on disease emergence. Nature 438:355–359.

Long, G. H., B. Chan, J. Allen, A. F. Read, and A. Graham. 2006. Parasite genetic diversity does not influence TNF-mediated effects on the virulence of primary rodent malaria infections. Parasitology 133:673–684.

Long, G. H., B. H. Chan, J. E. Allen, A. F. Read, and A. L. Graham. 2008. Experimental manipulation of immune-mediated disease and its fitness costs for rodent malaria parasites. BMC Evolutionary Biology 8:128.

López, C., C. Saravia, A. Gomez, J. Hoebeke, and M. A. Patarroyo. 2010. Mechanisms of genetically-based resistance to malaria. Gene 467:1–12.

Luzzatto, L. 2012. Sickle cell anaemia and malaria. Mediterranean Journal of Hematology and Infectious Diseases 4.

Macdonald, G. 1957. The epidemiology and control of malaria. Oxford University Press, Oxford.

Machain-Williams, C., K. Reagan, T. Wang, N. S. Zeidner, and C. D. Blair. 2013. Immunization with *Culex tarsalis* mosquito salivary gland extract modulates West Nile virus infection and disease in mice. Viral Immunology 26:84–92.

Mackinnon, M. J., and A. F. Read. 1999. Genetic relationships between parasite virulence and transmission in the rodent malaria *Plasmodium chabaudi*. Evolution 53:689–703.

Mandal, S., R. R. Sarkar, and S. Sinha. 2011. Mathematical models of malaria-a review. Malaria Journal 10:202.

Marois, I., A. Cloutier, É. Garneau, and M. V. Richter. 2012. Initial infectious dose dictates the innate, adaptive, and memory responses to influenza in the respiratory tract. Journal of Leukocyte Biology 92:107–121.

Martin, J. G., D. H. Nussey, A. J. Wilson, and D. Réale. 2011. Measuring individual differences in reaction norms in field and experimental studies: a power analysis of random regression models. Methods in Ecology and Evolution 2:362–374.

Matsuura, K., and C. J. Willmott. 2018. Terrestrial air temperature: 1900-2017 gridded monthly time series. `http://climate.geog.udel.edu/~climate/`. Accessed: 2018-10-17.

McAlister, R. O. 1977. Time-dependent loss of invasive ability of *Plasmodium berghei* merozoites in vitro. Journal of Parasitology pages 455–463.

McElreath, R. 2018. Statistical rethinking: A Bayesian course with examples in R and Stan. Chapman and Hall/CRC, London.

McLean, A. R., and C. J. Bostock. 2000. Scrapie infections initiated at varying doses: an analysis of 117 titration experiments. Philosophical Transactions of the Royal Society of London. Series B: Biological Sciences 355:1043–1050.

Mendis, K., A. Rietveld, M. Warsame, A. Bosman, B. Greenwood, and W. H. Wernsdorfer. 2009. From malaria control to eradication: The WHO perspective. Tropical Medicine & International Health 14:802–809.

Metcalf, C., A. Graham, S. Huijben, V. Barclay, G. Long, B. Grenfell, A. Read, and O. Bjørnstad. 2011. Partitioning regulatory mechanisms of within-host malaria dynamics using the effective propagation number. Science 333:984–988.

Metcalf, C. J. E., G. Long, N. Mideo, J. D. Forester, O. Bjørnstad, and A. L. Graham. 2012. Revealing mechanisms underlying variation in malaria virulence: effective propagation and host control of uninfected red blood cell supply. Journal of the Royal Society Interface 9:2804–2813.

Michael, E., and D. Bundy. 1989. Density dependence in establishment, growth and worm fecundity in intestinal helminthiasis: the population biology of *Trichuris muris* (nematoda) infection in CBA/Ca mice. Parasitology 98:451–458.

Michel, G., C. Pomares, B. Ferrua, and P. Marty. 2011. Importance of worldwide asymptomatic carriers of *Leishmania infantum* (*L. chagasi*) in human. Acta Tropica 119:69–75.

Mideo, N., S. Alizon, and T. Day. 2008*a*. Linking within-and between-host dynamics in the evolutionary epidemiology of infectious diseases. Trends in Ecology & Evolution 23:511–517.

Mideo, N., V. C. Barclay, B. H. Chan, N. J. Savill, A. F. Read, and T. Day. 2008*b*. Understanding and predicting strain-specific patterns of pathogenesis in the rodent malaria *Plasmodium chabaudi*. American Naturalist 172:E214–E238.

Mideo, N., T. Day, and A. F. Read. 2008*c*. Modelling malaria pathogenesis. Cellular Microbiology 10:1947–1955.

Mideo, N., S. E. Reece, A. L. Smith, and C. J. E. Metcalf. 2013. The Cinderella syndrome: why do malaria-infected cells burst at midnight? Trends in Parasitology 29:10–16.

Mideo, N., N. J. Savill, W. Chadwick, P. Schneider, A. F. Read, T. Day, and S. E. Reece. 2011. Causes of variation in malaria infection dynamics: insights from theory and data. American Naturalist 178:174–188.

Miller, M. R., L. Råberg, A. F. Read, and N. J. Savill. 2010. Quantitative analysis of immune response and erythropoiesis during rodent malarial infection. PLOS Computational Biology 6:e1000946.

Molina, R., C. Cafiavate, E. Cercenado, F. Lagunat, R. Lopez-Velez, and J. Alvar. 1994. Indirect xenodiagnosis of visceral leishmaniasis in 10 HIV-infected patients using colonized *Phlebotomus perniciosus*. AIDS 8:277–278.

Molineaux, L., H. Diebner, M. Eichner, W. Collins, G. Jeffery, and K. Dietz. 2001. *Plasmodium falciparum* parasitaemia described by a new mathematical model. Parasitology 122:379–391.

Mordecai, E. A., J. M. Cohen, M. V. Evans, P. Gudapati, L. R. Johnson, C. A. Lippi, K. Miazgowicz, C. C. Murdock, J. R. Rohr, S. J. Ryan, et al. 2017*a*. Detecting the impact of temperature on transmission of Zika, dengue, and chikungunya using mechanistic models. PLOS Neglected Tropical Diseases 11:e0005568.

———. 2017*b*. Model code, data, and output .

Mordecai, E. A., K. P. Paaijmans, L. R. Johnson, C. Balzer, T. Ben-Horin, E. Moor, A. McNally, S. Pawar, S. J. Ryan, T. C. Smith, et al. 2013. Optimal temperature for malaria transmission is dramatically lower than previously predicted. Ecology Letters 16:22–30.

Mordmüller, B., W. Metzger, P. Juillard, B. Brinkman, C. Verweij, G. Grau, and P. Kremsner. 1997. Tumor necrosis factor in *Plasmodium falciparum* malaria: high plasma level is associated with fever, but high production capacity is associated with rapid fever clearance. European Cytokine Network 8:29–35.

Morris, M. C., E. A. Gilliam, J. Button, and L. Li. 2014. Dynamic modulation of innate immune response by varying dosages of lipopolysaccharide (lps) in human monocytic cells. Journal of Biological Chemistry 289:21584–21590.

Moser, C., C. J. Lerche, K. Thomsen, T. Hartvig, J. Schierbeck, P. Ø. Jensen, O. Ciofu, and N. Høiby. 2019. Antibiotic therapy as personalized medicine–general considerations and complicating factors. APMIS 127:361–371.

Mugglin, A. S., N. Cressie, and I. Gemmell. 2002. Hierarchical statistical modelling of influenza epidemic dynamics in space and time. Statistics in Medicine 21:2703–2721.

Nahrendorf, W., P. J. Spence, I. Tumwine, P. Levy, W. Jarra, R. W. Sauerwein, and J. Langhorne. 2015. Blood-stage immunity to *Plasmodium chabaudi* malaria following chemoprophylaxis and sporozoite immunization. eLife 4:e05165.

Nie, P., and C. Kennedy. 1993. Infection dynamics of larval *Bothriocephalus claviceps* in *Cyclops vicinus*. Parasitology 106:503–509.

Nikinmaa, M., and K. Anttila. 2019. Individual variation in aquatic toxicology: Not only unwanted noise. Aquatic Toxicology 207:29–33.

Ockenfels, B., E. Michael, and M. A. McDowell. 2014. Meta-analysis of the effects of insect vector saliva on host immune responses and infection of vector-transmitted pathogens: a focus on leishmaniasis. PLOS Neglected Tropical Diseases 8:e3197.

Ohm, J. R., F. Baldini, P. Barreaux, T. Lefevre, P. A. Lynch, E. Suh, S. A. Whitehead, and M. B. Thomas. 2018. Rethinking the extrinsic incubation period of malaria parasites. Parasites and Vectors 11:178.

Oliveira, F., A. M. de Carvalho, and C. I. de Oliveira. 2013*a*. Sand-fly saliva-*Leishmania*-man: the trigger trio. Frontiers in Immunology 4:375.

Oliveira, F., P. G. Lawyer, S. Kamhawi, and J. G. Valenzuela. 2008. Immunity to distinct sand fly salivary proteins primes the anti-*Leishmania* immune response towards protection or exacerbation of disease. PLOS Neglected Tropical Diseases 2:e226.

Oliveira, F., B. Traoré, R. Gomes, O. Faye, D. C. Gilmore, S. Keita, P. Traoré, C. Teixeira, C. A. Coulibaly, S. Samake, et al. 2013*b*. Delayed-type hypersensitivity to sand fly saliva in humans from a leishmaniasis-endemic area of Mali is Th1-mediated and persists to midlife. Journal of Investigative Dermatology 133:452–459.

Omer, F. M., and E. M. Riley. 1998. Transforming growth factor $\beta$ production is inversely correlated with severity of murine malaria infection. Journal of Experimental Medicine 188:39–48.

Otto, S. P., and T. Day. 2011. A biologist's guide to mathematical modeling in ecology and evolution. Princeton University Press, Princeton.

Paaijmans, K. P., S. Blanford, B. H. Chan, and M. B. Thomas. 2011. Warmer temperatures reduce the vectorial capacity of malaria mosquitoes. Biology Letters 8:465–468.

Paaijmans, K. P., A. F. Read, and M. B. Thomas. 2009. Understanding the link between malaria risk and climate. Proceedings of the National Academy of Sciences of the United States of America 106:13844–13849.

Pagan, A. J., S. Levitte, R. D. Berg, L. Hernandez, J. Zimmerman, D. M. Tobin, and L. Ramakrishnan. 2016. mTOR deficiency reveals an immunological trade-off in innate resistance to mycobacterial infection in vivo. Journal of Immunology .

Paul, R., F. Ariey, and V. Robert. 2003. The evolutionary ecology of *Plasmodium*. Ecology Letters 6:866–880.

Pearson, T., T. G. Markees, D. V. Serreze, M. A. Pierce, M. P. Marron, L. S. Wicker, L. B. Peterson, L. D. Shultz, J. P. Mordes, A. A. Rossini, et al. 2003. Genetic disassociation of autoimmunity and resistance to costimulation blockade-induced transplantation tolerance in nonobese diabetic mice. Journal of Immunology 171:185–195.

Perelson, A. S., and R. M. Ribeiro. 2013. Modeling the within-host dynamics of HIV infection. BMC Biology 11:96.

Perkins, D. J., T. Were, G. C. Davenport, P. Kempaiah, J. B. Hittner, and J. M. Ong'echa. 2011. Severe malarial anemia: innate immunity and pathogenesis. International Journal of Biological Sciences 7:1427.

Perkins, T. A., R. C. Reiner Jr, G. España, A. Quirine, A. Verma, K. A. Liebman, V. A. Paz-Soldan, J. P. Elder, A. C. Morrison, S. T. Stoddard, et al. 2019. An agent-based model of dengue virus transmission shows how uncertainty about breakthrough infections influences vaccination impact projections. PLOS Computational Biology 15:e1006710.

Perkins, T. A., A. S. Siraj, C. W. Ruktanonchai, M. U. Kraemer, and A. J. Tatem. 2016. Model-based projections of Zika virus infections in childbearing women in the Americas. Nature Microbiology 1:16126.

Petersen, L. R., R. S. Nasci, C. B. Beard, and R. F. Massung. 2014. Emerging vector-borne diseases in the United States: What's next and are we prepared? Pages 258–285 *in* Forum on Microbial Threats; Board on Global Health; Health and Medicine Division; National Academies of Sciences, Engineering, and Medicine. Global Health Impacts of Vector-Borne Diseases: Workshop Summary. National Academies Press, Washington (DC).

Pingen, M., M. A. Schmid, E. Harris, and C. S. McKimmie. 2017. Mosquito biting modulates skin response to virus infection. Trends in Parasitology .

Pluess, B., F. Tanser, C. Lengeler, and B. Sharp. 2010. Indoor residual spraying for preventing malaria. Cochrane Database of Systematic Reviews page CD006657.

Poulin, R., and S. Morand. 2014. Parasite biodiversity. Smithsonian Institution, Washington, D.C.

Price, R. N., J. A. Simpson, F. Nosten, C. Luxemburger, L. Hkirjaroen, F. ter Kuile, T. Chongsuphajaisiddhi, and N. J. White. 2001. Factors contributing to anemia after uncomplicated falciparum malaria. American Journal of Tropical Medicine and Hygiene 65:614–622.

Prosser, J. I., B. J. Bohannan, T. P. Curtis, R. J. Ellis, M. K. Firestone, R. P. Freckleton, J. L. Green, L. E. Green, K. Killham, J. J. Lennon, et al. 2007. The role of ecological theory in microbial ecology. Nature Reviews Microbiology 5:384–392.

R Core Team. 2018. R: A language and environment for statistical computing. R Foundation for Statistical Computing, Vienna, Austria.

Rassi, A., and J. A. Marin-Neto. 2010. Chagas disease. Lancet 375:1388–1402.

Read, A. F., S. J. Baigent, C. Powers, L. B. Kgosana, L. Blackwell, L. P. Smith, D. A. Kennedy, S. W. Walkden-Brown, and V. K. Nair. 2015. Imperfect vaccination can enhance the transmission of highly virulent pathogens. PLOS Biology 13:e1002198.

Reiner, R. C., T. A. Perkins, C. M. Barker, T. Niu, L. F. Chaves, A. M. Ellis, D. B. George, A. Le Menach, J. R. Pulliam, D. Bisanzio, et al. 2013. A systematic review of mathematical models of mosquito-borne pathogen transmission: 1970–2010. Journal of The Royal Society Interface 10:20120921.

Reisen, W. K., Y. Fang, and V. M. Martinez. 2006. Effects of temperature on the transmission of West Nile virus by *Culex tarsalis* (diptera: Culicidae). Journal of Medical Entomology 43:309–317.

Rhodes, S. J., J. Guedj, H. A. Fletcher, T. Lindenstrøm, T. J. Scriba, T. G. Evans, G. M. Knight, and R. G. White. 2018. Using vaccine immunostimulation/immunodynamic modelling methods to inform vaccine dose decision-making. NPJ Vaccines 3:1–7.

Rhodes, S. J., G. M. Knight, D. E. Kirschner, R. G. White, and T. G. Evans. 2019. Dose finding for new vaccines: The role for immunostimulation/immunodynamic modelling. Journal of Theoretical Biology 465:51–55.

Ribeiro, J. M., and I. M. Francischetti. 2003. Role of arthropod saliva in blood feeding: Sialome and post-sialome perspectives. Annual Review of Entomology 48:73–88.

Riches, A., J. Sharp, D. B. Thomas, and S. V. Smith. 1973. Blood volume determination in the mouse. Journal of Physiology 228:279–284.

Rivas, A. L., G. Leitner, M. D. Jankowski, A. L. Hoogesteijn, M. J. Iandiorio, S. Chatzipanagiotou, A. Ioannidis, S. E. Blum, R. Piccinini, A. Antoniades, et al. 2017. Nature and consequences of biological reductionism for the immunological study of infectious diseases. Frontiers in Immunology 8:612.

Robert, M. A., R. C. Christofferson, P. D. Weber, and H. J. Wearing. 2019. Temperature impacts on dengue emergence in the United States: Investigating the role of seasonality and climate change. Epidemics 28:100344.

Roberts, A., F. P.-M. de Villena, W. Wang, L. McMillan, and D. W. Threadgill. 2007. The polymorphism architecture of mouse genetic resources elucidated using genome-wide resequencing data: implications for QTL discovery and systems genetics. Mammalian Genome 18:473–481.

Roche, D. G., V. Careau, and S. A. Binning. 2016. Demystifying animal 'personality'(or not): why individual variation matters to experimental biologists. Journal of Experimental Biology 219:3832–3843.

Rock, K. S., E. A. le Rutte, S. J. de Vlas, E. R. Adams, G. F. Medley, and T. D. Hollingsworth. 2015. Uniting mathematics and biology for control of visceral leishmaniasis. Trends in Parasitology 31:251–259.

Rockett, K., M. Awburn, B. Aggarwal, W. Cowden, and I. Clark. 1992. In vivo induction of nitrite and nitrate by tumor necrosis factor, lymphotoxin, and interleukin-1: possible roles in malaria. Infection and Immunity 60:3725–3730.

Rogers, D. J., and S. I. Hay. 2012. The climatic suitability for dengue transmission in continental Europe. European Centre for Disease Prevention and Control, Solna.

Rohoušová, I., J. Hostomská, M. Vlková, T. Kobets, M. Lipoldová, and P. Volf. 2011. The protective effect against *Leishmania* infection conferred by sand fly bites is limited to short-term exposure. International Journal for Parasitology 41:481–485.

Romeo-Aznar, V., R. Paul, O. Telle, and M. Pascual. 2018. Mosquito-borne transmission in urban landscapes: the missing link between vector abundance and human density. Proceedings of the Royal Society B: Biological Sciences 285:20180826.

Rosenberg, R., R. A. Wirtz, I. Schneider, and R. Burge. 1990. An estimation of the number of malaria sporozoites ejected by a feeding mosquito. Transactions of the Royal Society of Tropical Medicine and Hygiene 84:209–212.

Ross, R. 1897. On some peculiar pigmented cells found in two mosquitos fed on malarial blood. British Medical Journal 2:1786.

———. 1908. Report on the prevention of malaria in Mauritius. Waterlow, London.

———. 1911*a*. The prevention of malaria. John Murray, London.

———. 1911*b*. Some quantitative studies in epidemiology. Nature 87:466–467.

———. 1921. The principle of repeated medication for curing infections. British Medical Journal 2:1.

Rudolph, K. E., J. Lessler, R. M. Moloney, B. Kmush, and D. A. Cummings. 2014. Incubation periods of mosquito-borne viral infections: a systematic review. American Journal of Tropical Medicine and Hygiene 90:882–891.

Ryan, S. J., T. Ben-Horin, and L. R. Johnson. 2015. Malaria control and senescence: the importance of accounting for the pace and shape of aging in wild mosquitoes. Ecosphere 6:1–13.

Safeukui, I., J.-M. Correas, V. Brousse, D. Hirt, G. Deplaine, S. Mulé, M. Lesurtel, N. Goasguen, A. Sauvanet, A. Couvelard, et al. 2008. Retention of *Plasmodium falciparum* ring-infected erythrocytes in the slow, open microcirculation of the human spleen. Blood 112:2520–2528.

Santhanam, J., L. Råberg, A. F. Read, and N. J. Savill. 2014. Immune-mediated competition in rodent malaria is most likely caused by induced changes in innate immune clearance of merozoites. PLOS Computational Biology 10:e1003416.

Saul, A. 1998. Models for the in-host dynamics of malaria revisited: errors in some basic models lead to large over-estimates of growth rates. Parasitology 117:405–407.

Savill, N. J., W. Chadwick, and S. E. Reece. 2009. Quantitative analysis of mechanisms that govern red blood cell age structure and dynamics during anaemia. PLOS Computational Biology 5:e1000416.

Schaffner, F., and A. Mathis. 2014. Dengue and dengue vectors in the who european region: past, present, and scenarios for the future. Lancet Infectious Diseases 14:1271–1280.

Schmid-Hempel, P., and S. A. Frank. 2007. Pathogenesis, virulence, and infective dose. PLOS Pathogens 3:e147.

Schmidt, C., N. Schneble, J. Müller, R. Bauer, A. Perino, R. Marone, S. Rybalkin, M. Wymann, E. Hirsch, and R. Wetzker. 2013. Phosphoinositide 3-kinase $\gamma$ mediates microglial phagocytosis via lipid kinase-independent control of cAMP. Neuroscience 233:44–53.

Schmidt, C., N. Schneble, and R. Wetzker. 2014. The fifth dimension of innate immunity. Journal of Cell Communication and Signaling 8:363–367.

Schneider, B. S., C. E. McGee, J. M. Jordan, H. L. Stevenson, L. Soong, and S. Higgs. 2007. Prior exposure to uninfected mosquitoes enhances mortality in naturally-transmitted West Nile virus infection. PLOS One 2:e1171.

Schneider, B. S., L. Soong, N. S. Zeidner, and S. Higgs. 2004. *Aedes aegypti* salivary gland extracts modulate anti-viral and TH1/TH2 cytokine responses to sindbis virus infection. Viral Immunology 17:565–573.

Schneider, D. S. 2011. Tracing personalized health curves during infections. PLOS Biology 9:e1001158.

Schneider, D. S., and J. S. Ayres. 2008. Two ways to survive infection: what resistance and tolerance can teach us about treating infectious diseases. Nature Reviews Immunology 8:889.

Scott, J. A. G., J. A. Berkley, I. Mwangi, L. Ochola, S. Uyoga, A. Macharia, C. Ndila, B. S. Lowe, S. Mwarumba, E. Bauni, et al. 2011. Relation between falciparum malaria and bacteraemia in Kenyan children: a population-based, case-control study and a longitudinal study. Lancet 378:1316–1323.

Segueni, N., E. Tritto, M.-L. Bourigault, S. Rose, F. Erard, M. Le Bert, M. Jacobs, F. Di Padova, D. P. Stiehl, P. Moulin, et al. 2016. Controlled *Mycobacterium tuberculosis* infection in mice under treatment with anti-IL-17A or IL-17F antibodies, in contrast to TNF$\alpha$ neutralization. Scientific Reports 6:36923.

Serreze, D. V., J. W. Gaedeke, and E. H. Leiter. 1993. Hematopoietic stem-cell defects underlying abnormal macrophage development and maturation in NOD/Lt mice: defective regulation of cytokine receptors and protein kinase c. Proceedings of the National Academy of Sciences of the United States of America 90:9625–9629.

Shankar, A. H. 2000. Nutritional modulation of malaria morbidity and mortality. Journal of Infectious Diseases 182:S37–S53.

Shapiro, L. L., S. A. Whitehead, and M. B. Thomas. 2017. Quantifying the effects of temperature on mosquito and parasite traits that determine the transmission potential of human malaria. PLOS Biology 15:e2003489.

Shavit, J. A., A. Manichaikul, H. L. Lemmerhirt, K. W. Broman, and D. Ginsburg. 2009. Modifiers of von Willebrand factor identified by natural variation in inbred strains of mice. Blood 114:5368–5374.

Simpson, R. H. 1952. Infectiousness of communicable diseases in the household:(measles, chickenpox, and mumps). Lancet 260:549–554.

Siraj, A. S., R. J. Oidtman, J. H. Huber, M. U. Kraemer, O. J. Brady, M. A. Johansson, and T. A. Perkins. 2017. Temperature modulates dengue virus epidemic growth rates through its effects on reproduction numbers and generation intervals. PLOS Neglected Tropical Diseases 11:e0005797.

Smith, D. L., K. E. Battle, S. I. Hay, C. M. Barker, T. W. Scott, and F. E. McKenzie. 2012. Ross, Macdonald, and a theory for the dynamics and control of mosquito-transmitted pathogens. PLOS Pathogens 8:e1002588.

Smith, D. L., and F. E. McKenzie. 2004. Statics and dynamics of malaria infection in *Anopheles* mosquitoes. Malaria Journal 3:13.

Smith, H. 2011. Distributed delay equations and the linear chain trick. Pages 119–130 *in* An Introduction to Delay Differential Equations with Applications to the Life Sciences. Springer.

Smith, K. F., A. P. Dobson, F. E. McKenzie, L. A. Real, D. L. Smith, and M. L. Wilson. 2005. Ecological theory to enhance infectious disease control and public health policy. Frontiers in Ecology and the Environment 3:29–37.

Soetaert, K. 2009. rootSolve: Nonlinear root finding, equilibrium and steady-state analysis of ordinary differential equations.

Soetaert, K., T. Petzoldt, and R. W. Setzer. 2010. Solving differential equations in R: Package deSolve. Journal of Statistical Software 33:1–25.

Sorci, G., C. Lippens, C. Léchenault, and B. Faivre. 2017. Benefits of immune protection versus immunopathology costs: A synthesis from cytokine KO models. Infection, Genetics and Evolution 54:491–495.

Sorensen, T., S. Hohenstein, and S. Vasishth. 2016. Bayesian linear mixed models using Stan: A tutorial for psychologists, linguists, and cognitive scientists. Quantitative Methods for Psychology 12:175–200.

Stan Development Team. 2018. Stan Modeling Language User's Guide and Reference Manual, Version 2.18.0.

———. 2019. RStan: the R interface to Stan, version 2.18.2. `http://mc-stan.org`.

Stauch, A., R. R. Sarkar, A. Picado, B. Ostyn, S. Sundar, S. Rijal, M. Boelaert, J.-C. Dujardin, and H.-P. Duerr. 2011. Visceral leishmaniasis in the Indian subcontinent: modelling epidemiology and control. PLOS Neglected Tropical Diseases 5:e1405.

Stephens, R., R. L. Culleton, and T. J. Lamb. 2012. The contribution of *Plasmodium chabaudi* to our understanding of malaria. Trends in Parasitology 28:73–82.

Stevenson, M. M., and E. M. Riley. 2004. Innate immunity to malaria. Nature Reviews Immunology 4:169.

Stockdale, L., and R. Newton. 2013. A review of preventative methods against human leishmaniasis infection. PLOS Neglected Tropical Diseases 7:e2278.

Tan, G. K., J. K. Ng, S. L. Trasti, W. Schul, G. Yip, and S. Alonso. 2010. A non mouse-adapted dengue virus strain as a new model of severe dengue infection in AG129 mice. PLOS Neglected Tropical Diseases 4.

Tate, A. T. 2017. A general model for the influence of immune priming on disease prevalence. Oikos 126:350–360.

Thiakaki, M., I. Rohousova, V. Volfova, P. Volf, K.-P. Chang, and K. Soteriadou. 2005. Sand fly specificity of saliva-mediated protective immunity in *Leishmania* amazonensis-BALB/c mouse model. Microbes and Infection 7:760–766.

Timms, R., N. Colegrave, B. Chan, and A. Read. 2001. The effect of parasite dose on disease severity in the rodent malaria *Plasmodium chabaudi*. Parasitology 123:1–11.

Titus, R. G., and J. Ribeiro. 1988. Salivary gland lysates from the sand fly *Lutzomyia longipalpis* enhance *Leishmania* infectivity. Science 239:1306–1308.

Tomasello, D., and P. Schlagenhauf. 2013. Chikungunya and dengue autochthonous cases in Europe, 2007–2012. Travel Medicine and Infectious Disease 11:274–284.

Torres, B. Y., J. H. M. Oliveira, A. T. Tate, P. Rath, K. Cumnock, and D. S. Schneider. 2016. Tracking resilience to infections by mapping disease space. PLOS Biology 14:e1002436.

Tran, T. M., B. Samal, E. Kirkness, and P. D. Crompton. 2012. Systems immunology of human malaria. Trends in Parasitology 28:248–257.

Trochim, W. M., D. A. Cabrera, B. Milstein, R. S. Gallagher, and S. J. Leischow. 2006. Practical challenges of systems thinking and modeling in public health. American Journal of Public Health 96:538–546.

Tsutsui, N., and T. Kamiyama. 1999. Transforming growth factor $\beta$-induced failure of resistance to infection with blood-stage *Plasmodium chabaudi* in mice. Infection and Immunity 67:2306–2311.

Turlings, T. C., and M. Erb. 2018. Tritrophic interactions mediated by herbivore-induced plant volatiles: mechanisms, ecological relevance, and application potential. Annual Review of Entomology 63:433–452.

Vale, P. F., A. Fenton, and S. P. Brown. 2014. Limiting damage during infection: lessons from infection tolerance for novel therapeutics. PLOS Biology 12:e1001769.

Van Putten, L., and F. Croon. 1958. The life span of red cells in the rat and the mouse as determined by labeling with DFP32 in vivo. Blood 13:789–794.

VanderWaal, K. L., and V. O. Ezenwa. 2016. Heterogeneity in pathogen transmission: mechanisms and methodology. Functional Ecology 30:1606–1622.

Vazquez-Prokopec, G. M., T. A. Perkins, L. A. Waller, A. L. Lloyd, R. C. Reiner, T. W. Scott, and U. Kitron. 2016. Coupled heterogeneities and their impact on parasite transmission and control. Trends in Parasitology 32:356–367.

Verhoeff, R. P., M.-C. P. Knippels, M. G. Gilissen, and K. T. Boersma. 2018. The theoretical nature of systems thinking. Perspectives on systems thinking in biology education. Page 40 *in* Frontiers in Education, vol. 3.

Vindenes, Y., and Ø. Langangen. 2015. Individual heterogeneity in life histories and eco-evolutionary dynamics. Ecology Letters 18:417–432.

Wale, N., M. J. Jones, D. G. Sim, A. F. Read, and A. A. King. 2019. The contribution of host cell-directed vs. parasite-directed immunity to the disease and dynamics of malaria infections. Proceedings of the National Academy of Sciences of the United States of America 116:22386–22392.

Watson, F. L., R. Püttmann-Holgado, F. Thomas, D. L. Lamar, M. Hughes, M. Kondo, V. I. Rebel, and D. Schmucker. 2005. Extensive diversity of Ig-superfamily proteins in the immune system of insects. Science 309:1874–1878.

Weatherall, D. 2008. Genetic variation and susceptibility to infection: the red cell and malaria. British Journal of Haematology 141:276–286.

White, N., D. Chapman, and G. Watt. 1992. The effects of multiplication and synchronicity on the vascular distribution of parasites in falciparum malaria. Transactions of the Royal Society of Tropical Medicine and Hygiene 86:590–597.

White, N. J. 2017. Malaria parasite clearance. Malaria Journal 16:88.

Woolhouse, M. E., C. Dye, J.-F. Etard, T. Smith, J. Charlwood, G. Garnett, P. Hagan, J. Hii, P. Ndhlovu, R. Quinnell, et al. 1997. Heterogeneities in the transmission of infectious agents: implications for the design of control programs. Proceedings of the National Academy of Sciences of the United States of America 94:338–342.

World Health Organization. 2012*a*. Global strategy for dengue prevention and control 2012-2020. Geneva: World Health Organization, Geneva.

———. 2012*b*. Handbook for integrated vector management. Geneva: World Health Organization, Geneva.

———. 2014. A global brief on vector-borne diseases. Geneva: World Health Organization.

———. 2015. Global technical strategy for malaria 2016-2030. Geneva: World Health Organization.

———. 2017. Global vector control response 2017-2030. Geneva: World Health Organization.

Zhang, J., M. Teh, J. Kim, M. M. Eva, R. Cayrol, R. K. Meade, A. Nijnik, X. Montagutelli, D. Malo, and J. Jaubert. 2019. A loss-of-function mutation in Itgal contributes to the high susceptibility of Collaborative Cross strain CC042 to *Salmonella* infections. BioRxiv page 723478.